SCUOLA DI SCIENZE
Dipartimento di Chimica Industriale “Toso Montanari”

Corso di Laurea Magistrale in

Chimica Industriale

Classe LM-71 - Scienze e Tecnologie della Chimica Industriale

Synthesis, Characterization and Conformational Studies of Modified Carbazole-bis-aryl-boranes

Tesi di laurea sperimentale

CANDIDATO

Simone Foschi

RELATORE

Prof. Dr. Andrea Mazzanti

CORRELATORE

Dr. Michele Mancinelli

Daniel Pecorari

Anno Accademico 2019-2020

ABSTRACT

During this project we have synthetized different compounds belonging to the class of amino-boranes for the study of bis-aryl-B=N system. We have decided to keep unchanged the aryl components and change only the amine to observe the effect of that on the B=N bond. The used amines are modified carbazoles with functional groups chosen to amplify or disempower the steric and the conjugation effect. We have found that the evaluation of steric barrier was possible studying the gearing aryls rotation around the C-B bonds, while the conjugation barrier is instead given by the energy needed to break the formal double bond B=N and allow the amine rotation. The work started with a proposed synthesis, improved for every reaction, then the products are characterized by NMR, fluorometric spectroscopy, mass spectrometry and X-Ray diffraction on single crystal. The following study on rotational energy barrier was possible theoretically through DFT calculation and experimentally with techniques like Dynamic NMR and EXSY. The fluorometric analysis was done for the study of the solvatochromic propriety of the products.

SOMMARIO

Durante il progetto di tesi sono stati sintetizzati diversi composti appartenenti alla classe degli ammino-borani per lo studio del sistema B=N. Durante la scelta dei prodotti si è deciso di mantenere invariata la componente arilica modificando invece l'ammina per osservare l'effetto che si ha sul legame B=N. Le ammine utilizzate sono carbazoli sostituiti con gruppi funzionali, scelti in modo da amplificare o depotenziare gli effetti sterici o coniugativi del sistema. Abbiamo osservato il comportamento della barriera sterica riguardante la rotazione ad ingranaggio degli arili intorno ai legami C-B, e la barriera coniugativa data dall'energia necessaria a rompere il doppio legame B=N e permettere la rotazione dell'ammina. Il lavoro è iniziato con una proposta di sintesi, migliorata ad ogni reazione, e i prodotti ottenuti sono stati caratterizzati mediante spettroscopia NMR, fluorimetrica, spettrometria di massa, e diffrazione a raggi X sul singolo cristallo. Il successivo studio delle energie delle barriere rotazionali è stato possibile per via teorica mediante calcoli DFT e per via sperimentale con tecniche spettroscopiche come la dinamica NMR e l'EXSY. L'analisi fluorimetrica è stata fatta per osservare le proprietà solvatocromiche dei prodotti.

INDEX

1 Introduction

1.1 Amino-boranes

Amino-boranes are a new class of "smart materials"[1] useful for specialized and practical applications, owing to their low cost of production and their properties. The presence of a B-N bond isosteric and isoelectronic to a classic C=C double bond allow them to respond to external stimuli like heat,[2] pressure,[3] light,[4] electric field,[5] viscosity,[6] pH[7,8] or other molecules,[9] and to go through physical transformations such as isomerization,[10] phase transition[11] or change in intermolecular interaction.[12]

A strategy to obtain these compounds is the addition of a Lewis base (i.e. an amine) to the Lewis acid (i.e. boron) with an empty p_z-orbital and form a π-conjugated scaffold with a small HOMO-LUMO gap. This feature allows these molecules to be higly fluorescent, with huge Stokes-shift effects.[13] The use of bulky structural rigid groups close to the boron further increase the photophysical properties of amino-boranes. Another interesting property of amino-boranes is the highly emission quantum yield in the solid state and in solution, where a raise in the concentration or the addition of a non-solvent leads to aggregation induced emission (AIE). On the contrary, the classical organic luminophore exhibits aggregation-causing quenching (ACQ) and a low emission quantum yield in the solid state. The development of these luminescent molecules can be exploited in numerous applicative fields such as solid-state lasers, organic-light emitting diodes (OLEDs), solid state lighting or fluorescent sensors.[14]

In addition, amino-boranes are studied in medicine for their affinity to proteins in cellular membrane.[15] This type of drug can have a large range of biological activities among which antineoplastic, antiviral, hypolipidemic, anti-inflammatory activities, anti-osteoporotic and dopamine receptor antagonist activities.[16] For these applications it's very important the creation of stable and enantiopure compounds, that can be highly kindred with biological system.

1.2 Bis-arylboryl-amine based molecules

A subclass of amine-boranes of particular interest is bis-arylboryl-amine. Kalluvettukuzhy et al have designed and synthesized a starting compound using phenothiazine, a cyclic non-planar amine with strong electron donor propriety.[14] The resulting compound showed a large variety of luminescent proprieties like triboluminescence, mechanofluorochromism, temperature sensing, aggregation induced emission (AIE) and bright solid-state emission (Scheme 1).

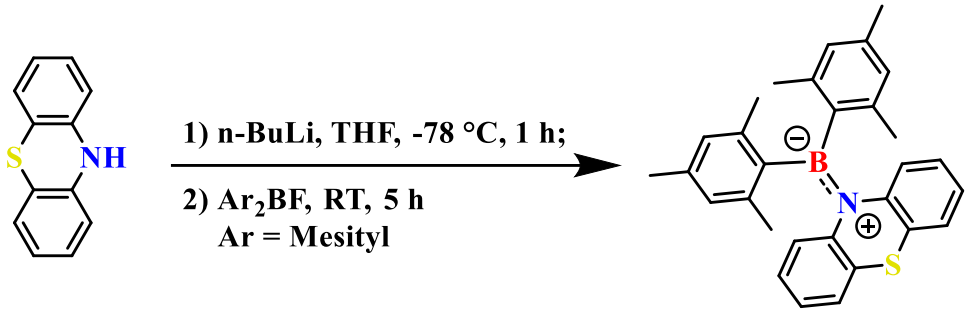

Scheme 1 *Synthetic route for bis-mesityl-boryl- phenothiazine.*

The compound is prepared by the lithiation of phenothiazine with *n*-BuLi at -78 °C, followed by nucleophilic attack of the nitrogen anion to bis-mesityl-boron-fluoride. The final compound is stable under ambient conditions (towards both air and moisture) and it is thermally stable up to +250 °C.

Other example can be found in literature like:

- Bis-arylborylanilines where the nitrogen is not directly bond whit the boron;[17]
- Boron−Nitrogen−Boron Zig zag-edged where we have multiple boron and nitrogen differently bond with each other;[18]
- Substituted Borazaronaphthalene where a cross-coupling reactions fused to an azaborine core via a one-pot nucleophilic tandem reaction.[19]

All these compounds show some kind of luminescent propriety when a suitable donor site is attached at the boron. Arylboranes exhibit intense intramolecular charge transfer (ICT) and a subsequent ligand centered (LC) emission.

1.3 Chirality

The first example of chirality was observed in 1848 by a 25 years old Louis Pasteur. He found that a tartaric acid salt formed two different type of crystals and the solution of this crystals rotate polarized light clockwise or counter clockwise.[20] After this discovery he postulated that the difference in the crystals derived from different shape of the molecules that he calls "right- and left-handed". Later in his life Pasteur observed that a mould ground on a petri dish had changed an inactive solution in ones that can rotate light. Only with this few clue he hypothesized that the solution was composed of the same amount of two contrary optical active compounds nullifying each other. The mould had only metabolised one of the two, changing the ratio of the solution, thus turning on the optical activity. This discovered laid the bases to understand the importance of chiral compounds in biological system, where the two opposite forms called "enantiomers" can, and usually have, different effect. An awful example that makes us realize the importance and the potential of enantiomers is Thalidomide, a sleeping drug/sedative which caused fetus malformation when prescribed to pregnant women for the relief of morning sickness.[21] This experience changed the way we test end develops drug. Thalidomide has a stereogenic center and it exists in two enantiomeric forms: *R* (which produces the therapeutic effect) and *S* (responsible for teratogenic side effects). Both of the form was equally present in the drug marketed like a racemate (a 1:1 blend of the two compounds). It's unclear if a pure solution of the (*R*)-enantiomer would have avoided the side effect. Due to the inversion of the stereogenic center the drug can racemize in vivo (the transformation of one enantiomer into the other which leads to the racemate) and can form the teratogenic compound. Nowadays the drug is now used as antiretroviral for HIV and to cure myeloma.

The word "chirality" defines the properties of a rigid object (or atoms) of being non-superposable on its mirror image. This mean that the object doesn't have any symmetry elements, on contrary if it is superposable on its mirror image it is called "achiral".[22] The term was coined in 1893 from Lord Kelvin during a lecture at the Oxford university. He used the Greek words χειρ (*kheir*) that means hands, because it is a very good and simple example of chirality. The branch of chemistry that study chirality is stereochemistry and the most common source of chirality is a stereogenic center, usually a carbon atom with four different substituents with the same connectivity but different space disposition. In this work we focus our interest in a less common type of chirality, i.e. atropisomerism.

1.4 Atropisomerism

Atropisomers are enantiomers or diastereoisomers that result from the frozen rotation of a single bond (Fig.1).[23] This is due to steric hindrance and/or electronic factors. The racemization rates of atropisomers on a choose temperature can vary depending on solvents and environment.

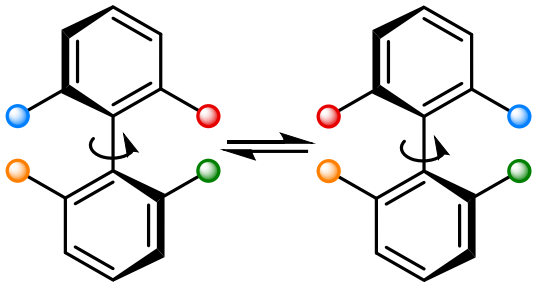

Fig.1 *Example of atropisomers with axial chirality.*

To distinguish between atropisomers and non-atropisomers a 20 kcal/mol rotational energy barrier was established as a suitable threshold to predict atropisomerization with an accuracy. With a new subclass of stereoisomer comes the need for new IUPAC rules for terminology, so we have two possibility:

- R_a and S_a where "a" indicates the presence of axial chirality.
- *M* and *P*.

The first one uses a Newman projection along the chiral axis and rank the groups as "far" and "close" to the observer with CIP (Cahn-Ingold-Prelog) rules. The "close" substituent is considered having higher priority (Scheme 2, top). The second one uses the dihedral angle concept where "B-C" corresponds to the chiral axis and the atoms A and D are assigned thanks to CIP rules to the highest-ranking atom. If the rotation from "A" to "D" turns clockwise the absolute configuration is *P*, and if it goes counter-clockwise is *M* (Scheme 2, bottom).[24]

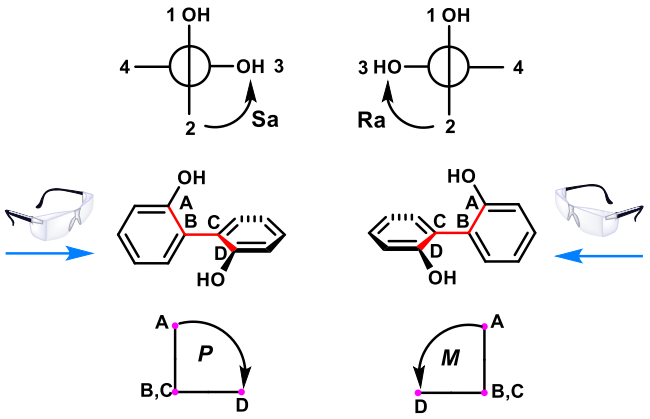

Scheme 2 *R_a/S_a (top) and M/P (bottom) nomenclature of stereogenic axes.*

1.5 Molecular Propellers

When at least two aryl rings are attached to a single atomic center (X) the rotation about the aryl-X bond axis by one of the aryls can cause the motion of all the other rings. Due to the steric hindrance none of the rings moves independently of the other.[25] The structure adopts a propeller-like conformation in which all rings have the same direction of twist and are all out of the plane. This arrangement allows the formation of two structure for two and three-bladed propellers namely right-handed (*P*) and left-handed (*M*). These propeller-shaped molecules usually display a lower isomerization barrier than expected. This is given by a crimped rotation where all the ring moves together.[26]

This configuration is also present when two aryl rings are bonded to the same sp^2-hybridized carbon. Here the rotation of any combination of aryl ring (n-ring flip) reverses the helicity of the conformational enantiomers.[27] In this case we can have isomerization trough a disrotatory (n=1) or a conrotatory (n=2) motion of the two rings of the propeller passing through a plane orthogonal to that of the C=X and his binders. The transition state changes dependently on the sense of rotation, in this case we can have three possible routes (Scheme 3).

When:

- n=0 the two rings cross simultaneously through a plane coincident with that of C=X in a conrotatory motion, usually this transition state is too hindered to occur;
- n=1 one ring is orthogonal and the other is parallel to the C=X plane, the same transition state take place when the two rings revers.
- n=2 the two rings are orthogonal to the C=X plane at the same time.

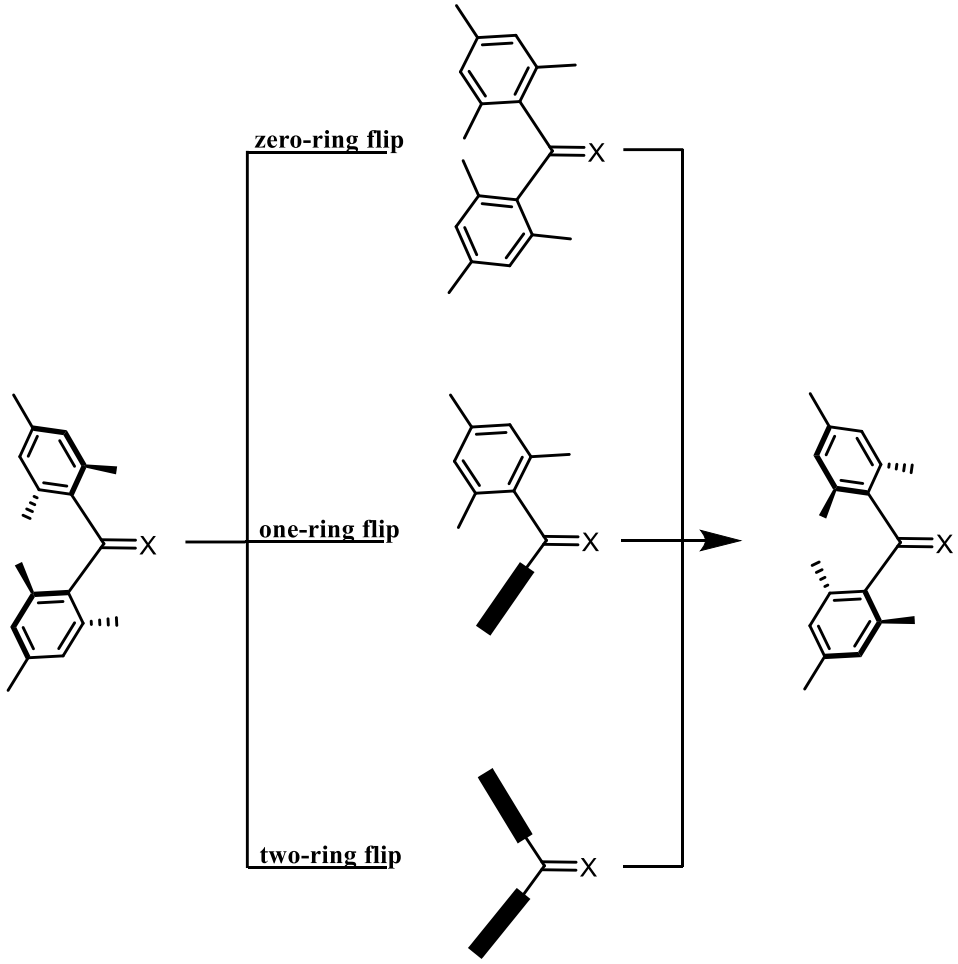

Scheme 3 *Representation of the transition state for zero-one-two-ring flip pathway that interconvert the enantiomeric propeller conformations.*

Considering that, the enantiomerization is a thermal phenomenon where a variation of the temperature results in a variation of the rotation speed that leads to racemization. Lowering enough the temperature freezes the molecules in a "two-blade propeller" conformation that can be studied. The spectroscopic technique that can study this phenomenon at different temperatures is called Dynamic NMR (DNMR). With that, we can follow the change of ^{1}H-NMR anisochronous signals. When the conformations are locked the symmetrical twist of the two mesityl rings makes the *ortho*/*meta* diastereotopic positions. This lead to two ^{1}H-NMR signals for *ortho*-methyl and two for *meta*-aryl protons. On raising the temperature, the rotation of the aryls is faster, with exchange of the protons in the space. This brings to a fast enantiomerization where only one signal for the ^{1}H-NMR *ortho*-methyls and one for *meta*-aryl protons are detected. The simulation of these spectra gives us the rotational energy barrier.

1.6 Dynamic NMR and EXSY

Reversible processes that can change the NMR spectrum (like chemical shift or coupling constant), can be observed and studied at various temperature to extrapolate the energy of these processes.[24] This technique is called variable-temperature NMR (dynamic NMR or DNMR) spectroscopy and allows to observe racemization energies. With this technique it is possible to study the rotational barrier of aryl atropisomers or propellers. When a structure lacks diasterotopic signal we can add a chiral probe (like an isopropyl group) to the molecular scaffold. Once the experimental acquisition at different temperature is done we can proceed to the simulation of the line shape and the determination of the rate constant for the process. This constant can be converted to the racemization energy ($\Delta G^{\neq}$) through the Eyring equation. DNMR is a reliable technic that can observe racemization energy from ~4.3 to ~22.2 Kcal/mol (Fig.2).

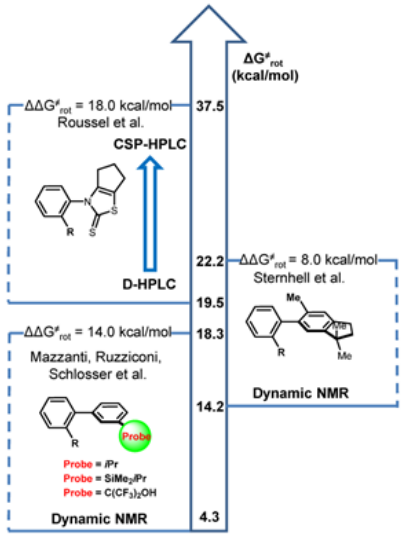

Fig.2 *Different technics used to evaluate steric factors.*

In the range between ~19.5 to ~22.2 kcal/mol, therefore in the limits from DNMR and Dynamic HPLC (DHPLC) we can use another experiment called EXchange SpectroscopY (EXSY). This technic uses a lower range of temperatures than DNMR and consists of a Nuclear Overhauser Effect SpectroscopY (NOESY) but with a smaller mixing time, so the nearest protons do not develop NOE. EXSY requires the irradiation of a single peak that interchange with another in response to an exchange of the two in space. The mixing time is proportional to the rate of exchange of the signal. The activation energy $\Delta G^{\neq}$ of the exchange (racemization barrier) can be interpolated from the integration of the peaks by assuming a first-order reversible kinetic.

1.7 Density functional theory (DFT)

Introduced in the late 60's Density Functional Theory (DFT) is a computational methodology used to predict the conformation of big molecules, bulk materials, atomization energies, ionization energies, electric and magnetic properties, reaction paths and a lot more. The DFT model is based on the theory that all molecular electron propriety is a result of the electron probability density ρ(x,y,z). Particularly, it is based on the determination of electron density and wave function in a many-electron system. With DFT we can determinate the property of many-electron systems, using functionals (function of function), which in this case are the spatially dependent electron density.[29] B3LYP is the most used hybrid functional that stand for "Becke, 3-parameter, Lee–Yang–Parr". It's called hybrid because it uses a weighted average of interaction from Hartree–Fock and DFT theory. The basis set used in our computational studies is 6-311G(d,p) where 6 is the number of function that describe the core electron and 311 are three contraction that describe the valence electron, the first with three function and the other two with one each.

DFT calculation has been successfully used for modelling Ground State (GS) and Transition State (TS) that can be univocally identifies trough vibrational state.[28] TS display one negative frequency meanwhile GS display all positive frequencies. The negative TS frequency has large value for high-energy processes like chemical reaction. When instead the transition state involves internal dynamic processes, the vibrational frequencies are usually smaller. The transition state energy and the molecular structure are very important for stereodynamic analysis. Because the TS is a peak of energy that link two ground state it well represents the energy barrier that block the interconversion between atropisomers. The results found with DFT calculation are easily checked thanks to experimental analysis like X-ray in the case of structure geometry and kinetic studies in case of relative energy.

1.8 Fluorescence

Luminescence is a radiative decay that occurs from electronically excited states, from substances called fluorophores.[30] This phenomenon is divided into fluorescence and phosphorescence depending on the nature of the excited state. To give rise to a radiative emission at room temperature the compounds usually follow certain geometric, structural and electronic requirements. One of them is structural rigidity, like in aryl ligands π-conjugated, that allows to minimize vibrational relaxations that leads to a non-radiative decay. Other factors are the degree of distortion together with the entity of the energetic separation ("energy gap law") between the excited and the fundamental state.

First, we have an absorption and the promotion of an electron from a fundamental state S0 to a higher vibrational level S1. From here the fluorophore can exhibit fluorescence and emits from S1 → S0. Otherwise, it can undergo trough a spin conversion to the first triplet state T1 and emit from there, in this case we have phosphorescence (Fig.3).

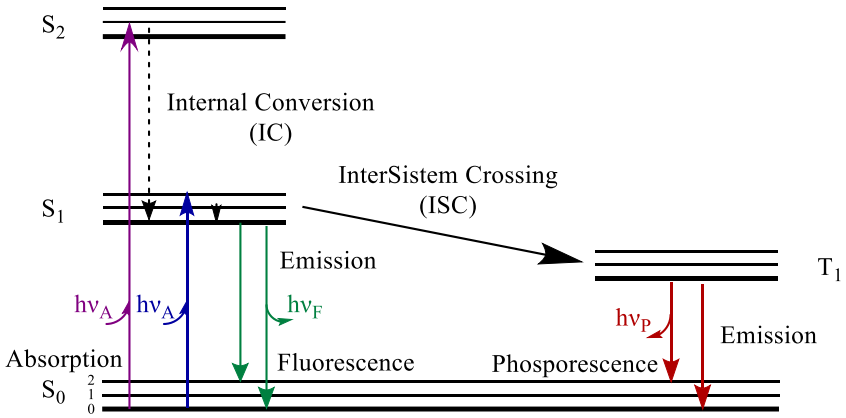

Fig.3 *Jablonski diagram.*

The emission spectrum is a plot of the fluorescence intensity versus wavelength (nanometers) or wavenumber (cm^{-1}) and is typically a mirror image of the absorption spectrum of the S0 → S1 transition (Fig.4). This is due to the unwilling of electronic excitement to altering nuclear geometry. Another property of fluorescence is that the emission spectrum is generally observed irrespective of the excitation wavelength.

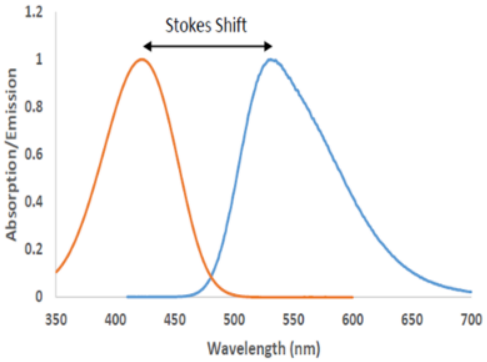

Fig.4 *Example of an emission/absorption spectrum.*

The Jablonski diagram (Fig.4) reveals that the energy of the emission is usually less than that of absorption, leading to the so called "Stokes shift". This Stokes shift is usually caused by the decay to the lowest vibrational level of S1 (internal conversion) (Fig.5). In addition to these effects, we can have Stokes shifts due to solvent effects, excited-state reactions, complex formation, and/or energy transfer.

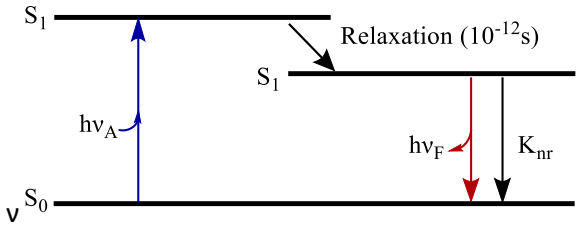

Fig.5 *Simplified Jablonski diagram to illustrate quantum yield and lifetime for fluorescence.*

Other important characteristics for a fluorophore are quantum yield and fluorescence lifetime. The quantum yield is the ratio of emitted to the absorbed photons and it ranges from 0 to 1. The lifetime, instead, is the time that the fluorophore spends in the excited state and it determines the time it has to interact with the environment, and hence the information available from its emission.

As said before, boron compounds show luminescent propriety especially when we increase the delocalization on it. High emission shifts from polar to non-polar solvent allows us to have a large variety of colors at different emission wavelengths (called solvatochromic effect) spanning from green to the Near Infra-Red (NIR). The outcome is a diversity of molecules that exhibiting interesting and tunable spectroscopic, electrochemical and chemical properties.[31]

2 Aim of the Thesis

The aim of this thesis is the synthesis of compounds that allow the study of the rotational energy barriers of B=N and B-C, and the use of modified carbazoles that can tune the fluorescence spectra. We started with the previously cited bis-arylboryl-phenothiazine synthesis and developed an alternative route that uses bis-mesityl-boron-fluoride prepared *in situ*. Once all the synthetic steps were optimized, we tried different cyclic secondary amines (**8**, **9**, **10**) and decided to use carbazole (**10**) as a suitable primary scaffold thanks to its stiffness and ease of modification. We have divided the products in two main class of carbazoles (Scheme 4). The first class exhibit a substituted carbazole (**10a-d**) and is used to determine the B=N rotational energy barrier in the presence of a small steric hindrance in the ground state geometry. The second class of compound bear a benzo-carbazole (**11a-d**), that implies higher steric hindrance in the ground state geometries. The different geometries have a strong influence on the B-C and B-N rotational barriers.

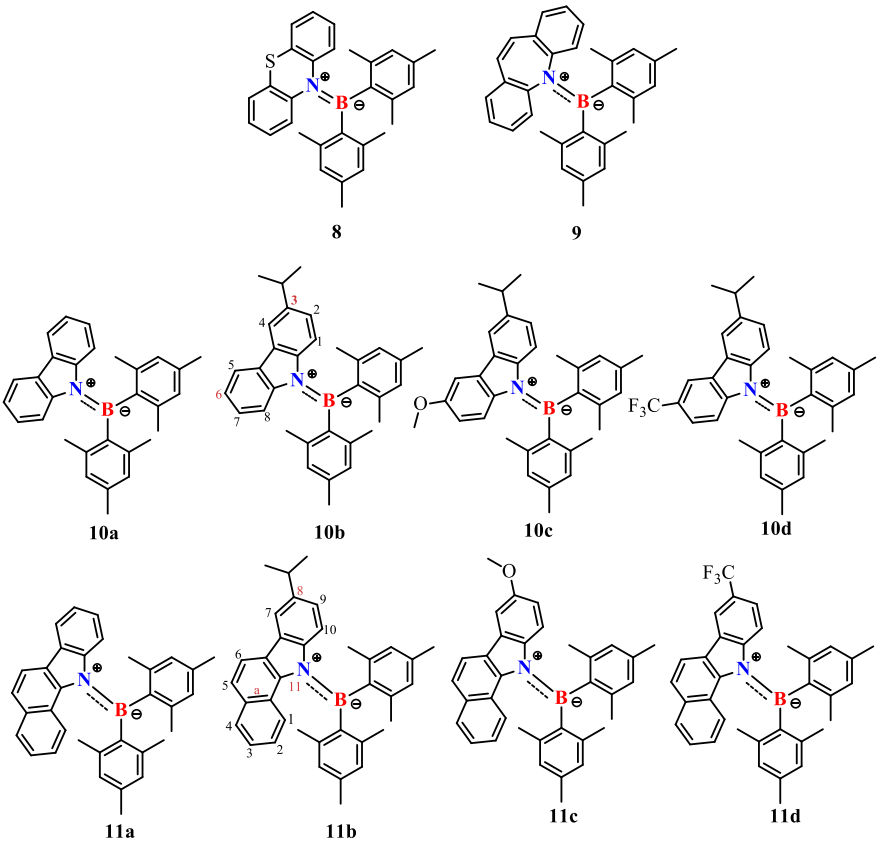

Scheme 4 *Products divided into classes given by different amines.*

The carbazole and benzocarbazole scaffolds were then substituted respectively in the 3 and 8 positions with isopropyl, methoxy (OMe) and trifluoromethyl (CF_3) groups, in order to modify the electronic features of the nitrogen, and to observe how the conjugation of B-N bond changes from an electron-attractor to an electron-donator group.

All the compounds were prepared using the same reaction reported above (see Experimental section for details), and each compound was characterized in the following steps:

1. Structure determination by means of NMR, Mass spectroscopy and single crystal X-Ray analysis;
2. DNMR and/or EXSY studies for the experimental determination of the B-N and B-C rotational energy barriers;
3. Comparison of the experimental and the computational DFT values, previously calculated and based on a propeller transitions state.
4. Fluorescence characterization of the solvatochromic properties (Stokes shifts), quantum yield, lifetime of the exited state and solid-state emission.

Preliminary conformational studies have been done with DFT calculations to better understand the dynamics of the rotations around the C-B and B=N bonds.

3 Results and Discussion

3.1 Conformational Studies and DFT Calculations

To optimize the ground state geometries (GS) and their transition states (TS) with good accuracy we used DFT calculations. The chosen functional was B3LYP combined with a 6-311G(d,p) basis set. For the synthesized compounds we identified the ground states and all the possible rotational transition states. The first two compounds (**8** and **9**) that we have synthetized and studied displayed a non-planar cyclic secondary amine. This adds a transition state that involve the inversion of the butterfly-like structure of the amine that we name amine-flip. To avoid this issue, in Scheme 6 are shown the stereochemical pathway of carbazole **10**, a planar cyclic secondary amine. The possible transition states for this kind of propeller-like molecules are six (Scheme 6). In order to identify all of them, we have positioned the three rings alternately parallel or perpendicular to the boron-binders plane until we have covered all the possible conformations. For example, a "**2ring-flip** carb-mes" identifies a transition state where there is

one parallel (one aryl) and **two perpendicular** groups (the carbazole and the other aryl) to the plane formed by boron and its binders.

The calculated ground states have been confirmed thanks to the X-ray analysis that allows to define unequivocally the molecular structures.

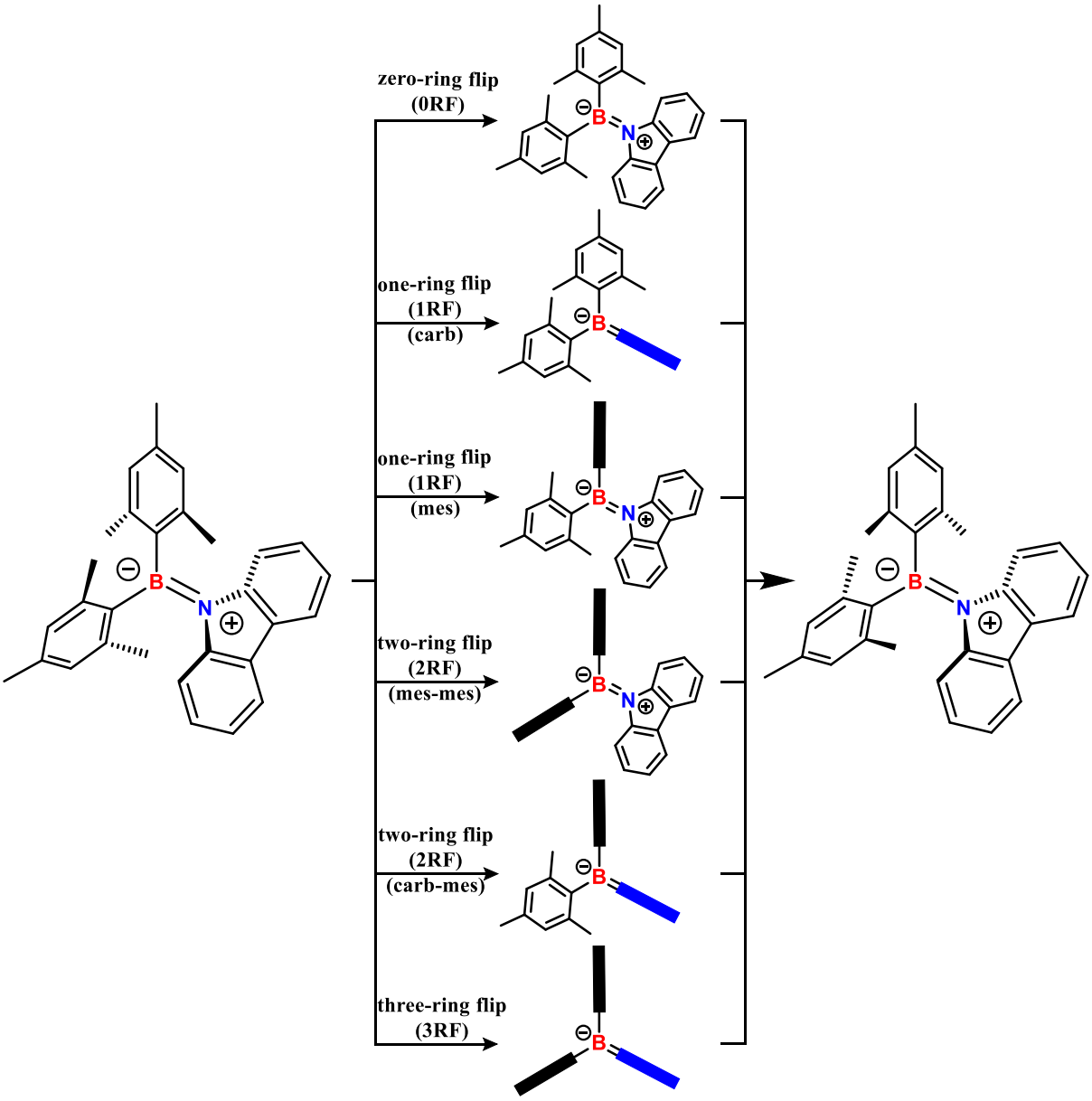

Scheme 5 *All the possible TS of enantiomerization for* ***10a****.*

The zero-ring flip is too sterically hindered to exist, due to the presence of all the three rings sharing the same plane. The two one-ring flips (**1RF**) put alternatively the carbazole or the mesityl perpendicular and the other groups planar to the boron-binders plane. In the two-ring

flips (**2RF**) we have two perpendicular groups and the last planar. Finally, three-ring flip (**3RF**) shows all groups perpendicular to the boron-binders plane.

In Table 1 are shown all GSs and TSs geometries and their relative energies in kcal/mol. The values of $\Delta G^{\neq}$ calculated for **1RF**s (62.29-45.58 kcal/mol) and the **3RF** (50.1 kcal/mol) are too high to be accessible. This means that other internal motion of the molecule at lower energy are allowed well before. So, we focus our attention on **2RF**s that in this case are the lower energy ones.

The first TS, **2RF-(mes-mes)**, has lower energy (11.15 kcal/mol) and could easily be identifies experimentally with DNMR because of the exchange of the two *ortho* methyl and *meta*-hydrogens and define the B-C rotational energy barrier. The second TS **2RF-(carb-mes)** at higher energy (22.42 kcal/mol) identify the B=N rotational barrier provided by the carbazole rotation. In this case, the barrier cannot be identified experimentally for the structure symmetry.

Table 1. DFT calculation of ground and transition state for **10a**.

State	2D structure	3D structure	Total Energy (a.u.)	Rel. E. Calculated (kcal/mol)
GS	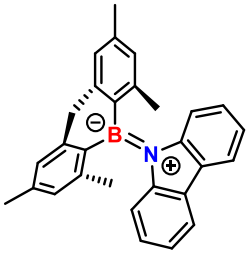	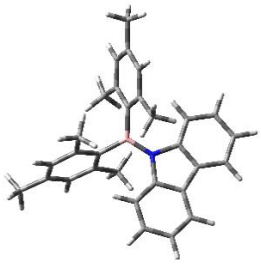	-1241.257571	0.00
1RF-TS (one-ring-flip) Carb	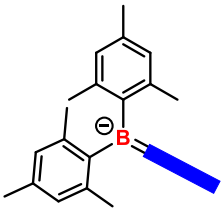	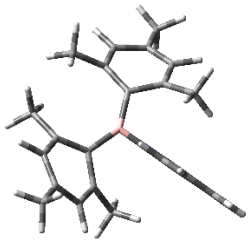	-1241.158301	62.29
1RF-TS (one-ring-flip) Mes	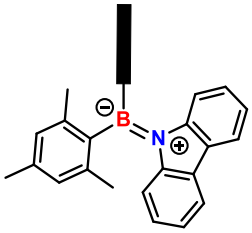	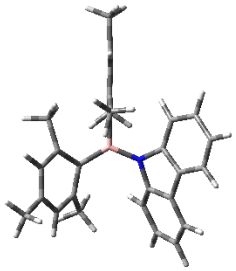	-1241.184930	45.58
2RF-TS (two-ring-flip) mes-mes	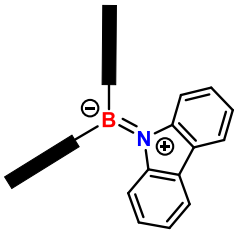	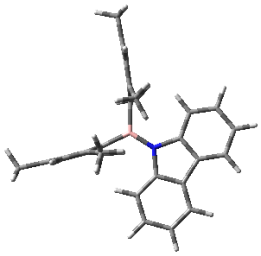	-1241.239799	**11.15**
2RF-TS (two-ring-flip) mes-carb	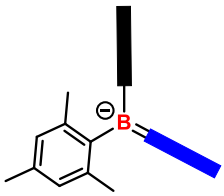	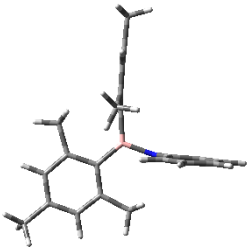	-1241.221838	**22.42**
3RF-TS (three-ring-flip)	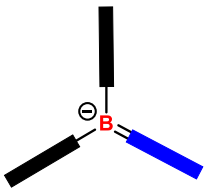	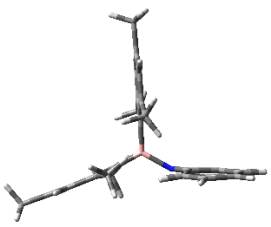	-1241.177714	50.11

For the compounds **8** and **9**, we must introduce an additional degree of freedom due to the cyclic amine-flip.

In table 2, we show the transition state for the phenothiazine and iminostylbene flip and the calculated DFT results.

The calculated energies of this kind of flip are in the range of the B=N or the B-C rotation energies. This overlap of internal movement makes the single effect hard to study experimentally, therefore we keep our attention only to the more planar carbazoles.

Table 2. GSs and TSs states of compounds **8** and **9**.

State	2D structure	3D structure	Total Energy (a.u.)	Rel. E. Calculated (kcal/mol)
GS-Phen	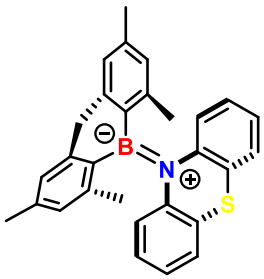	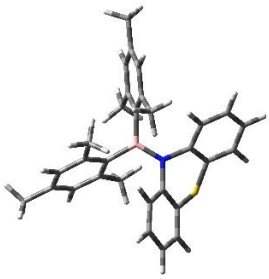	-1639.442855	0.0
TS-Phen-flip	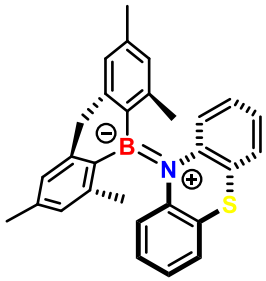	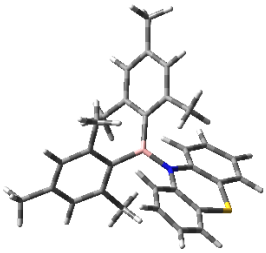	-1639.426312	**10.4**
GS-imino	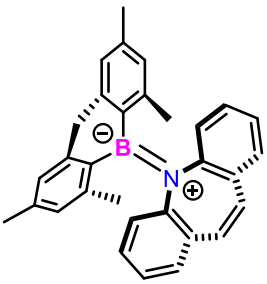	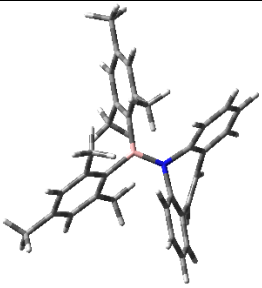	-1318.653243	0.0
TS-imino-flip	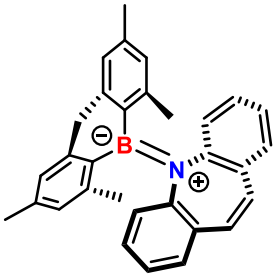	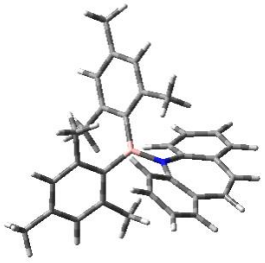	-1318.621613	**19.8**

3.1.1 DFT Calculations for bis-mesityl-11-benzo-carbazole-borane 11a

In this class of compounds, we use a bulkier carbazole as the benzocarbazole **11a**. The steric hindrance places benzocarbazole outside of the plane, conferring higher helicity in its ground state compared to carbazole **10**. Instead the same approach was done to calculate the TSs. The variations are very small and do not change neither the number of possible TS neither the attribution of the movements to the chosen **2RF**. Even if the effect of these modifications are not marked on the geometry of the transition states, they can be easily seen in the TS energies. The modification in the Ground State lead to a higher energy for B-C rotation (**2RF-TS mes-mes**, 16.5 kcal/mol, Tab.3) and at a lower energy for B=N rotation (**2RF-TS mes-carb**, 18.8 kcal/mol, Tab.3).

Table 3. DFT calculations of GS and TSs state of compound **11a**

State	2D structure	3D structure	Total Energy (a.u.)	Rel. E. Calculated (kcal/mol)
GS	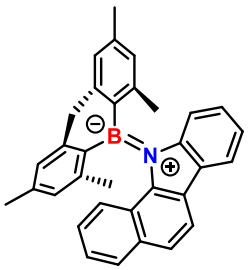	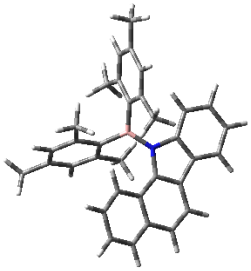	-1394.921874	0.0
1RF-TS (one-ring-flip) carb	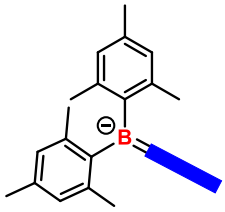	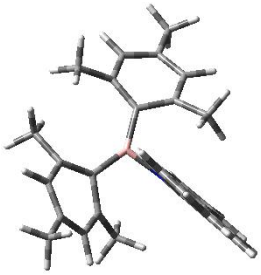	-1394.831329	56.8
1RF-TS (one-ring-flip) mes	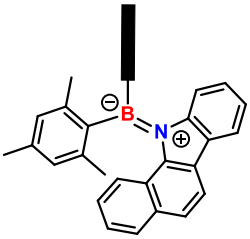	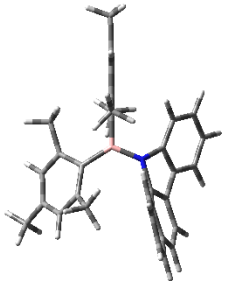	-1394.853451	42.9
2RF-TS (two-ring-flip) mes-mes	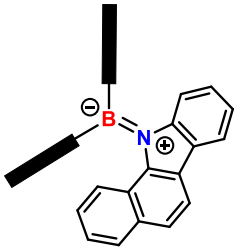	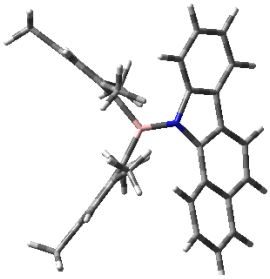	-1394.895614	**16.5**
2RF-TS (two-ring-flip) mes-carb	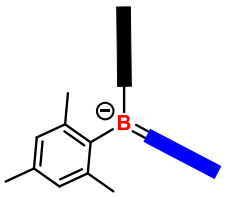	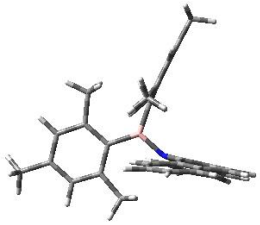	-1394.891869	**18.8**
3RF-TS (three-ring-flip)	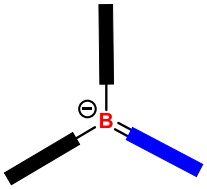	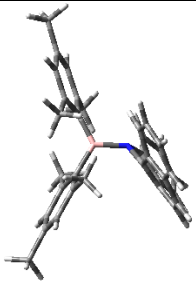	-1394.851153	44.4

3.1.2 DFT Calculations for modified-carbazole-borane

We have successfully found all the rotational energy barrier due to B-C and B=N rotation for each synthetized compound. **2RS-TS mes-mes** can be attributed at the B-C rotational energy barrier for every carbazole. Instead, the B=N rotational energy barrier continues to be ascribed at **2RS-TS mes-carb**.

All the calculated data for the two rotational barriers of ever compounds of Scheme 4 are shown in Tab.4.

Table 4. *Calculated rotational energy barrier $\Delta G^{\neq}$ (kcal/mol).*

Prodotto	**$\Delta G^{\neq}_{cal}$ rotation (kcal/mol)**		
	N=B	**C-B**	**Amine-Flip**
8	19.4	5.4	10.4
9	24.0	4.2	19.8
10a	22.4	11.1	not present
10b	22.6	11.1	
10c	23.2	10.8	
10d	21.9	11.2	
11a	18.8	16,5	
11b	19.0	1.4	
11c	19.4	16.1	
11d	18.4	16.9	

3.2 Synthesis

To produce the modified carbazoles we have chosen a Fischer–Borsche one-pot reaction (Scheme 6 and 7), a metal free synthesis that gives us a wide range of possible modification.[32]

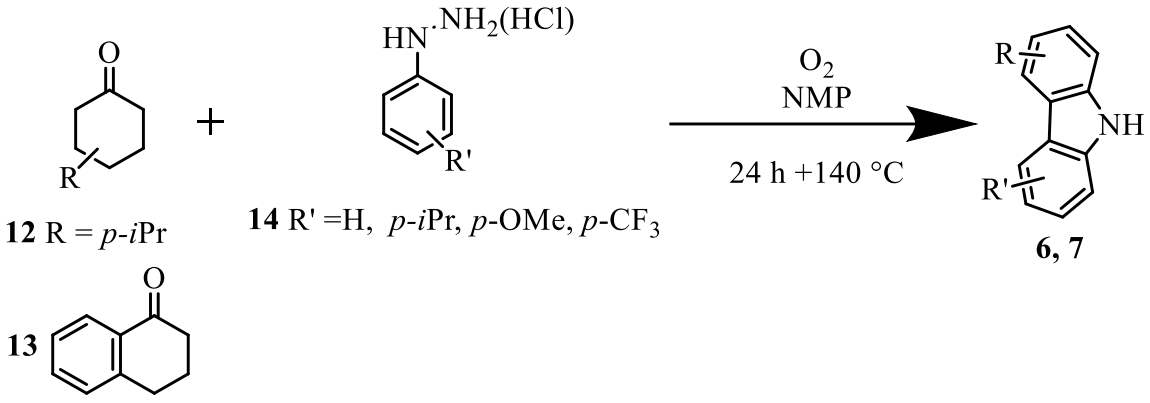

Scheme 6 *Generalized synthesis for modified carbazole.*

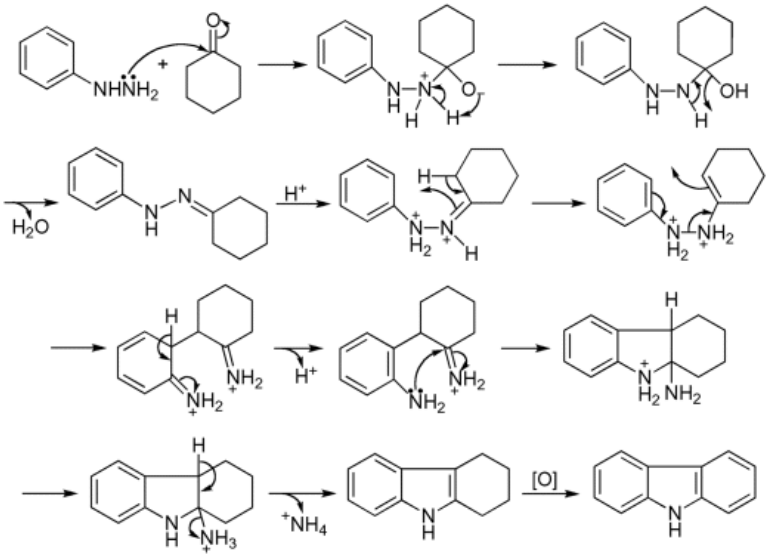

Scheme 7 *Fischer–Borsche reaction mechanism.*

The reaction starts with the condensation under acidic condition of phenylhydrazine and cyclohexanone. Then we have the formation of an indole intermediate by cyclization and a subsequent aromatization via oxidation to obtain the wanted carbazole.

Seven different carbazoles was synthetized with this method, three of which are not present in the literature (Scheme 9).

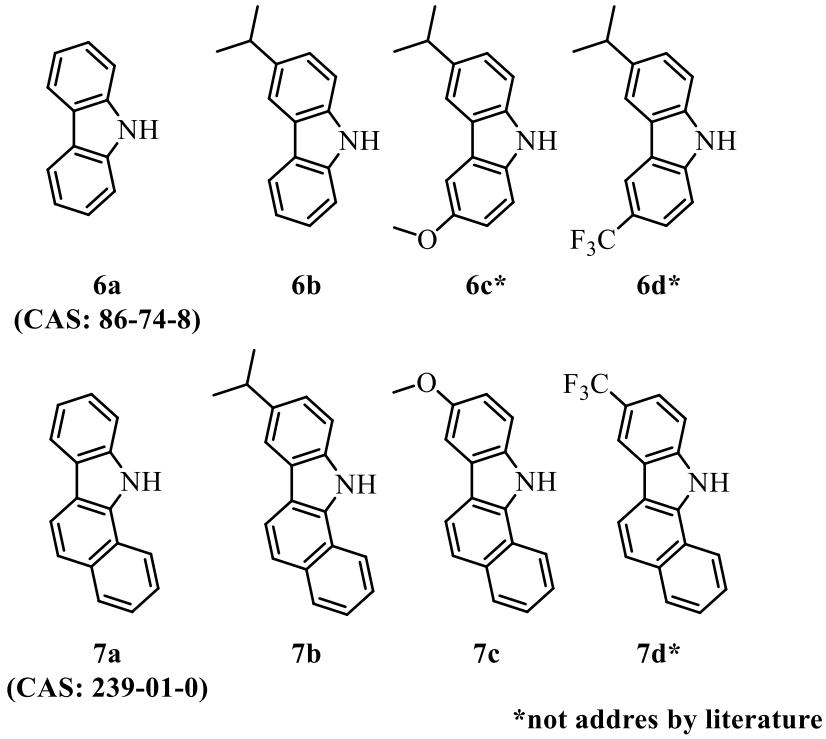

Scheme 8 *Synthetize carbazole.*

The fluctuations of the yields can be attributed at the amount O_2 atmosphere that we provide with an impermeable-gas balloon. The oxygen is needed for the aromatization so his absence or is inhomogeneous distribution lead to low yields. This assumption is corroborated from the presence of the non-aromatized by-products in the reaction mixture.

The synthesis of all the bis-mesityl-amino-boranes start with the preparation of the bis-mesityl-boryl-fluoride (Ar_2BF). Then the solution is added dropwise to a solution of a deprotonated amine, obtained by reacting carbazole with KHMDS. (Scheme 9-10).

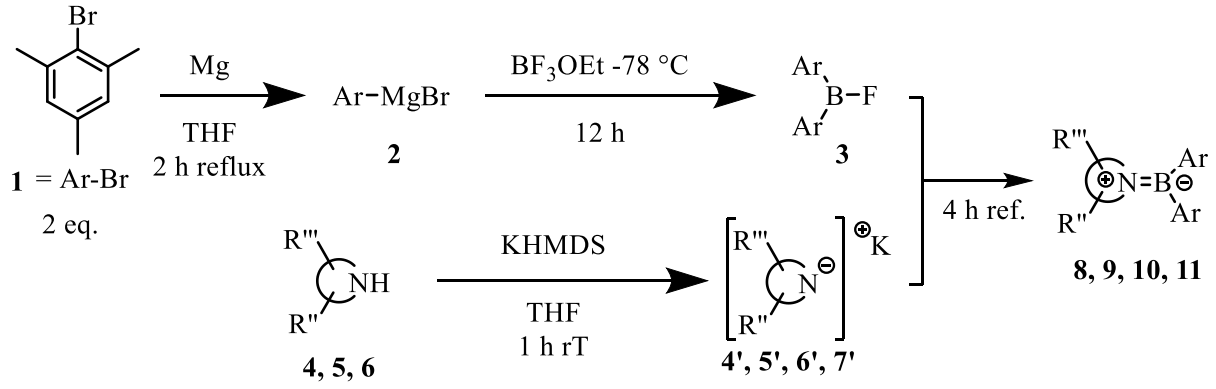

Scheme 9 *Generalized synthesis of bis-mesityl-amino-boranes.*

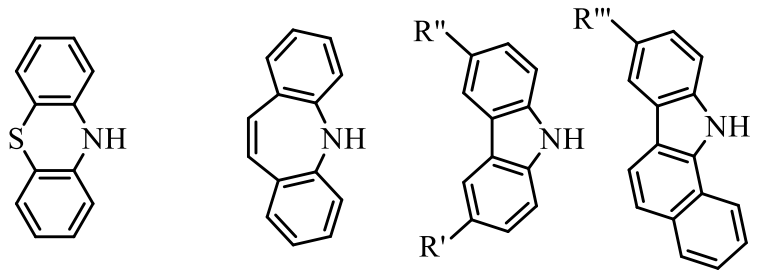

4 **5** **6** **7**

(CAS: 92-84-2) **(CAS: 256-96-2)**

Scheme 10 *Aromatic amines used in the reaction.*

We started with a Grignard reagent made from 2-bromomesitylene and magnesium, catalysed by iodine. The only solvent suitable for this reaction is dry THF, other solvents showed very low yields. After the addition of BF_3*OEt and the formation of Ar_2BF, before proceeding with the reaction, a sample was carried out and analyzed by ^{19}F-NMR spectroscopy. We observed that both Ar_2BF (15.9 ppm) and $ArBF_2$ (152.1 ppm) was present at this point with a 2:1 stoichiometry. This is not a concern because we observed that only Ar_2BF react. Meanwhile in another pot we prepared the anion of the amine by acid-base reaction between the aromatic amine and KHMDS. The subsequent addition of Ar_2BF solution in the anion pot turned out to be complex due to its incomplete solubility. This was partially resolved by the use of a large needle. After the dropwise addition of Ar_2BF we quenched the reaction with DCM. Finally, we proceed to purification with chromatography separation on silica gel and a gradient eluent mixture of Hexane/DCM (9:1→7:3). For a further purification of the products, we used crystallization with various mixtures like acetonitrile/DCM or hexane/DCM. We preferred this technique for its low cost, low effort, high purification rate and the need of a single crystal for diffraction X-ray characterization.

The final compounds are highly stable to air, and they are stable up to 120°C in DMSO.

3.3 Experimental conformational studies

Once we obtain the data on rotational energy barriers with computational methods, we analyse them with experimental kinetics studies that can double check the data. It's noteworthy that the DFT calculation for transition states are usually ≈2 kcal/mol smaller the experimental one.

The best suitable techniques that we can use with the rotational energy barriers found in computational calculations are DNMR and EXSY. The first one uses the simulation of ^{1}H spectra taken at various temperature to determine the experimental $\Delta G^{\neq}$. $^{\neq}$. For doing that we use a diastereotopic signal that differs when the rotation is blocked and become enantiotopic when the rotation is free. In our case we rely on *meta*-mesityl-proton or *orto*-mesityl-methyl ^{1}H signals for the simulation of the B-C rotational energy barrier.

The program used for this simulation is DNMR-6 QCPE n°633 (Dynamic Nuclear magnetic Resonance - Quantum Chemistry Program Exchange). This program simulates a theoretical NMR spectrum at various kinetic constant k (s^{-1}), and then we compare them with the experimental ones in order to obtain the value of the $\Delta\mathbf{G}^{\neq}$ at different temperatures.

The second one, EXSY, requires the saturation of a single peak, in a ^{1}H NMR spectra, that interchanges with another in response to the chemical exchange due to rotation. In our case the groups suitable for the purpose are the two *para*-mesityl-methyl. When permitted from the upper limit of the technics (~22.2 Kcal/mol) this exchange shows us the B=N rotational energy barrier.

The ^{1}H NMR signal of one *para*-methyl is irradiated at three temperatures for six different mixing times. At a defined temperature the rotational rate is fixed, so with an increase of the mixing time the molecule has more time to rotate, and the signal of the exchanged proton raises. The results are taken at different temperature in order to obtain more accuracy in the calculation of the $\Delta G^{\neq}$, this is obtained from the average of the $\Delta G^{\neq}$ calculated at every temperature.

The EXSY experiment is considered a reaction with a kinetic of the first order reversible to equilibrium like the following one:

$$\ln(C_{irr} - C_{irr\,eq}) = -2k \cdot t_{mix} + \ln\,(C_{irr\,0} - C_{irr\,eq})$$

Where:

- C_{irr} is the percentage of the irradiated signal;
- $C_{irr\,eq}$ corresponds to the equilibrium (which in our case is 0.5);
- C_{irr0} is the percentage at t_{mix}=0 (which is 1);
- t is the mixing time;
- k is the value of the kinetic constant;

At 0.00 ms of mixing time we have 100% of the irradiated proton, while at infinite mixing time the equilibrium is reached, and we have 50% of irradiated proton and 50% of the exchanged proton.

3.3.1 Dynamic NMR of carbazole

At +26 °C the ^{1}H-specrum of **10b** show really board and narrow signals. The four *orto*-mesityl-methyl signals that we have chosen for the study are shown like two close singlets, each one integrates 6 protons. This means that the B-C rotation is unlocked, and this results in an exchange of CH_3 in space that lead at only one methyl NMR signal for each mesityl. When we decreased the temperature, the B-C rotation becomes slow and both the *orto*-methyl NMR signal begin to widen, until they reach coalescence at -42 °C.

Underneath this temperature four broad signals divided in two groups are visible, and eventually four definite signals are visible at -99 °C. This means, that the B-C rotation is locked, and the two enantiomeric conformations are stable.

Thanks to the simulation of this experimental spectrum we have found a $\Delta G^{\neq}$ for the B-C rotational energy of 10.9±0.15 kcal/mol (Fig.6), fully consistent with the calculated one (11.1 kcal/mol). This result is an average of all the $\Delta G^{\neq}$ values derived from the rate constants obtained from the line shape simulations at each temperature.

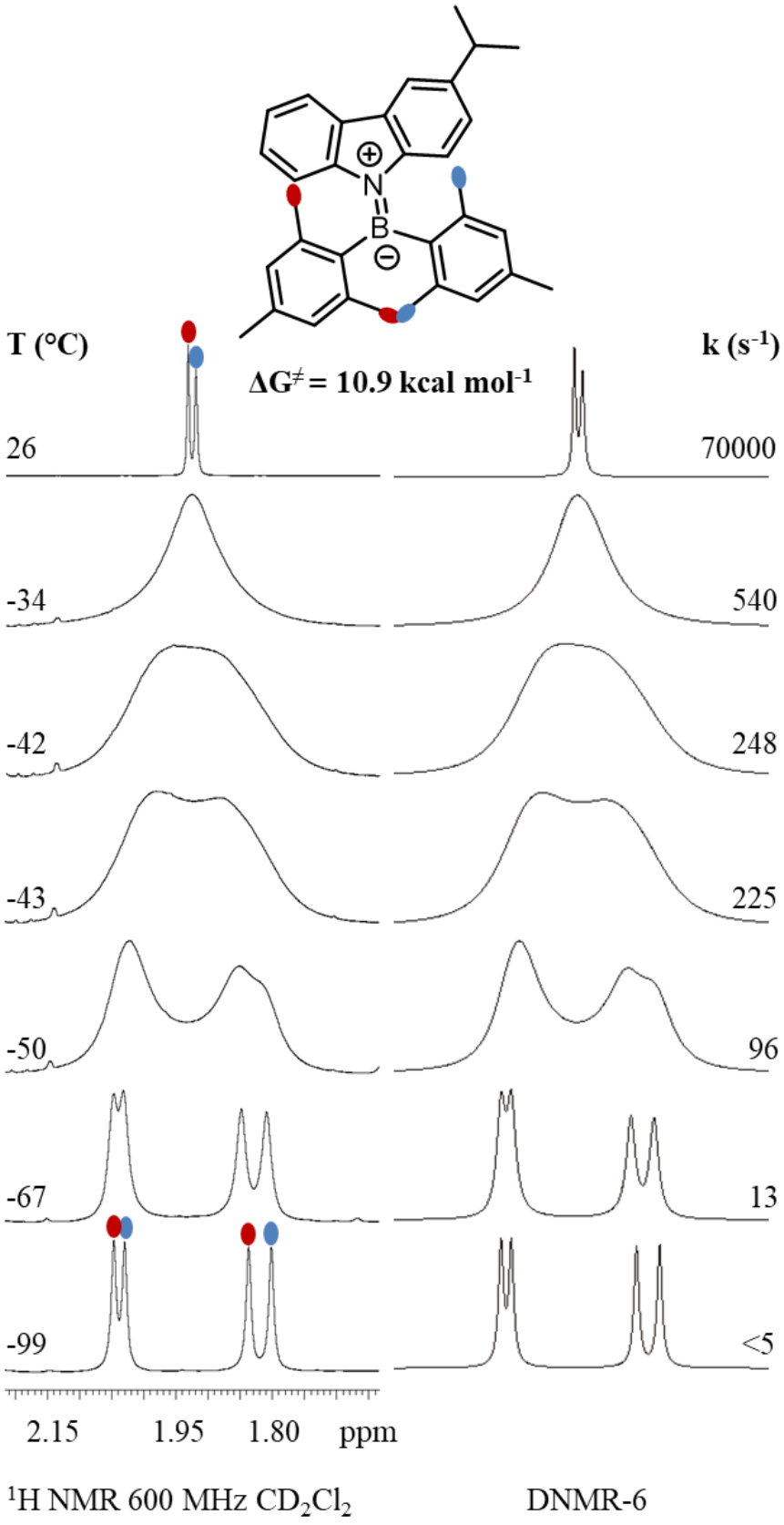

Fig.6 *DNMR of* ***10b****. left experimental spectra at different temperatures; right simulated spectra with different kinetic constants.*

For simple carbazole we are only able to detect the B-C rotational energy barrier with DNMR. The energy needed to break the conjugation and permit the B=N rotation is too high for this class of compounds and exceed the limit of the technique (~22.2 Kcal/mol). Indeed, the presence of two signals for the ortho-methyls at high temperature implies that the two mesityl rings are not exchanged by the B-N 180° rotation.

3.3.2 Dynamic NMR and 1D-EXSY of benzo-carbazole

At +25 °C the ^{1}H-NMR spectrum of **11b** show board and narrow signals except for two *meta*-mesityl-proton singlets that are broaden, this mean that the B-C rotation is almost unlocked. If we decrease the temperature the rotation stops and at -12 °C the singlet returns narrow. Instead, if we increase the temperature, we accelerate the rotational speed and reach coalescence at +50 C°. Over this temperature only one widen signals is present that narrow at +103 °C. This means that the B-C rotation is completely free to rotate.

From the simulation we found a $\Delta G^{\neq}$ for the B-C rotational energy of 16.2±0.15 kcal/mol (Fig.7) fully consistent with the calculated one (16.4 kcal/mol).

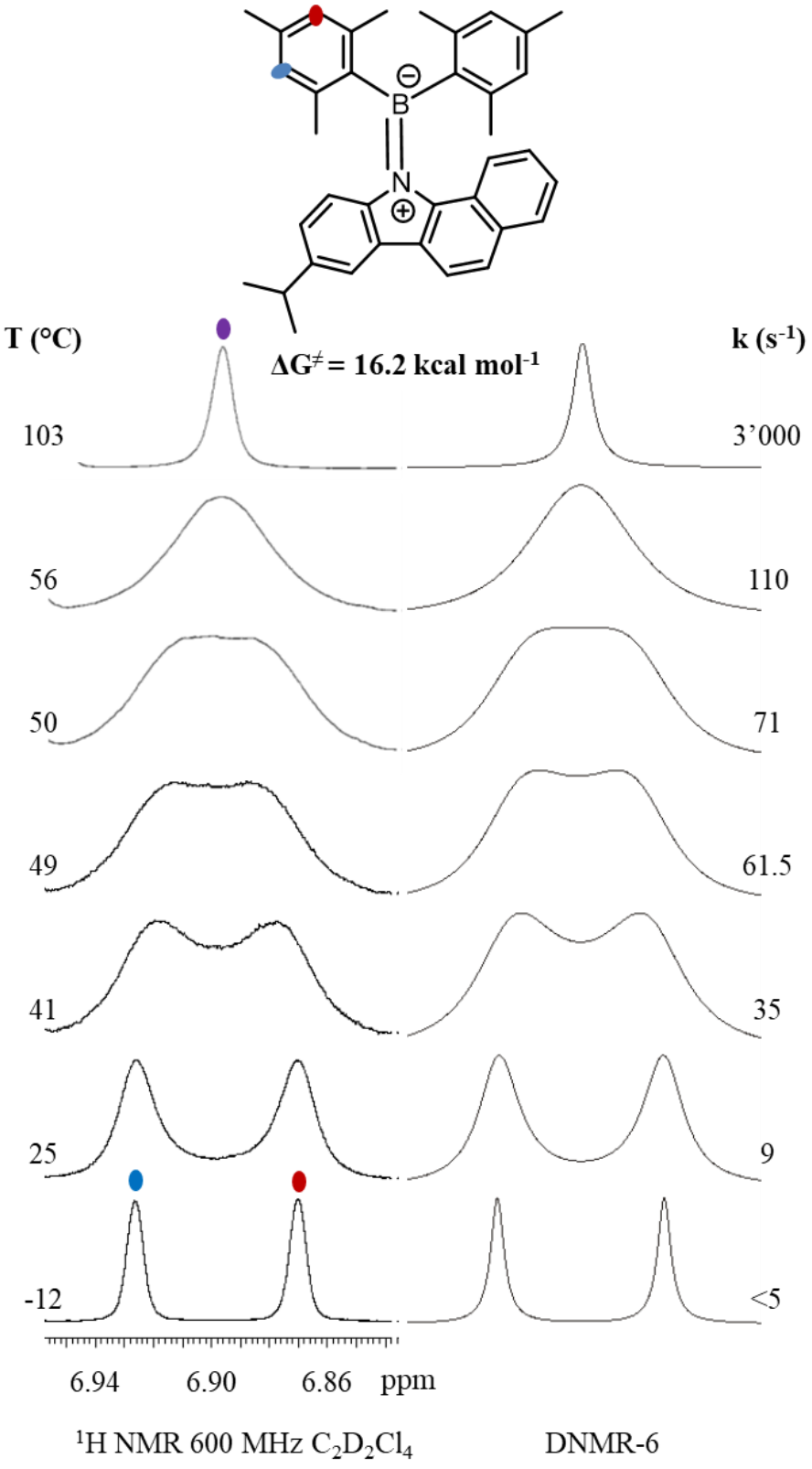

Fig.7 *DNMR of* ***11b****. left experimental spectra at different temperatures; right simulated spectra with different kinetic constants.*

We can study the B=N rotational energy barrier for benzocarbazole for its asymmetry that change the magnetic environment around the two mesityl. The exchange of these are detected on *para*-methyl NMR signals. We use the EXSY NMR experiment to measure the higher energy barrier of B=N because the para-methyl NMR signals are still narrow at the high temperature limit of NMR. We can be sure that those signals monitor the inversion of the benzocarbazole because the B-C rotation don't change the topicity of *para*-mesityl-methyl groups.

We irradiate one of the *para*-mesityl-methyl ^{1}H-signal with six different mixing times (20, 40, 60, 80, 100, 120 ms). The rate of increase in relationship to the mixing time give us the kinetic constant (K) of the process. This procedure is repeated at three different temperature and we obtain different value of k (0.93 s^{-1}, at +93 °C, 1.29 s^{-1} at +98 °C and 1.84 s^{-1} at +103 °C), this result is averaged in order to minimise the error. The K are obtained assuming a kinetic of the first order for each experimental analysis. Then we use the Eyring equation to convert the K to $\Delta G^{\neq}$, and we obtained a value of 21.7 ± 0.2 kcal/mol (Fig.8) comparable with the calculated one (19.0 kcal/mol).

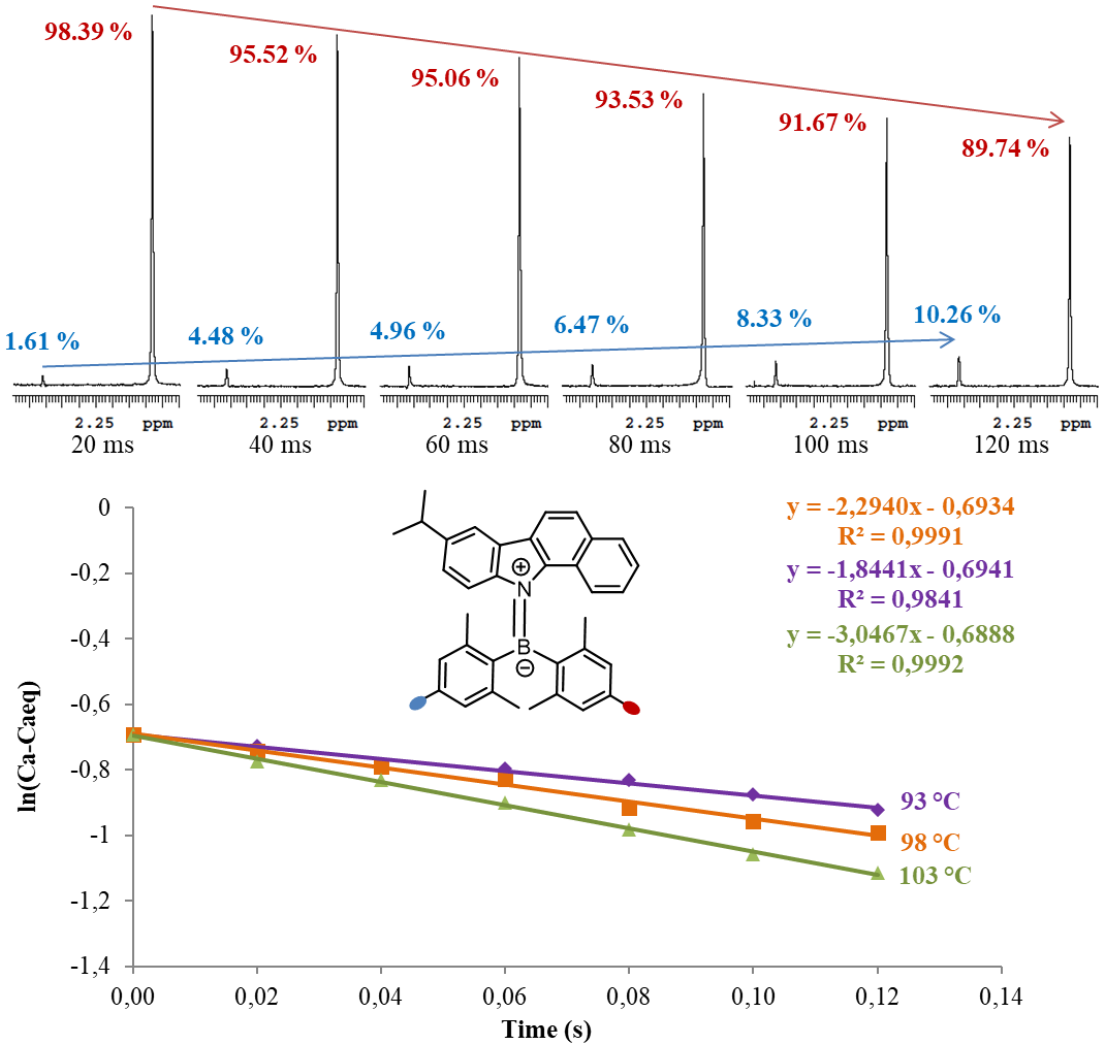

t (s)	T (°C)		
	93	98	103
	ln (Ca - Caeq)		
0	-0.693	-0.693	-0.693
0.02	-0.733	-0.743	-0.780
0.04	-0.779	-0.789	-0.844
0.06	-0.809	-0.828	-0.909
0.08	-0.839	-0.915	-1.002
0.1	-0.876	-0.957	-1.061
0.12	-0.924	-0.991	-1.141
$\Delta G^{\neq}$ (kcal/mol)	21.63	21.69	21.73
	21.7		

Fig.8 *EXSY of* ***11b****. Up experimental spectra at different mixing time; middle plotted mixing time and K values; down a tab. of k and relative* $\Delta G^{\neq}$ *at various T.*

3.3.3 Dynamic NMR and 1D-EXSY of modified-carbazole-borane

Al the other compounds was studied at the same way based on the class of the belonging of the carbazole. For all the simple carbazoles **10** we can only studied the B-C rotational energy barrier with DNMR. Unfortunately, the study of B=N conjugational energy barrier is prohibited due to the energy needed to unlock the rotation of the amine that exceed the limit of the NMR technique.

Instead for benzo-carbazole the hindrance lowers the conjugational energy barrier enough to permit the study. With this class of compounds **11** we can study the rotational energy barrier of B=N with EXSY and of B-C with DNMR like before.

The DNMR and EXSY figure are shown in the experimental data and reported the free energy barriers in the table 5.

The B-C rotational energy barrier the results are fully consistent with the DFT calculation. Instead, for the conjugational B=N rotational energy barrier we have a consistent difference in energetic levels between the calculated and the experimental results (Tab.5 and Scheme 4). This difference of ≈2.5 kcal/mol can be ascribed of an underestimation of the DFT calculation.

Tab.5 *Calculated and experimental rotational energy barrier $\Delta G^{\neq}$ (kcal/mol) for all products **8**, **9**, **10** and **11**.*

Prodotto	**$\Delta G^{\neq}$ rotation (kcal/mol)**					
	N=B		**C-B**		**Amin-Flip**	
	$\Delta G^{\neq}_{cal}$	**$\Delta G^{\neq}_{exp}$**	**$\Delta G^{\neq}_{cal}$**	**$\Delta G^{\neq}_{exp}$**	**$\Delta G^{\neq}_{cal}$**	**$\Delta G^{\neq}_{exp}$**
8	19.4	simmetric	5.4	/	10.4	11.0
9	24.0	simmetric	4.2	/	19.8	16.5
10a	22.4	simmetric	11.1	11.0	not possible	
10b	22.6	out of scale	11.1	10.7		
10c	23.2	out of scale	10.8	10.6		
10d	21.9	out of scale	11.2	/		
11a	18.8	21.5	16.5	15.0		
11b	19.0	21.7	16.4	16.2		
11c	19.4	21.6	16.1	15.8		
11d	18.4	21.0	16.9	15.6		

4 Fluorescence Analysis

All carbazole compounds were tested for fluorescence properties. In particular we are looking for solvatochromic properties, that is the propriety of solute to change the emission spectrum when it is dissolved in different solvents. This difference is called “Stokes shift”.
For this analysis we prepared five 10^{-5} M solutions with different solvents (acetonitrile, toluene, hexane, DCM and THF), and the neat solid. For all the compounds we first found the absorption peak and then registered the normalized fluorescence spectra with that excitation wavelength. Other studies were conducted for quantum yield, lifetime and aggregation induced emission (AIE). In our case the solute display different emission wavelength depending on the polarity of the solvent. For each analysis we have an λ_{exc} of 350 nm.

4.1 Absorption and emission spectra for carbazole

The compound **10b** show a peak of absorption at ≈323nm independently from the used solvent (Fig.9). UV spectra were recorded in the 300-600 nm region because of the absorption of some solvents below 300 nm.

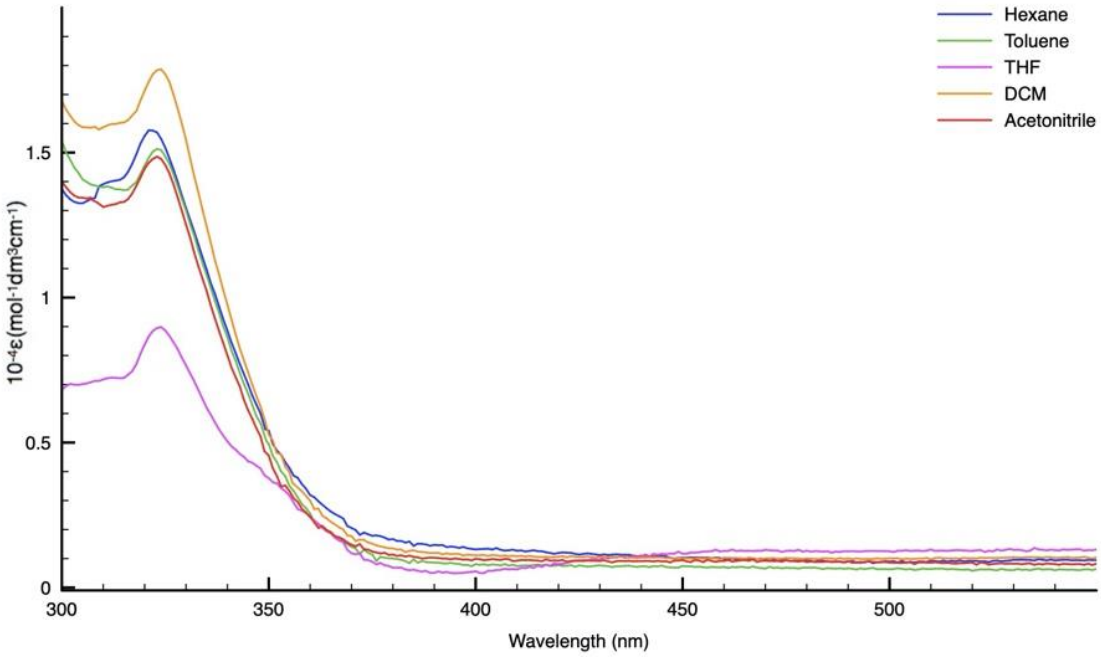

Fig.9 *Absorption Profiles of* ***10b*** *in different solvent at 298K.*

In the normalized emission spectra, we can easily see the solvent "Stokes shift". This goes from the least polar solvent (Hexane) that peak at 446nm from to the most polar (acetonitrile) that peak at 492 nm. This leads to a "Stokes shift" of ≈123 nm for hexane that reaches ≈169 nm for acetonitrile (Fig.10). The quantum yield (ϕ_{ox}*) is maximum in THF where reach 35% and minimum in hexane with only 8%. The lifetime of the excited state (τ_{ox}) is ≈13 ns with a minimum of 5 ns for hexane.

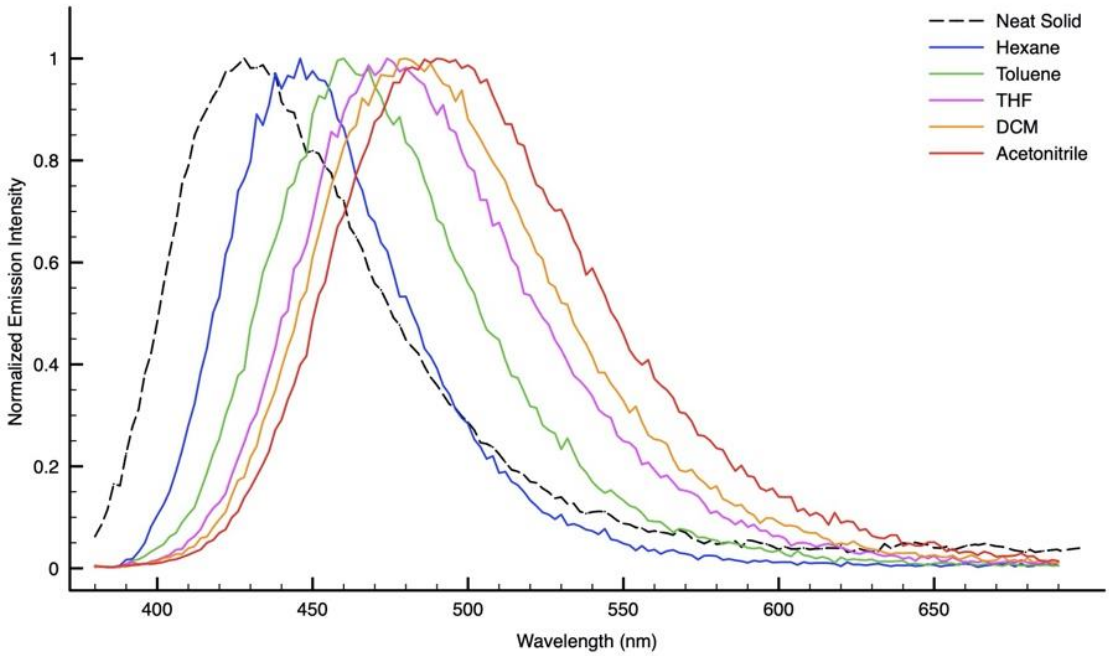

Fig.10 *Normalized Emission Profiles of* ***10b*** *in different solvent at 298K.*

4.2 Absorption and emission for benzo-carbazole

The compound **11a** does not show a clean peak of absorption as the simple carbazole but instead it display a decreasing logarithmic trend with a hump at ≈352nm independently from the used solvent except THF, that shows a defined peak at 350 nm (Fig.11).

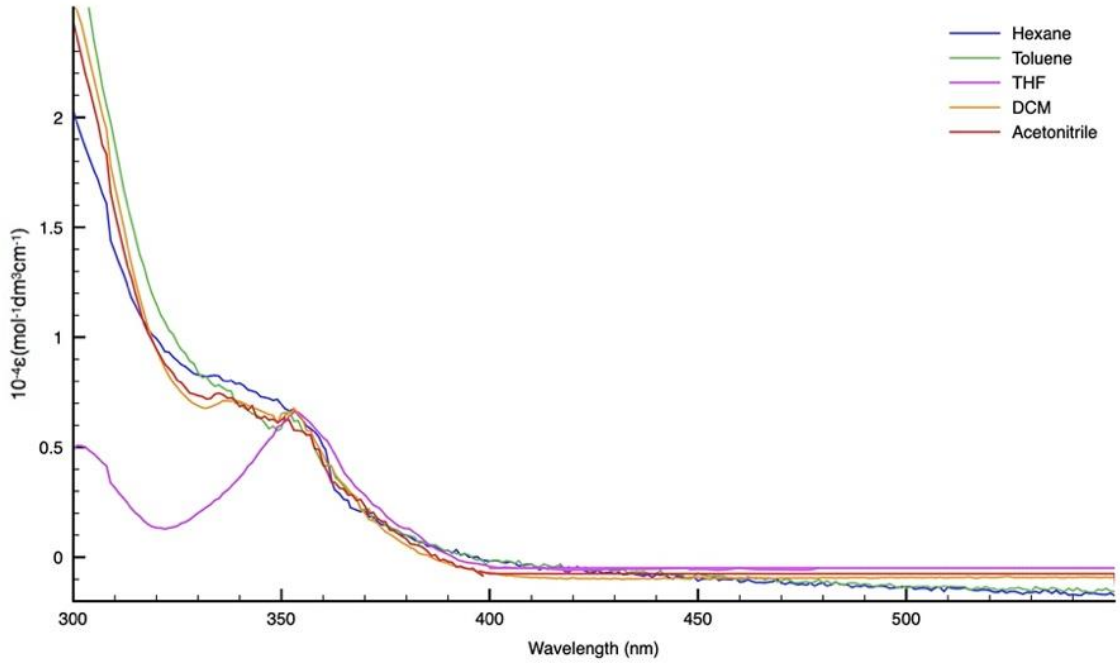

Fig.11 *Absorption Profiles of* ***11a*** *in different solvent at 298K.*

In the normalized emission spectra of **11a** the emissions are shifted to higher wavelength than in the carbazole compound. The pattern instead remains unchanged. In this case the emission of the Hexane solution peaks at 466nm and the acetonitrile one peaks at 504 nm. This leads to a "Stokes shift" of ≈114 nm for hexane that reaches ≈152 nm for acetonitrile (Fig.12). The quantum yield (ϕ_{ox}*) is maximum in DCM where reach 40% and minimum in hexane and acetonitrile with only 9%. The lifetime of the excited state (τ_{ox}) is ≈15 ns with a minimum of 10 ns for hexane.

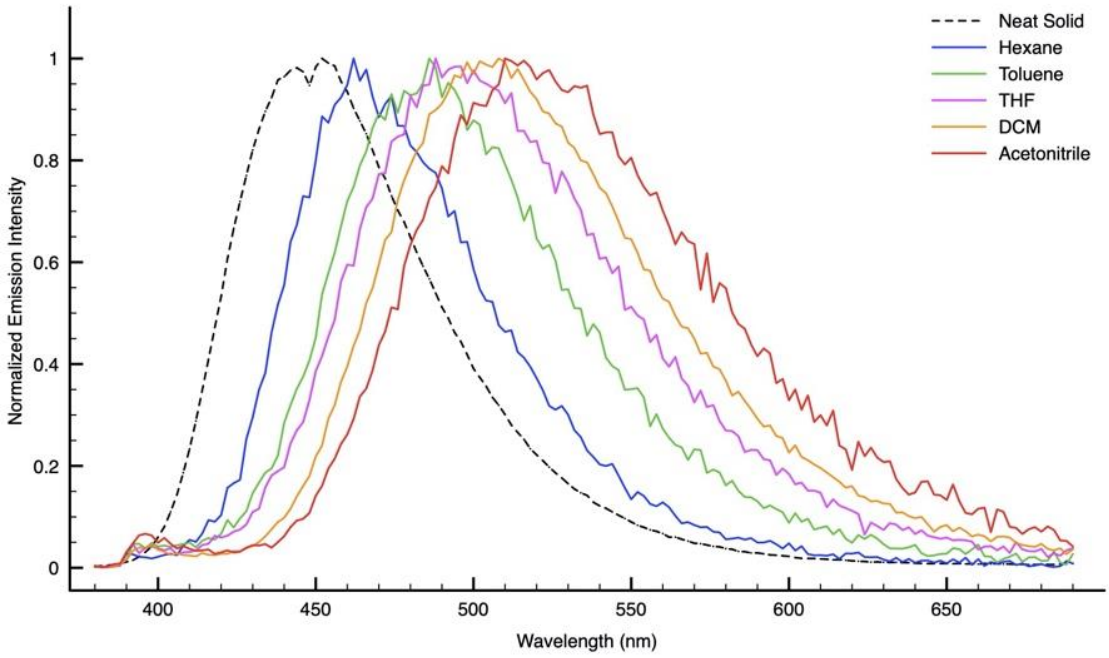

***Fig.12**. Normalized Emission Profiles of **11a** in different solvent at 298K.*

5 Conclusions

At first, we focused our attention at the optimization of the synthesis for the Bis-mesityl-amino-boranes, with good yields (see experimental section). Then we started characterized the 8-9-10 compounds, here we have understood that the cyclic amino-flip can resulted in difficult data elaboration and switch our attention on the possibility of using modified carbazoles that have planar conformation. After the development of the synthesis for the modified carbazoles we have characterized of products. For this purpose, we combine different techniques such as NMR, mass spectroscopy and X-rays on single crystals. Meanwhile, we elaborated the conformations and the possible internal movements of these molecule with DFT calculations. With this analysis we found all the possible Ground and Transition States and started to understand that the two main movement of the molecule are the B-C and the B=N rotation. After that, with DNMR and EXSY, it was possible to determine the experimental rotational energy barriers and compare the results with the energy found with the computational methodologies. At the end, we conducted fluorescence analysis of emission in different solvents which showed the solvatochromic properties of the compounds. With the luminescent properties and the high resistance of this compounds a future development can lead to applications in the field of the smart materials.

6 Experimental Section

6.1 Materials

The commercially available reagents are the following: 2-bromomesitylene, magnesium, iodine, boron trifluoride diethyl etherate (BF_3OEt_2), phenothiazine, iminostilbene, carbazole, gas hydrochloric acid, phenylhydrazine hydrochloride, 4-isopropilphenylhydrazine hydrochloride 4-methoxyphenylhydrazine hydrochloride, 4-(Trifluoromethyl)phenylhydrazine hydrochloride, cyclohexanone, 4-isopropicyclohexanone, α-Tetralone, potassium bis(trimethylsilyl)amide (KHMDS) 0.5 M in toluene. The solvents used are anhydrous tetrahydrofuran (THF), 1-methyl-2-pyrrolidinone (NMP), dichloromethane (DCM) and hexane. Anhydrous THF was odtained by distillation over sodium/benzophenone. Deuterated solvents for NMR spectra are commercially available. The reactions that lead to products are conducted under a constant flux of N_2, filtered through molecular sieves and KOH. The reaction for the synthesis of the modified carbazoles are conduct under oxygen from tank.

6.2 Instruments

All the glassware is clean with acetone, water and DCM and leaved at +70 °C inside an oven for about four hours for make it anhydrous.

The used stationary phases for chromatography are:

- Thin Layer Chromatography (TLC) plates in Silica gel 60 F254 on aluminium sheets.
- Column chromatography Silica gel (Merck Grade 9385) 60 Å (230-400 mesh Sigma Aldrich).

Mass spectrum are registered with a spectrometer MICROMASS ZQ 4000 in Electron Spray Ionisation (ESI). The NMR spectra ^{1}H-NMR, ^{13}C-NMR and ^{11}B-NMR ^{19}F-NMR are acquired with Varian Inova 600 (600 MHz). Fluorescence spectra were recorded on a EDINBURG H620 spectrometer.

6.3 Synthesis of amine see Scheme 7

Generalizable procedure for **7a** with which we had prepared compound **6b**, **6c**, **6d**, **7a**, **7b**, **7c**, **7d**.

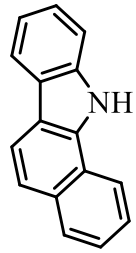

7a
(CAS: 239-01-0)

In a 25 mL oven-dried reaction vessel is added α-Tetralone **13** (0.67ml, 5 mmol), phenylhydrazine hydrochloride **14** (1.084g, 7.5 mmol), N-methyl-2-pyrrolidone (10 mL) under oxygen (1atm). The resulting solution was stirred at +140 °C for 24 h. After cooling to room temperature, the volatiles were removed under vacuum and the NMP was distilled away in high vacuum at +100 °C. The residue was filtered on Celite®, then the product was purified by chromatography separation (silica gel, Hexane/DCM= 7:3). Evaporated the solvents, a white solid was obtained (0.815g, 59%).

6.4 Synthesis of product see Scheme 10

Generalizable procedure for **11c** with which we had prepared compound **8**, **9**, **10a**, **10b**, **10c**, **10d**, **11a**, **11b**, **11c**, and **11d.**

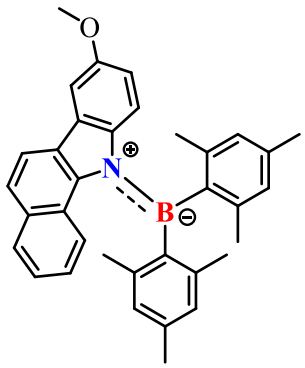

11c

In a 25 mL oven-dried reaction vessel is add 2-bromomesitylene (13, 0.45 mL, 6 mmol), magnesium (0.2 g), dry THF (6 mL) and a tip of iodine under nitrogen flow, stirred and left to reflux for 2 hours. After that the solution is bring to -78 °C in an acetone bath and is add boron trifluoride diethyl etherate (BF_3OEt_2) (0.41 mL, 3mmol) dropwise. After reached room temperature the resulting solution was stirred for 12h and add dropwise to a second solution than refluxed for 4h. The second solution is prepared in a 25 mL oven-dried reaction vessel where is added 8-OMe-11-benzo[a]carbazole (**7c**, 0.68 g, 3mmol), dry THF (6 mL) and stirred before the dropwise addition of potassium bis(trimethylsilyl)amide (KHMDS) (6 mL, 3mmol) than leave to react 1h. After cooling to room temperature, the reaction is quenched with DCM, brought to dryness, filtered on Celite®, purified by chromatography separation (silica gel, Hexane/DCM= 7:3) and by a crystallization in DCM. After evaporation of the solvents, a white solid was obtained (0.966g, 65%).

6.5 Characterization of compounds

For every not known compound we shown below the caracterization in this order:

I. Structure and identification code
II. ^{1}H-NMR
III. ^{13}C-NMR
IV. ^{11}B-NMR (if present)
V. ^{19}F-NMR (if present)
VI. Yield
VII. DFT calculations
VIII. DNMR (if present)
IX. EXSY (if present)
X. Absorption Profiles at 298K (if present)
XI. Normalized Emission Profiles at 298K (if present)
XII. "Stokes shift", quantum yield (ϕ_{ox}*) and lifetime of the excited state (τ_{ox}) values for each solvent
XIII. X-ray diffraction structure (if present)

6.5.1 Bis-mesityl-fhenotiazine 8

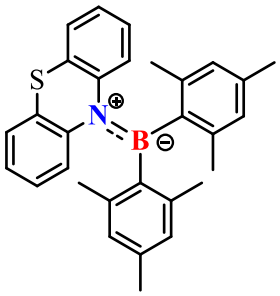

8

^{1}H,^{13}C, ^{11}B-NMR spectra agree with that reported in letterature.

The product **8** was obtained from general procedure with a yield of 24%.

For DFT calculations of GS and TSs state of compound **8** see Table 2 at 3.1 Conformational Studies and DFT Calculations.

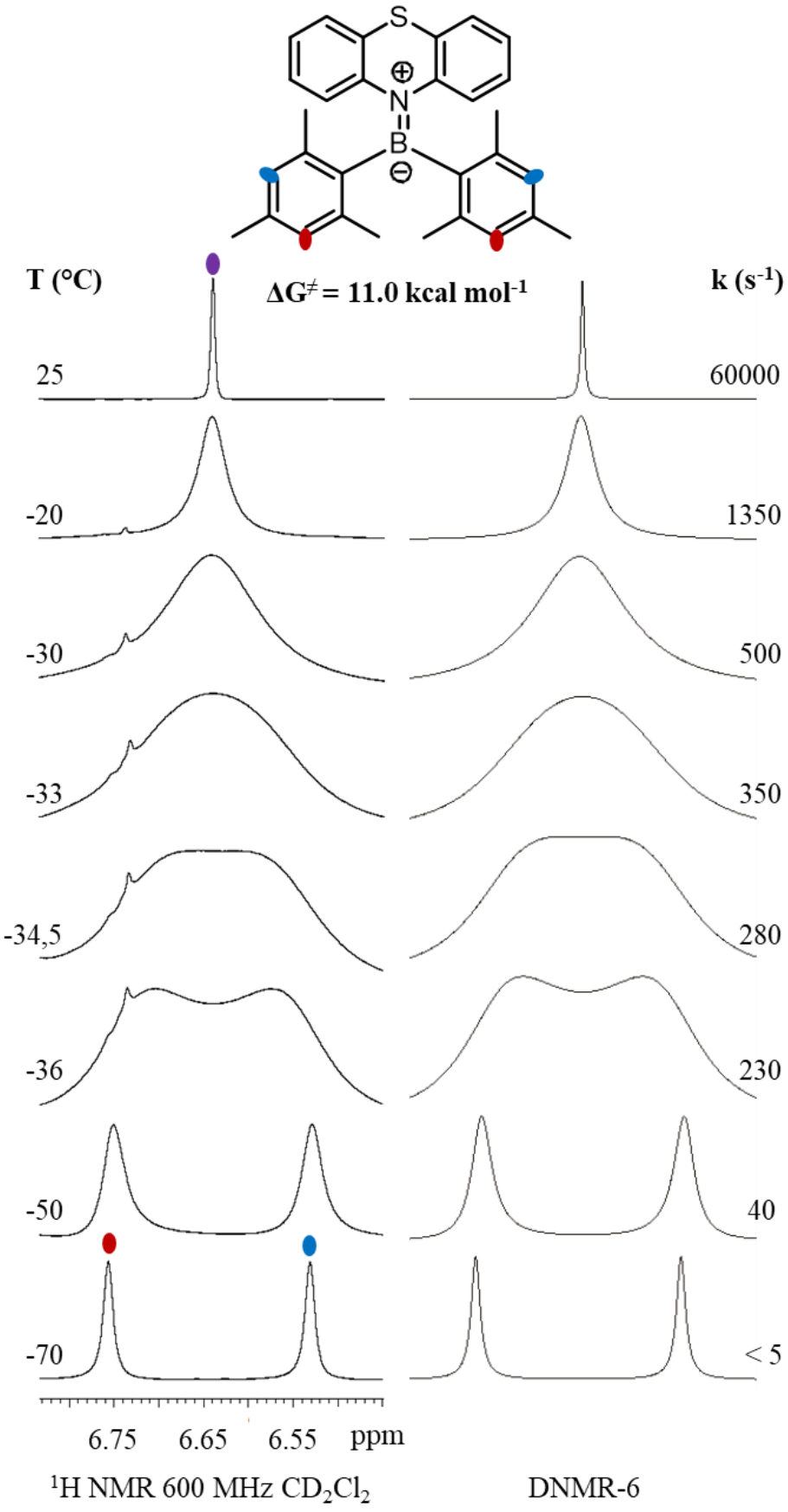

Fig.13 *DNMR of* ***8****. left experimental spectra at different temperatures; right simulated spectra with different kinetic constants.*

6.5.2 Bis-mesityl-iminostilbene 9

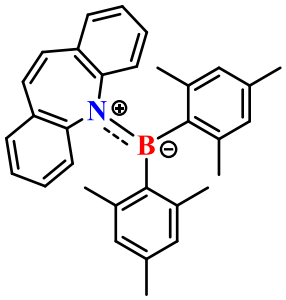

9

^{1}H NMR (600 MHz, Tetrachloroethane-d_2, 6.0ppm, +25°C) δ 7.33 (dd, *J* = 7.9, 1.4 Hz, 1H), 7.21 (dd, *J* = 7.4, 1.7 Hz, 1H), 7.12 (dtd, *J* = 24.3, 7.3, 1.5 Hz, 2H), 7.00 (s, 1H), 6.69 (s, 1H), 6.49 (s, 1H), 6.00 (d, *J* = 1.5 Hz, 1H), 2.69 (s, 3H), 2.14 (s, 3H), 2.11 (s, 3H), 1.60 (s, 1H).

^{13}C NMR (151 MHz, Tetrachloroethane-d_2, 74.0ppm, +25°C) δ 145.4, 140.1, 140.0, 136.2, 133.4, 131.5, 128.7, 128.6, 128.2, 127.9, 127.2, 125.8, 74.3, 74.2, 74.0, 73.8, 27.4, 24.8, 21.0.

^{11}B NMR (192 MHz, Tetrachloroethane-d_2, Rif.BF_3OEt_2, +25°C) δ 46.2.

The product **9** was obtained from general procedure with a yield of 46%.

For DFT calculations of GS and TSs state of compound **9** see Table 2 at 3.1 Conformational Studies and DFT Calculations.

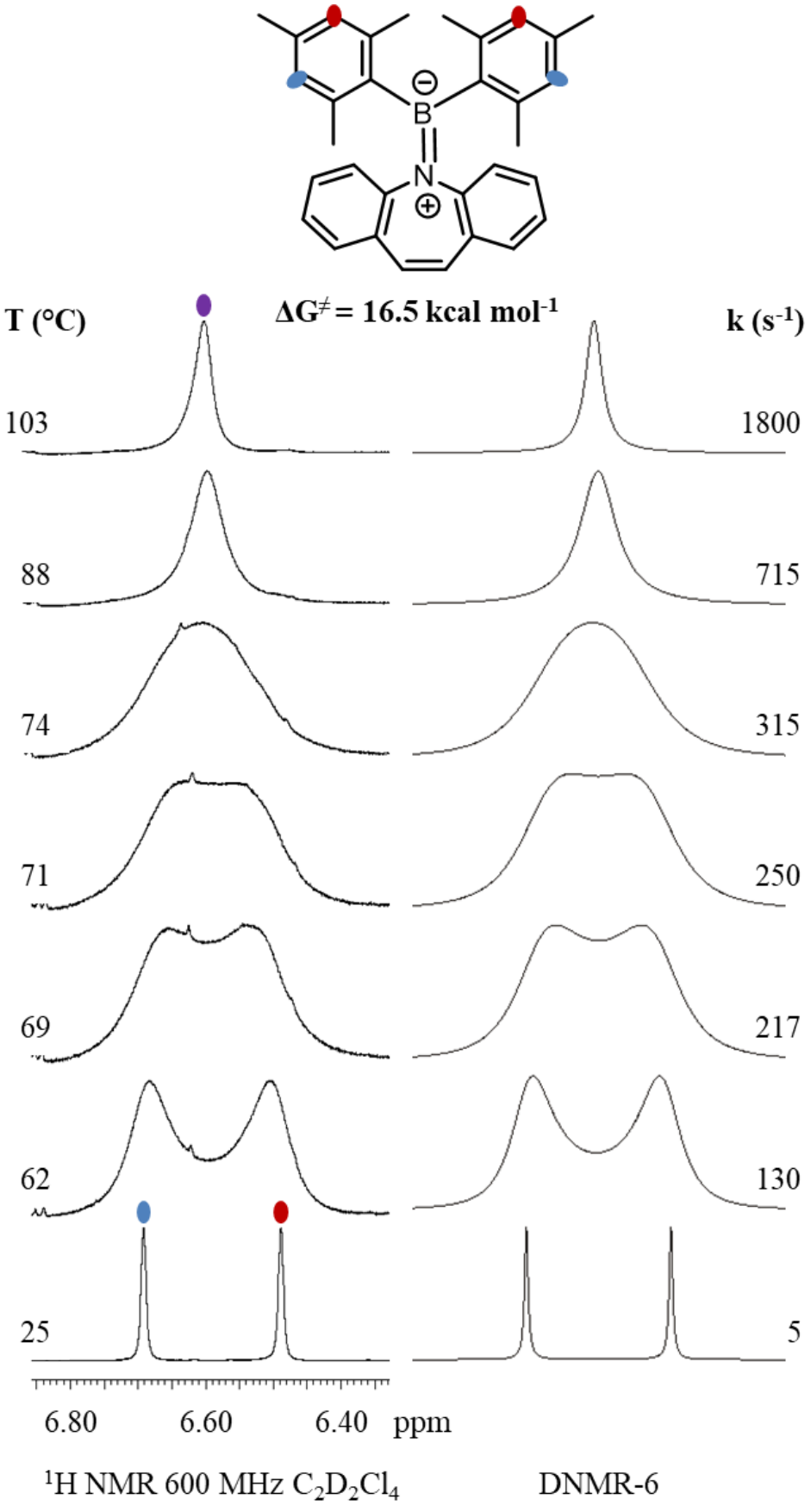

Fig.14 *DNMR of* ***9****. left experimental spectra at different temperatures; right simulated spectra with different kinetic constants.*

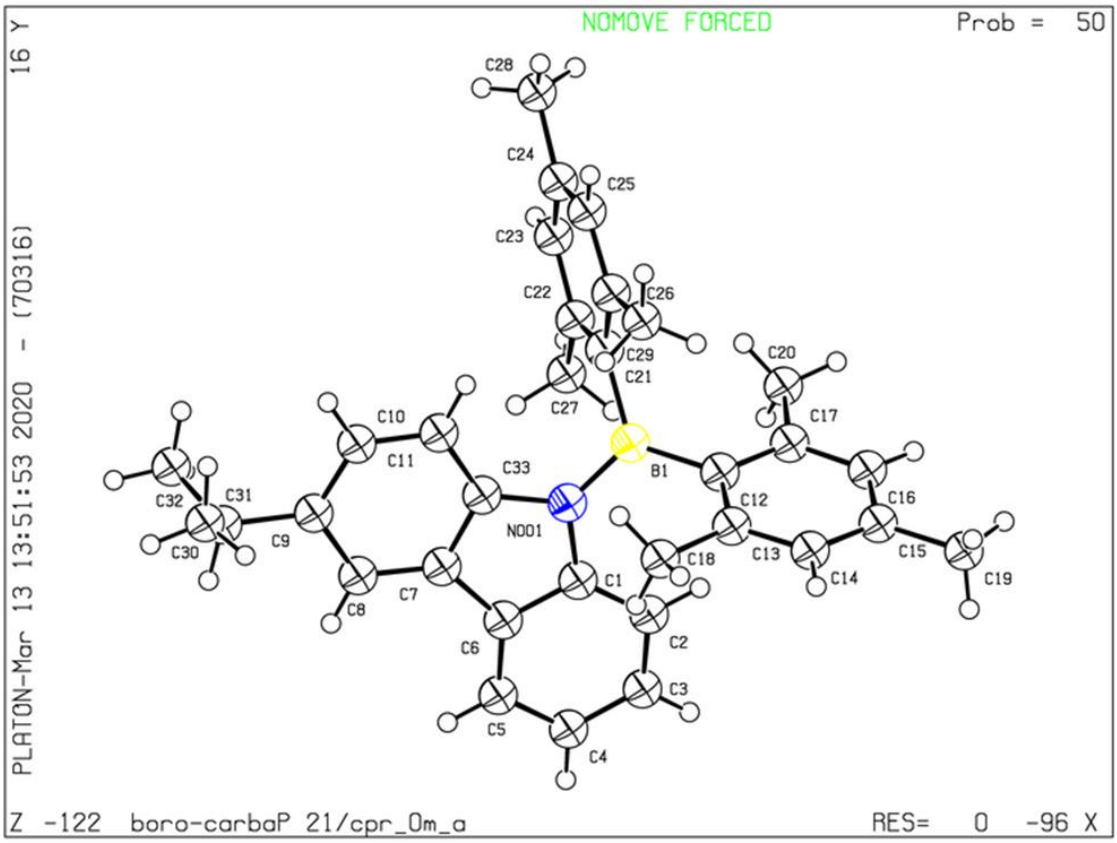

Cell:	a=9.81(5)	b=11.79(5)	c=23.06(10)
	alpha=90	beta=92.61(10)	gamma=90

Fig.15 *Crystal structure and cell data of compound* ***9***.

6.5.3 Bis-mesityl-carbazole-borane 10a

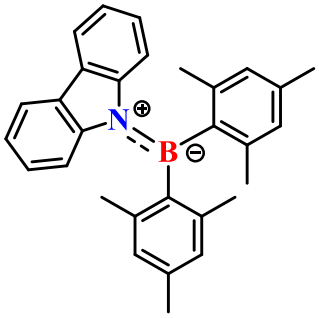

10a

^{1}H,^{13}C, ^{11}B-NMR spectra agree with that reported in letterature.

The product **10a** was obtained from general procedure with a yield of 38%.

For DFT calculations of GS and TSs state of compound **10a** see Table 1 at 3.1 Conformational Studies and DFT Calculations.

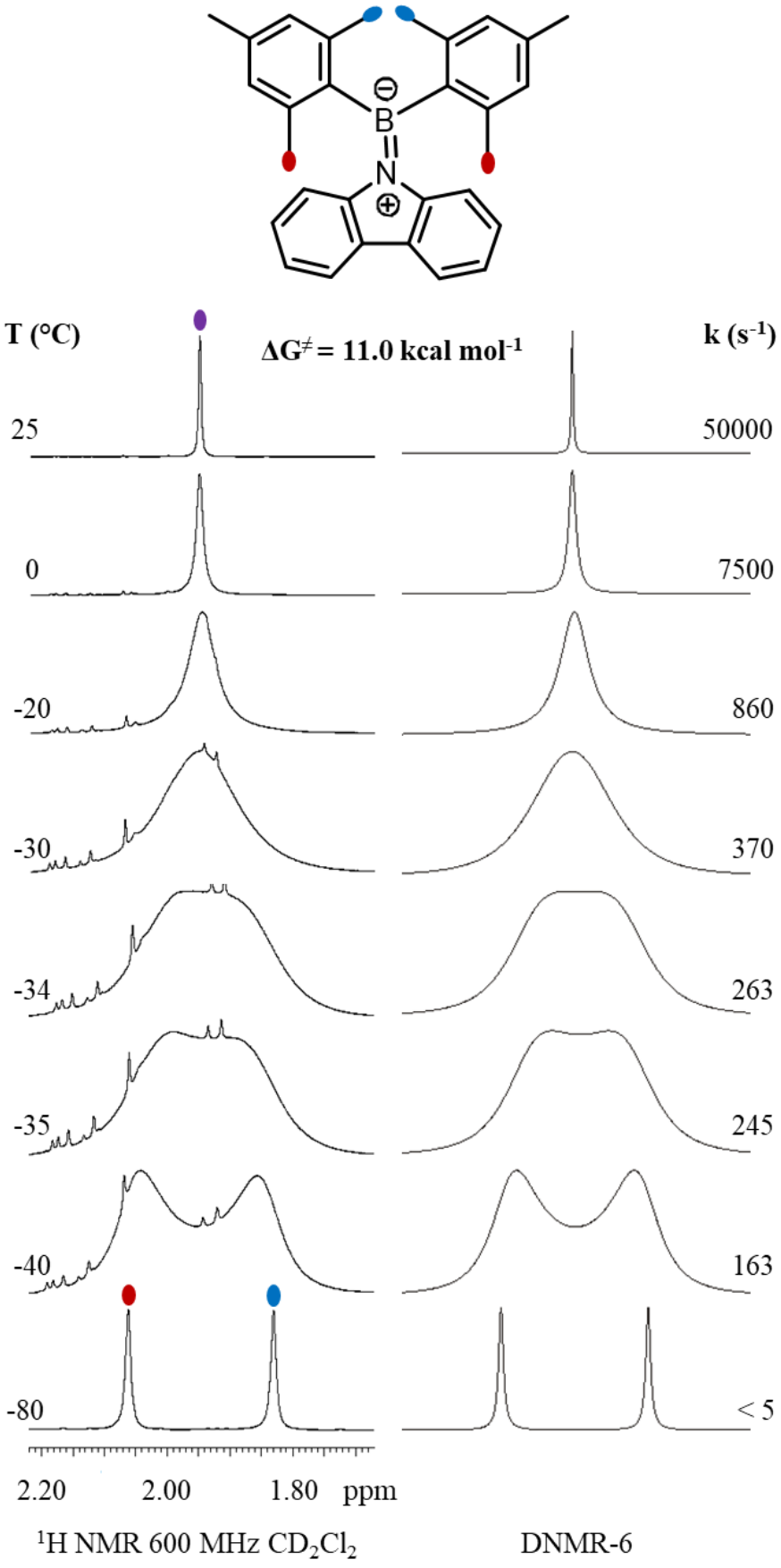

Fig.16 *DNMR of* ***10a****. left experimental spectra at different temperatures; right simulated spectra with different kinetic constants.*

6.5.4 Bis-mesityl-3-isopropil-carbazole-borane 10b

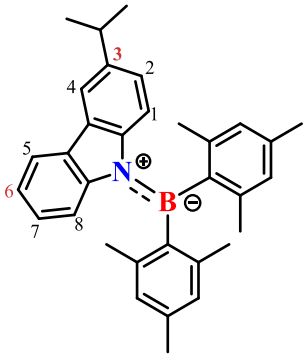

10b

^{1}H-NMR (600 MHz, Methylene Chloride-d$_2$, 5.32 ppm, +25°C) δ 7.97 (ddd, J = 7.7, 1.4, 0.7 Hz, 1H), 7.83 (d, J = 1.8 Hz, 1H), 7.27 – 7.21 (m, 1H), 7.04 (ddd, J = 8.5, 7.2, 1.3 Hz, 1H), 6.96 (dd, J = 8.6, 1.9 Hz, 1H), 6.91 (dt, J = 8.5, 0.9 Hz, 1H), 6.84 (d, J = 4.0 Hz, 4H), 6.81 (dd, J = 8.7, 0.6 Hz, 1H), 3.01 (p, J = 6.9 Hz, 1H), 2.33 (d, J = 3.2 Hz, 6H), 2.01 (d, J = 7.3 Hz, 12H), 1.30 (d, J = 6.9 Hz, 6H).

^{13}C-NMR (151 MHz, Methylene Chloride-d$_2$, 53.4 ppm, +25°C) δ 143.5, 143.5, 141.5, 140.9, 139.2$_5$, 139.2, 128.6, 128.5$_8$, 128.2, 128.0, 125.9, 125.0, 122.5, 119.3, 116.7, 115.4, 115.0, 53.7, 53.6, 53.4, 53.2, 53.0, 33.9, 24.1, 21.6, 21.0.

^{11}B-NMR (192 MHz, Methylene Chloride-d$_2$, Rif.BF$_3$OEt$_2$, +25°C) δ 52.0.

The product **10b** was obtained from general procedure with a yield of 9%.

Table 6. DFT calculations of GS and TSs state of compound **10b**.

State	2D structure	3D structure	Total Energy (a.u.)	Rel. E. Calculated (kcal/mol)
GS	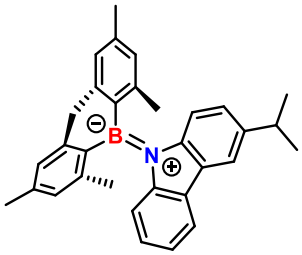	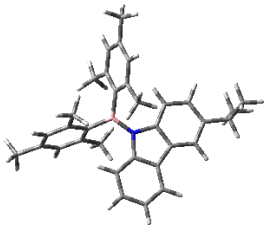	-1359.23226500	0.0
2RF-TS (two-ring-flip) mes-mes	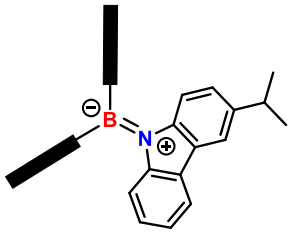	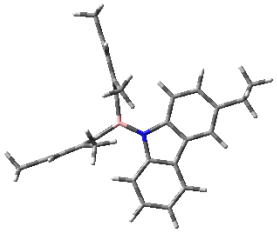	-1359.21462200	**11.07**
2RF-TS (two-ring-flip) mes-carb	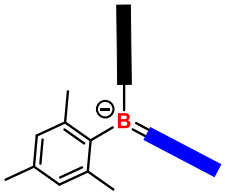	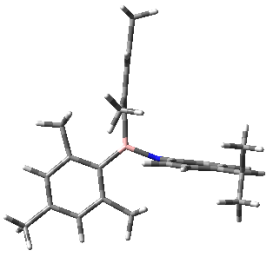	-1359.19619600	**22.6**

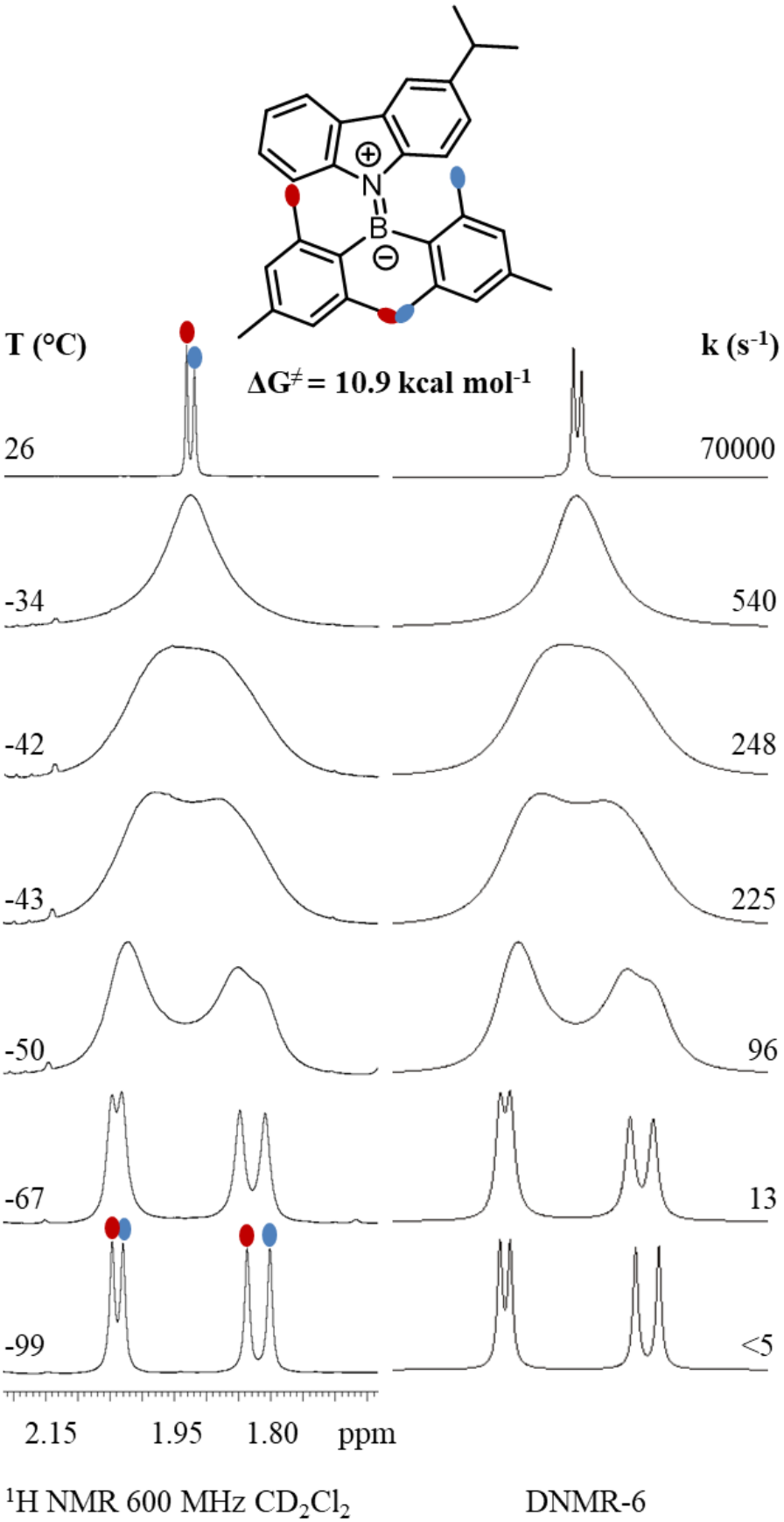

Fig.17 *DNMR of* ***10b****. left experimental spectra at different temperatures; right simulated spectra with different kinetic constants.*

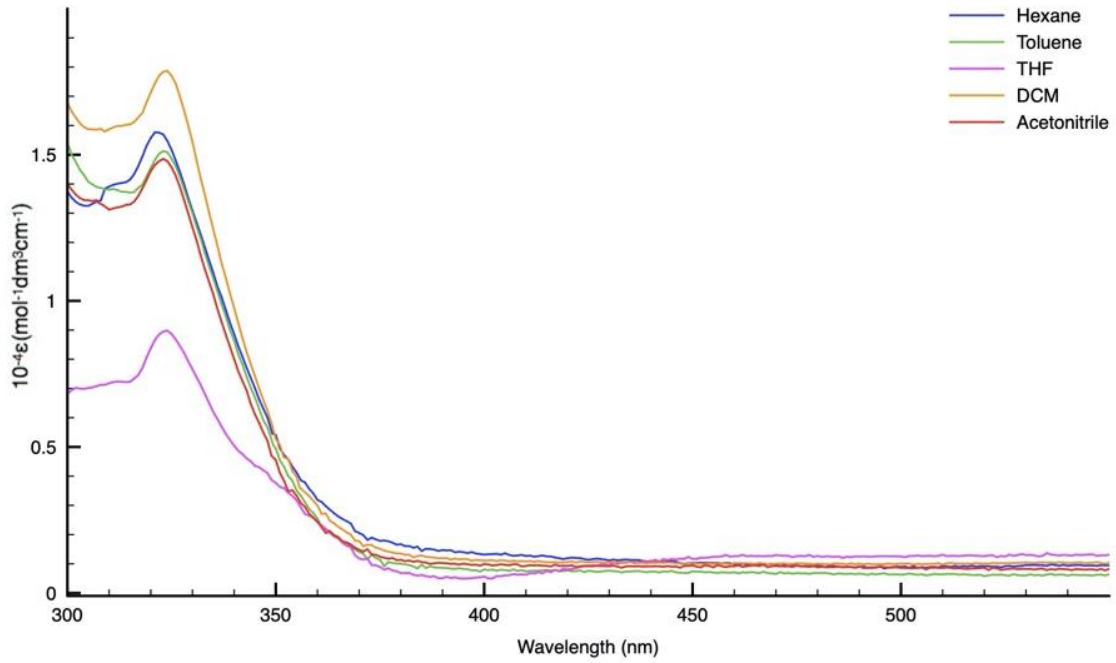

Fig.18 *Absorption Profiles of* ***10b*** *in different solvent at 298K.*

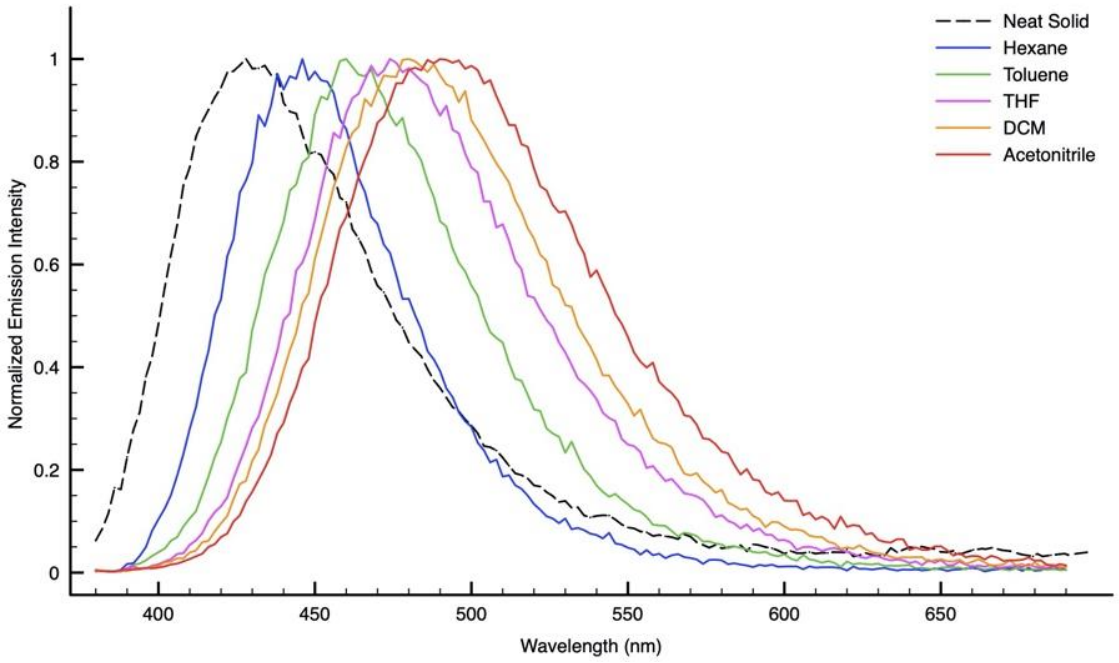

Fig.19 *Normalized Emission Profiles of* ***10b*** *in different solvent at 298K.*

Tab.7 *Fluorescence values for* ***10b*** *vs Quinine Sulphate/0.05 M H_2SO_4, Φ = 0.53 [i], λ_{exc} = 350 nm.*

Compound	Solvent	Absorption	Emission 298K			Emission Neat Solid Matrix 298K	
		λ(nm) $10^{-4}\varepsilon$ ($cm^{-1}M^{-1}$)	λ_{em} (nm)	τ_{ox} (ns)	ϕ_{ox}* (%)	λ_{em} (nm)	τ (ns)
10b	solid	/	/	/	/	430	5
	Hex	310 (1.39), 322 (1.58)	446	5	8.23	/	/
	Toluene	323 (1.51)	460	8.6	23.5	/	/
	THF	323 (0.89)	476	12.4	34.8	/	/
	DCM	324 (1.79)	482	15.1	28.5	/	/
	CH_3CN	306 (1.34), 323 (1.49)	492	13.3	20.4	/	/

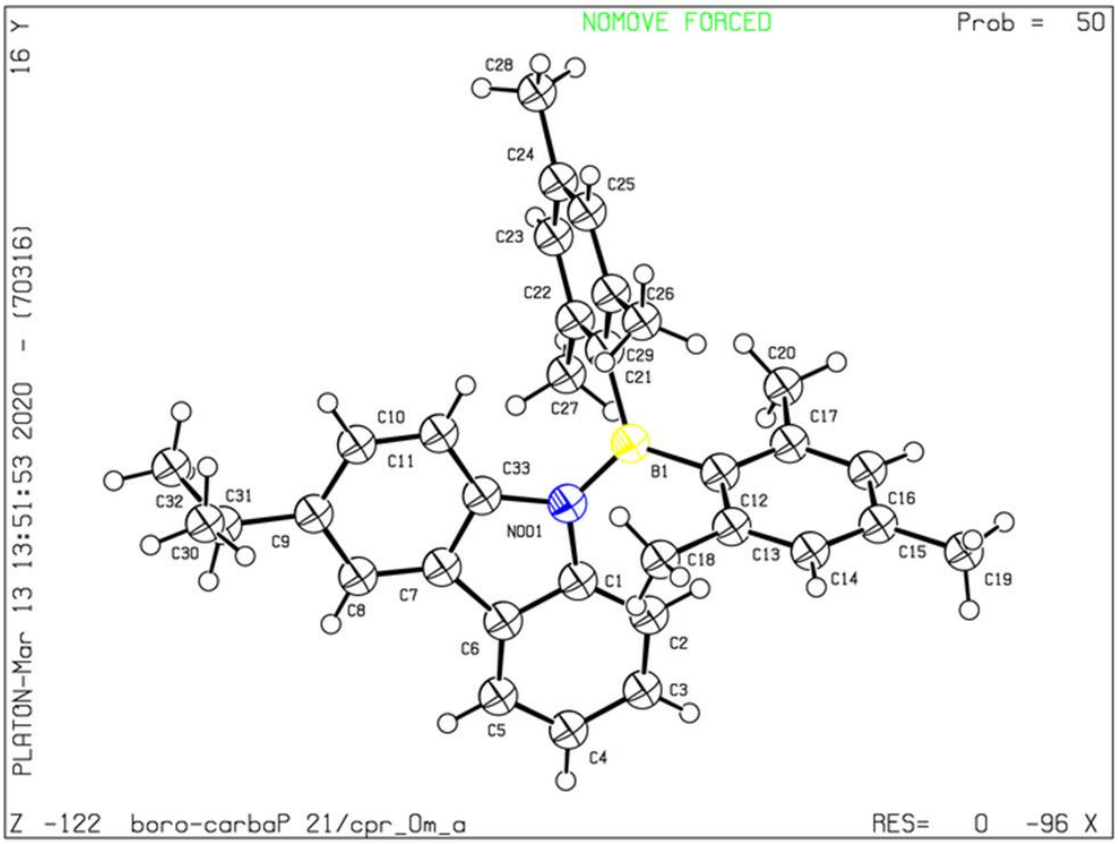

Cell: a=9.81(5) b=11.79(5) c=23.06(10)
alpha=90 beta=92.61(10) gamma=90

Fig.20 *Crystal structure and cell data of compound* ***10b****.*

6.5.5 Bis-mesityl-3-isopropil-6-Ome-carbazole-borane 10c

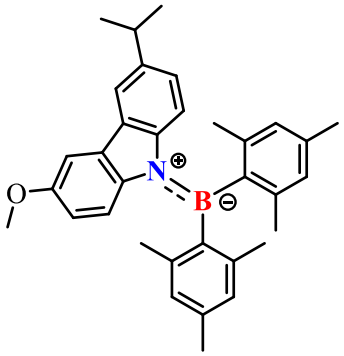

10c

^{1}H-NMR (600 MHz, Methylene Chloride-d$_2$, 5.32 ppm, +25°C) δ 7.80 (d, *J* = 1.8 Hz, 1H), 7.44 (d, *J* = 2.6 Hz, 1H), 6.95 (dd, *J* = 8.6, 1.9 Hz, 1H), 6.84 (d, *J* = 5.4 Hz, 4H), 6.79 (dd, *J* = 11.7, 8.8 Hz, 2H), 6.64 (dd, *J* = 9.0, 2.7 Hz, 1H), 3.87 (s, 3H), 3.02 (p, *J* = 6.9 Hz, 1H), 2.33 (d, *J* = 4.3 Hz, 6H), 2.02 (d, *J* = 10.0 Hz, 12H), 1.31 (d, *J* = 6.9 Hz, 6H).

^{13}C-NMR (151 MHz, Methylene Chloride-d$_2$, 53.4 ppm, +25°C) δ 156.0, 143.4, 142.2, 141.0, 141.0, 139.1$_3$, 139.1, 137.8, 129.1, 128.6, 128.5$_6$, 128.1, 125.2, 116.6, 116.3, 115.2, 114.0, 102.1, 55.5, 53.7, 53.6, 53.4, 53.2, 53.0, 33.9, 24.1, 21.6, 21.6, 20.9$_7$, 20.9$_6$.

^{11}B-NMR (192 MHz, Methylene Chloride-d$_2$, Rif.BF$_3$Oet$_2$, +25°C) δ 51.51.

The product **10c** was obtained from general procedure with a yield of 88%.

Table 8. DFT calculations of GS and TSs state of compound **10c**.

State	2D structure	3D structure	Total Energy (a.u.)	Rel. E. Calculated (kcal/mol)
GS	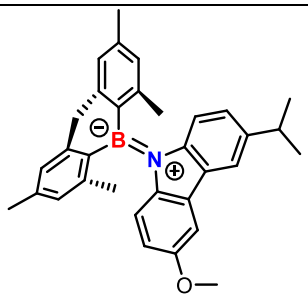	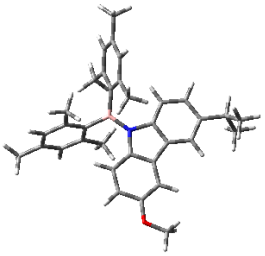	-1473.78422800	0.0
2RF-TS (two-ring-flip) mes-mes	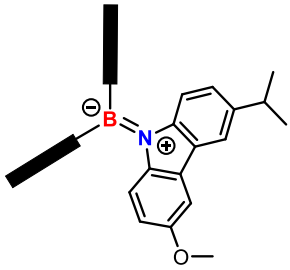	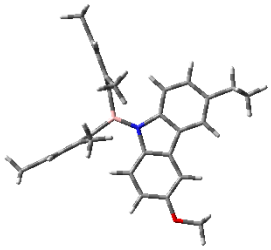	-1473.766971	**10.8**
2RF-TS (two-ring-flip) mes-carb	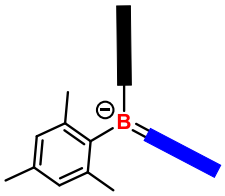	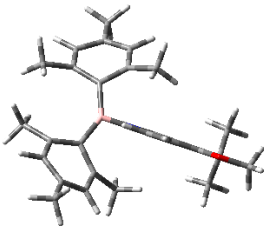	-1473.747193	**23.2**

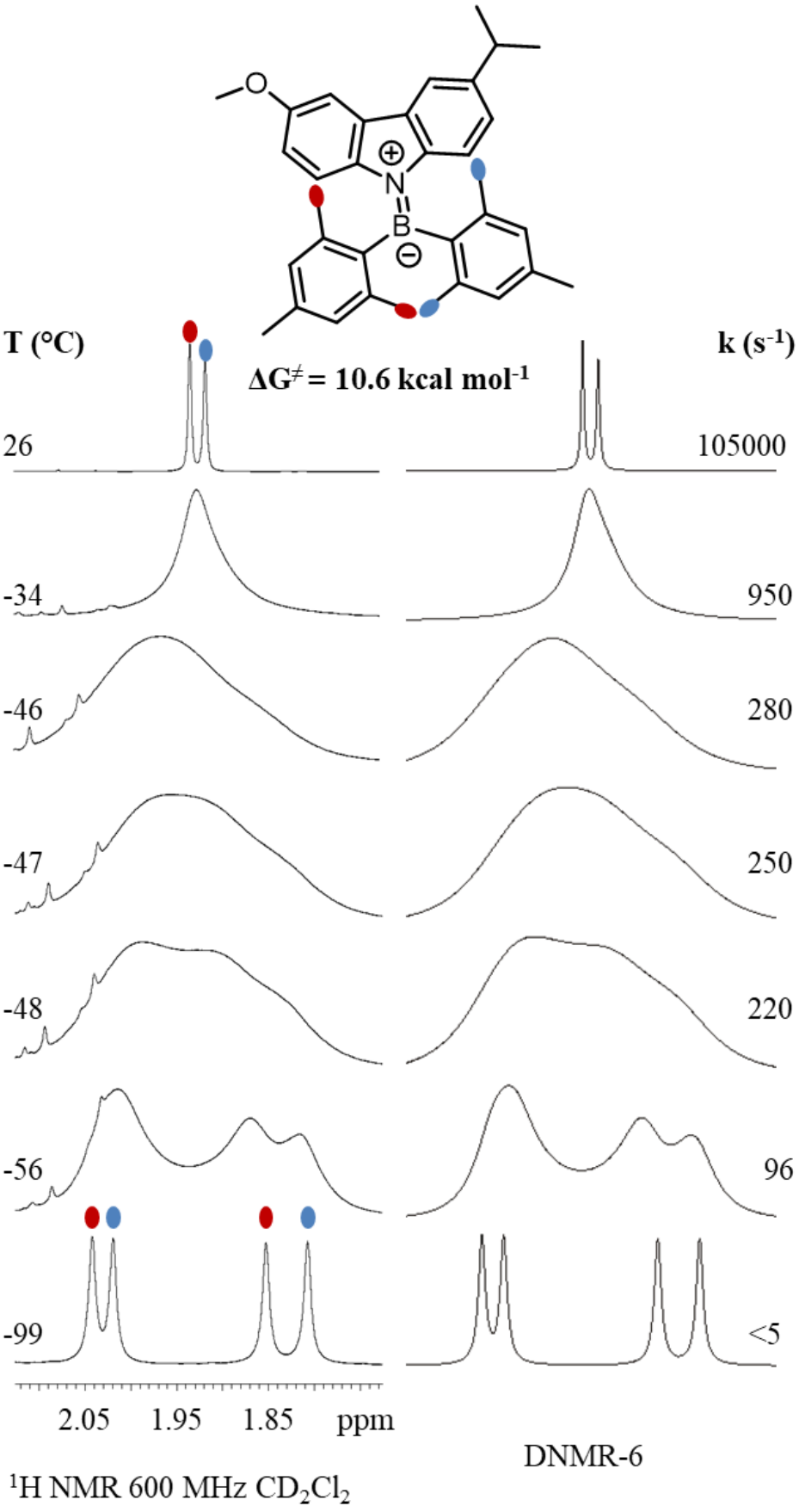

Fig.21 *DNMR of* ***10c****. left experimental spectra at different temperatures; right simulated spectra with different kinetic constants.*

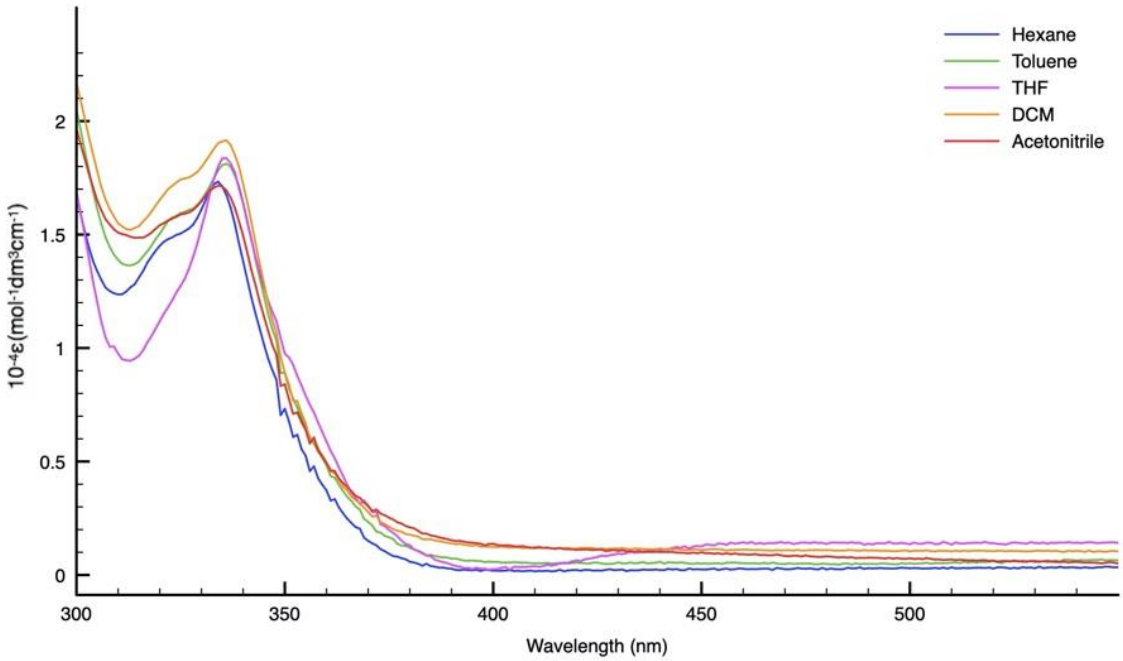

Fig.22 *Absorption Profiles of* ***10c*** *in different solvent at 298K.*

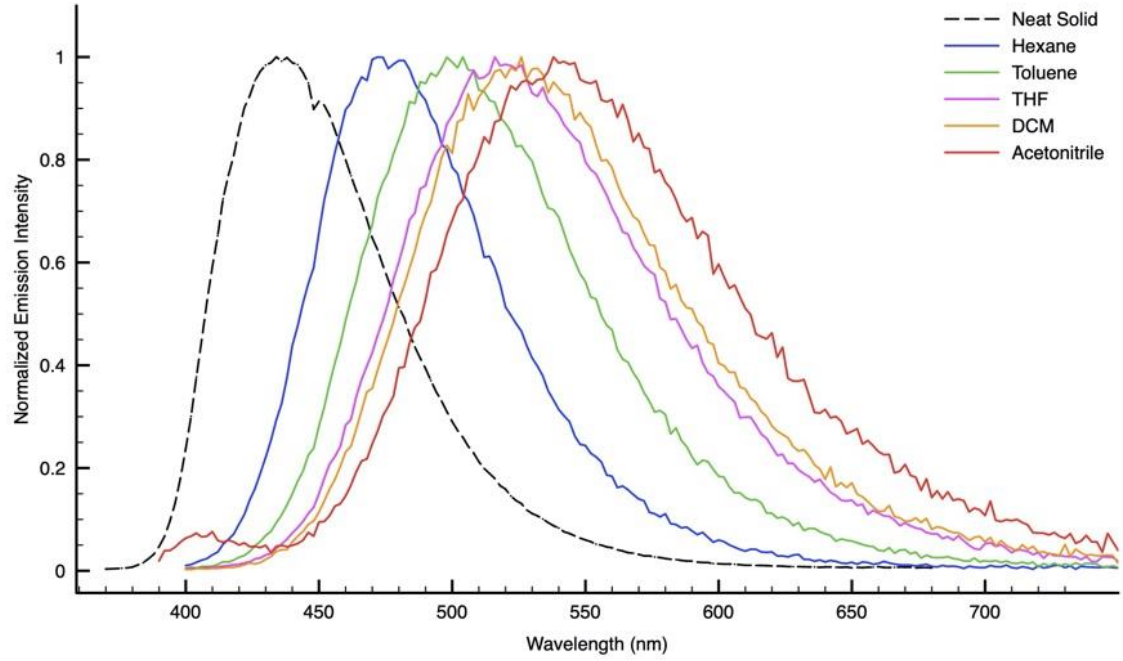

Fig.23 *Normalized Emission Profiles of* ***10c*** *in different solvent at 298K.*

Tab.9 *Fluorescence values for* ***10c*** *vs Quinine Sulphate/0.05 M H_2SO_4, Φ = 0.53 [ii], λ_{exc} = 350 nm.*

Compound	Solvent	Absorption	Emission 298K			Emission Neat Solid Matrix 298K	
		λ(nm) $10^{-4}\varepsilon$ ($cm^{-1}M^{-1}$)	λ_{em} (nm)	τ_{ox} (ns)	ϕ_{ox}* (%)	λ_{em} (nm)	τ (ns)
10c	solid	/	/	/	/	436	6
	Hex	321 (1.46), 334 (1.73)	476	9	22	/	/
	Toluene	325 (1.59), 336 (1.81)	500	13	28.5	/	/
	THF	336 (1.83)	520	19	49.7	/	/
	DCM	323 (1.71), 336 (1.92)	524	17	27	/	/
	CH_3CN	325 (1.59), 335 (1.71)	542	10	11.5	/	/

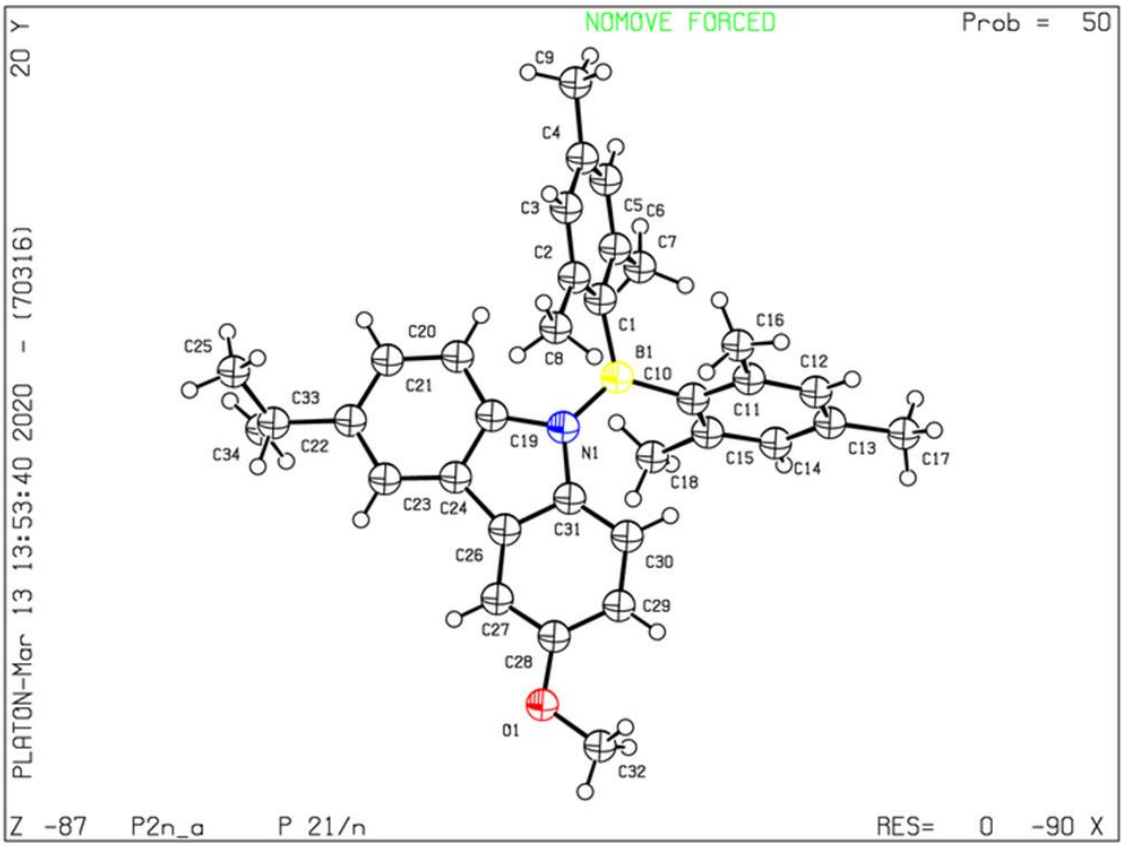

Cell: a=11.3267(5) b=24.625(1) c=11.5176(5)

alpha=90 beta=117.302(1) gamma=90

Fig.24 *Crystal structure and cell data of compound* ***10c****.*

6.5.6 Bis-mesityl-3-isopropil-6-CF_3-carbazole-borane 10d

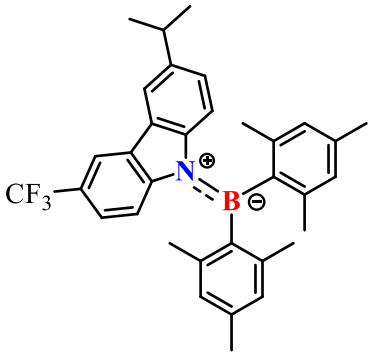

10d

^{1}H-NMR (400 MHz, Methylene Chloride-d_2, 5.35 ppm, +25°C) δ 8.28 (dt, *J* = 1.7, 0.8 Hz, 1H), 7.90 (d, *J* = 1.9 Hz, 1H), 7.31 (ddd, *J* = 8.7, 2.0, 0.7 Hz, 1H), 7.08 – 6.96 (m, 2H), 6.89 – 6.79 (m, 5H), 3.04 (h, *J* = 6.9 Hz, 1H), 2.35 (d, *J* = 1.9 Hz, 6H), 2.02 (d, *J* = 4.2 Hz, 12H), 1.32 (d, *J* = 6.9 Hz, 7H).

^{19}F NMR (376 MHz Methylene Chloride-d_2, Rif.BF_3OEt_2, +25°C) δ -61.35.

The product **10d** was obtained from general procedure with a yield of 54%.

Table 10. DFT calculations of GS and TSs state of compound **10d**.

State	2D structure	3D structure	Total Energy (a.u.)	Rel. E. Calculated (kcal/mol)
GS	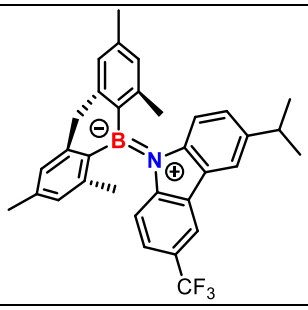	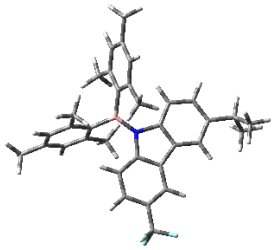	-1696.372691	0.0
2RF-TS (two-ring-flip) mes-mes	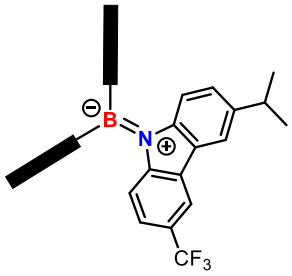	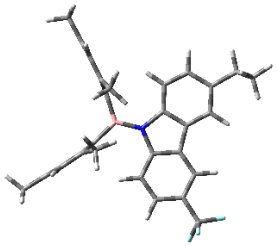	-1696.354719	**11.3**
2RF-TS (two-ring-flip) mes-carb	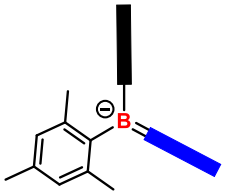	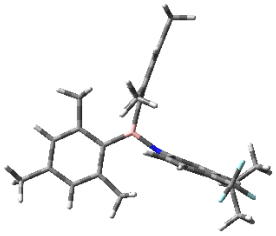	-1696.337780	**21.9**

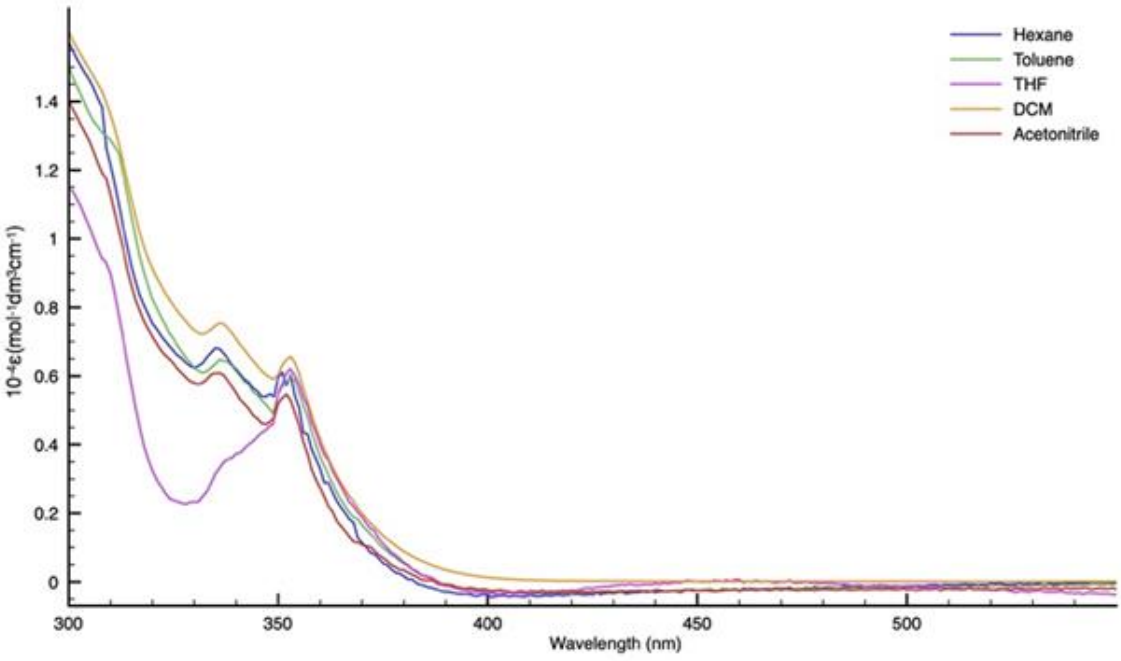

Fig.25 *Absorption Profiles of* ***10d*** *in different solvent at 298K.*

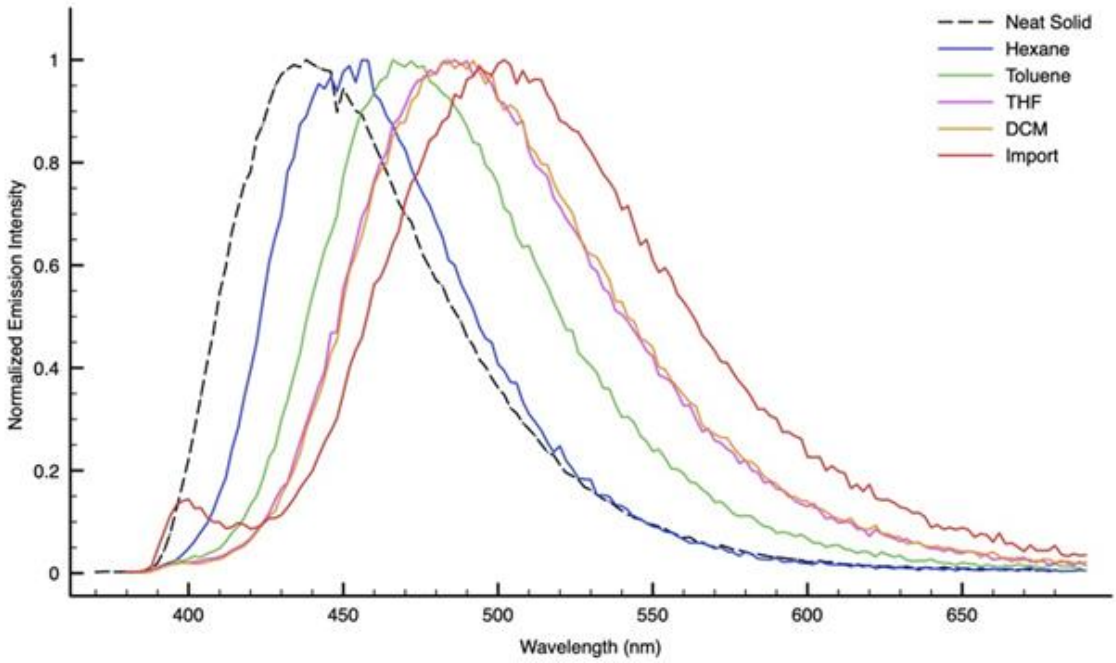

Fig.26 *Normalized Emission Profiles of* ***10d*** *in different solvent at 298K.*

Tab.11 *Fluorescence values for* ***10d*** *vs Quinine Sulphate/0.05 M H_2SO_4, $\Phi = 0.53$ [iii], $\lambda_{exc} = 350$ nm.*

Compound	**Solvent**	**Absorption**	**Emission 298K**			**Emission Neat Solid Matrix 298K**	
		λ(nm) $10^{-4}\varepsilon$ ($cm^{-1}M^{-1}$)	λ_{em} (nm)	τ_{ox} (ns)	ϕ_{ox}* (%)	λ_{em} (nm)	τ (ns)
10d	solid	/	/	/	/	438	9
	Hex	335 (0.68), 351 (0.61)	450	6	28.5	/	/
	Toluene	337 (0.64), 353 (0.60)	470	11.5	46.8	/	/
	THF	337 (0.49), 353 (0.77)	484	15	32.9	/	/
	DCM	336 (0.75), 353 (0.66)	486	17	36.2	/	/
	CH_3CN	335 (0.61), 352 (0.55)	500	14.7	35.7	/	/

6.5.7 Bis-mesityl-11-benzo[a]carbazole-borane 11a

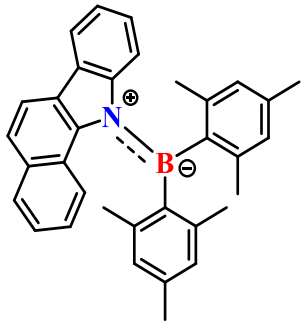

11a

^{1}H-NMR (600 MHz, Methylene Chloride-d$_2$, 5.32 ppm, +25°C) δ 8.12 (d, *J* = 8.4 Hz, 1H), 8.07 (d, *J* = 7.7 Hz, 1H), 8.02 (d, *J* = 8.5 Hz, 1H), 7.85 (d, *J* = 8.1 Hz, 1H), 7.78 (d, *J* = 8.4 Hz, 1H), 7.28 (dt, *J* = 14.1, 7.5 Hz, 2H), 7.11 (dt, *J* = 14.8, 7.7 Hz, 2H), 6.98 (s, 1H), 6.94 – 6.89 (m, 2H), 6.77 (s, 1H), 6.27 (s, 1H), 5.31 (s, 3H), 2.52 (s, 3H), 2.39 (s, 3H), 2.33 (s, 3H), 2.08 (s, 3H), 1.80 (s, 3H), 0.94 (s, 3H), 0.08 (s, 0H).

^{13}C NMR (151 MHz, Tetrachloroethane-*d*$_2$, 53.4ppm, +25°C) δ 148.7, 142.9, 142.8, 141.4, 141.2, 140.97, 140.6, 140.1, 140.0, 139.4, 138.7, 133.2, 132.2, 129.2, 129.1, 129.0, 128.7, 128.2, 128.1, 128.0, 127.7, 127.5, 125.8, 125.5, 125.4, 124.3, 124.2, 123.9, 123.7, 122.2, 119.2, 118.0, 114.6, 53.7, 53.6, 53.4, 53.2, 53.0, 29.6, 22.8, 22.7, 22.5, 21.9, 21.1, 20.8, 20.7, 20.2, 19.9, 17.0.

^{11}B-NMR (192 MHz, Methylene Chloride-d$_2$, Rif.BF$_3$OEt$_2$, +25°C) δ 55.48.

The product **11a** was obtained from general procedure with a yield of 10%.

For DFT calculations of GS and TSs state of compound **11a** see Table 3 at 3.1 Conformational Studies and DFT Calculations.

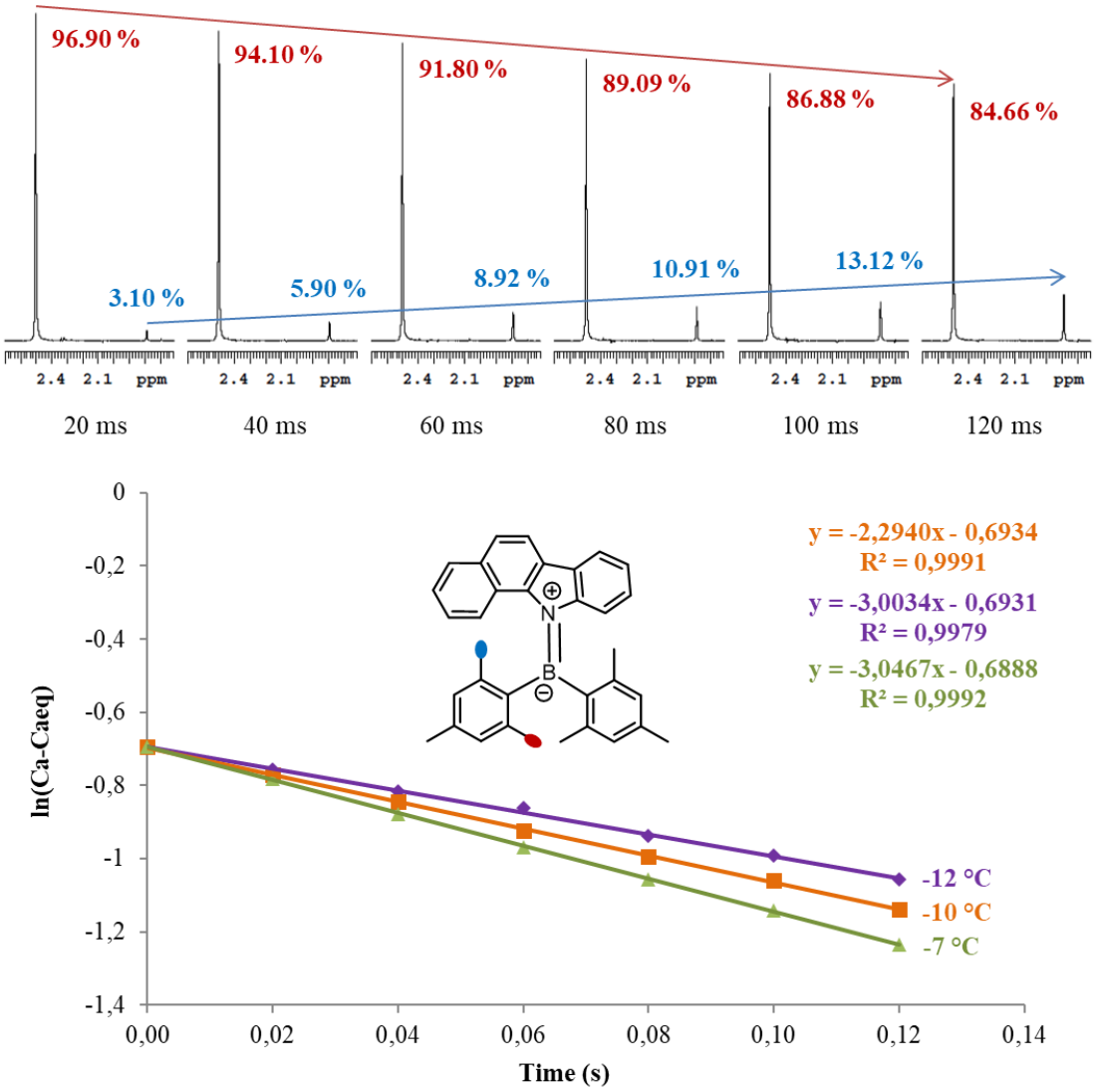

t (s)	T (°C)		
	-12	-10	-7
	ln (Ca - Caeq)		
0.0	-0.693147181	-0.693147181	-0.693147181
0.02	-0.757152511	-0.772190388	-0.783071888
0.04	-0.818710404	-0.84304027	-0.87803202
0.06	-0.872273846	-0.922560345	-0.968110481
0.08	-0.939303506	-0.99479296	-1.056127677
0.10	-0.997500787	-1.060161102	-1.141624179
0.12	-1.059583902	-1.140059479	-1.233744963
$\Delta G^{\neq}$ (kcal/mol)	15.00	15.01	15.08
	15.0		

Fig.27 *EXSY of* ***11a****. Up experimental spectra at different mixing time; middle plotted mixing time and K values; down a tab. of k and relative* $\Delta G^{\neq}$ *at various T.*

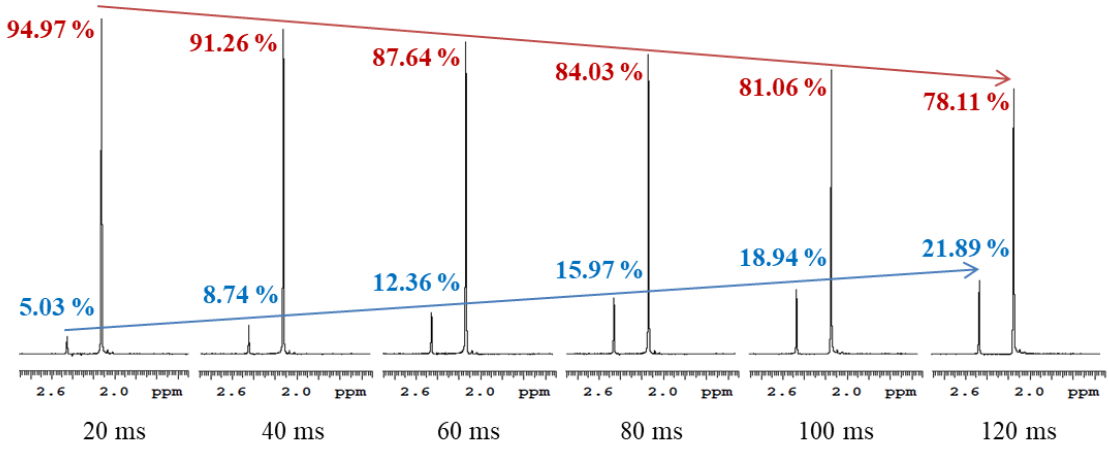

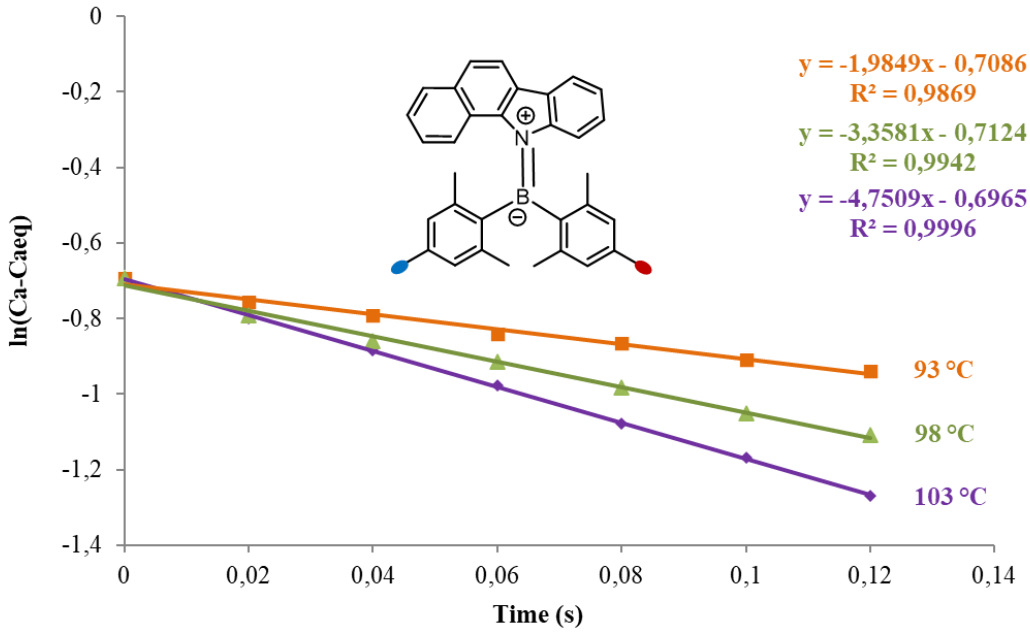

t (s)	T (°C)		
	93	98	103
	ln (Ca - Caeq)		
0	-0.693147181	-0.693147181	-0.693147181
0.02	-0.756299996	-0.792083928	-0.799174585
0.04	-0.792304752	-0.858257701	-0.885276678
0.06	-0.841183259	-0.915041512	-0.977102871
0.08	-0.86441011	-0.981896489	-1.077927697
0.1	-0.908322562	-1.049536451	-1.169249368
0.12	-0.93828075	-1.10714862	-1.269044801
$\Delta G^{\neq}$ (kcal/mol)	21.58	21.50	21.54
	21.5		

Fig.28 *EXSY of* ***11a****. Up experimental spectra at different mixing time; middle plotted mixing time and K values; down a tab. of k and relative* $\Delta G^{\neq}$ *at various T.*

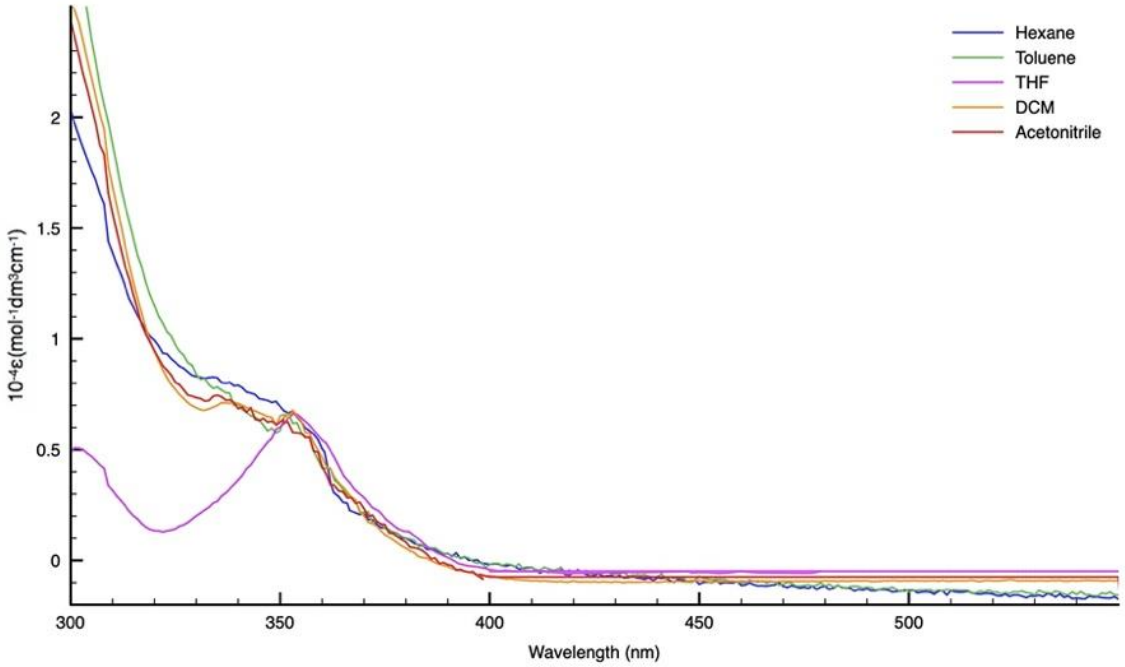

Fig.29 *Absorption Profiles of* ***11a*** *in different solvent at 298K.*

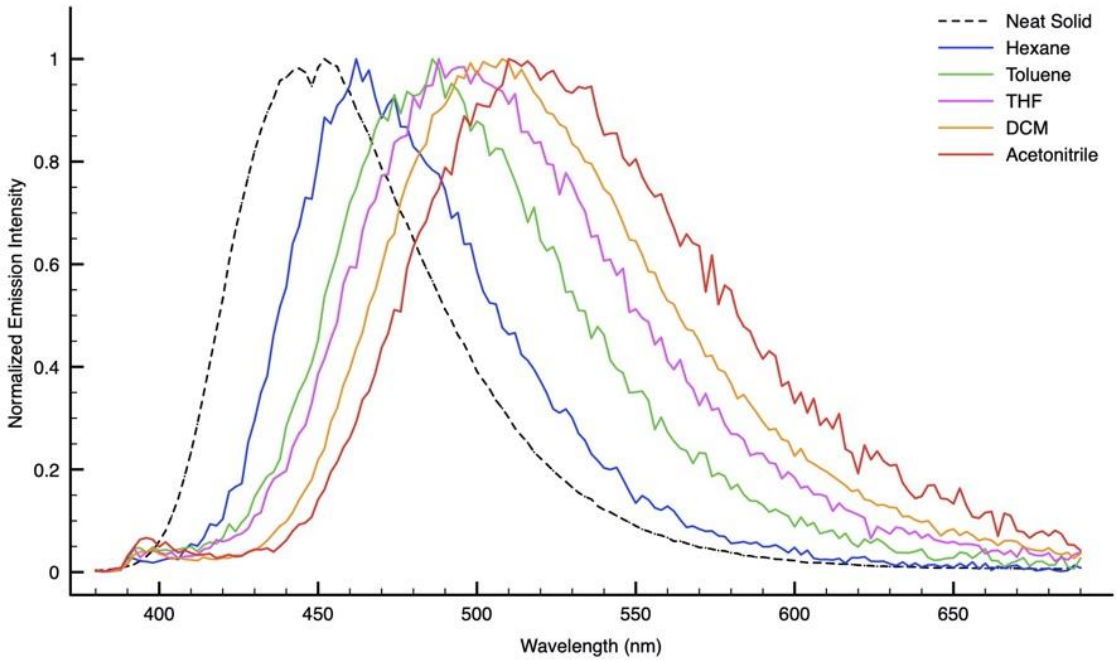

Fig.30 *Normalized Emission Profiles of* ***10a*** *in different solvent at 298K.*

Tab.12 *Fluorescence values for* ***11a*** *vs Quinine Sulphate/0.05 M H_2SO_4, Φ = 0.53 [iv], λ_{exc} = 350 nm.*

Compound	Solvent	Absorption	Emission 298K			Emission Neat Solid Matrix 298K	
		λ(nm) $10^{-4}\varepsilon$ ($cm^{-1}M^{-1}$)	λ_{em} (nm)	τ_{ox} (ns)	ϕ_{ox}* (%)	λ_{em} (nm)	τ (ns)
11a	solid	/	/	/	/	448	6
	Hex	351 (0.71)	466	9.7	9.12	/	/
	Toluene	352 (0.66)	486	12.5	14.2	/	/
	THF	353 (0.66)	496	14.3	13.9	/	/
	DCM	353 (0.68)	516	18.9	40	/	/
	CH_3CN	353 (0.58)	504	15	9.7	/	/

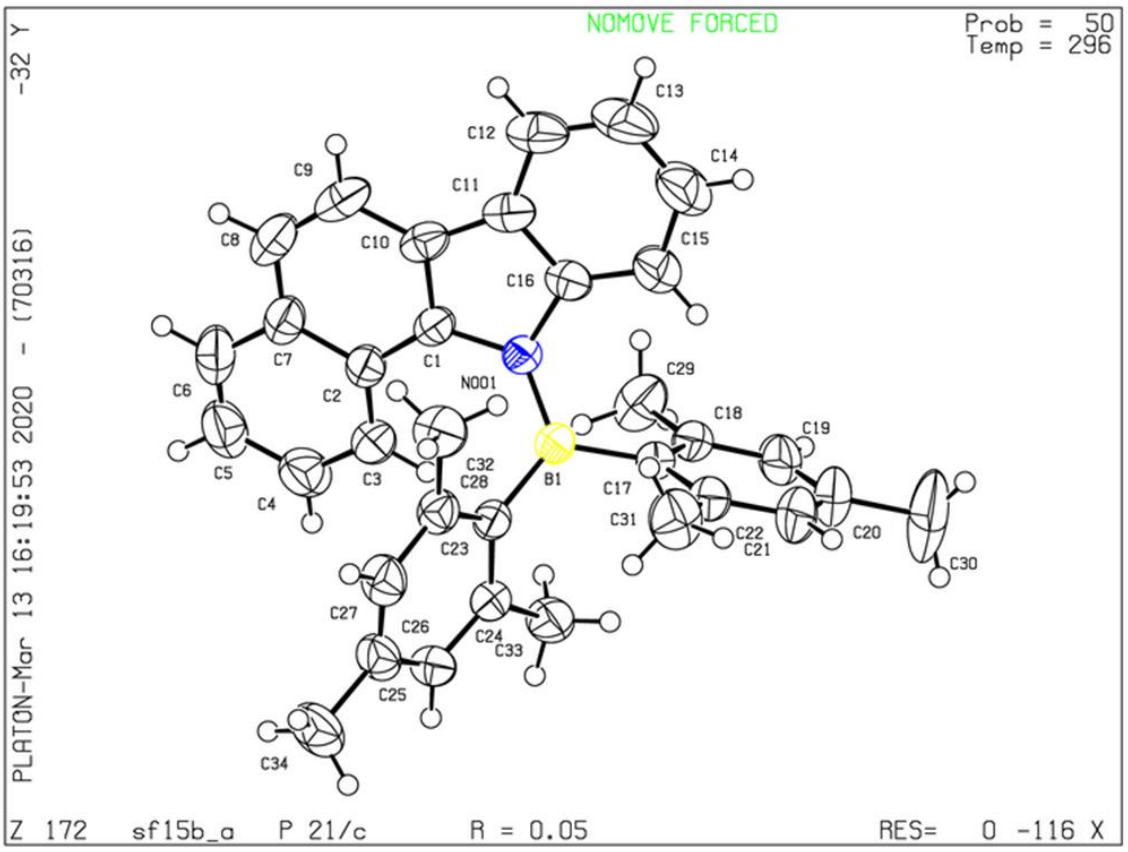

Cell: a=11.5407(6) b=8.4893(5) c=27.6625(15)
alpha=90 beta=98.960(2) gamma=90

Fig.31 *Crystal structure and cell data of compound* ***11a***.

6.5.8 Bis-mesityl-8-isopropil-11-benzo[a]carbazole-borane 11b

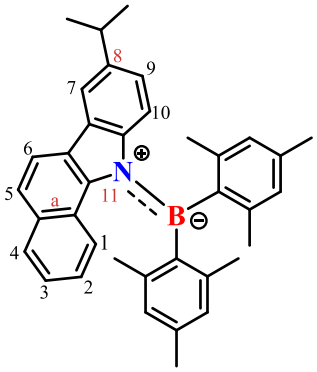

11b

^{1}H-NMR (600 MHz, Methylene Chloride-d$_2$, 5.33 ppm, +25°C) δ 8.13 (d, *J* = 8.4 Hz, 1H), 8.02 (dd, *J* = 8.6, 1.0 Hz, 1H), 7.92 (d, *J* = 1.9 Hz, 1H), 7.88 – 7.83 (m, 1H), 7.78 (d, *J* = 8.3 Hz, 1H), 7.27 (ddd, *J* = 8.0, 6.8, 1.1 Hz, 1H), 7.12 (ddd, *J* = 8.3, 6.8, 1.3 Hz, 1H), 7.03 – 6.98 (m, 2H), 6.93 (s, 1H), 6.81 – 6.77 (m, 2H), 6.29 (s, 1H), 3.06 (p, *J* = 6.9 Hz, 1H), 2.53 (s, 3H), 2.41 (s, 3H), 2.35 (s, 3H), 2.10 (s, 3H), 1.82 (s, 3H), 1.34 (dd, *J* = 7.0, 4.1 Hz, 7H), 1.28 (s, 1H), 0.98 (s, 3H), 0.09 (s, 1H).

^{13}C-NMR (151 MHz, Tetrachloroethane-*d*$_2$, 53.4ppm, +25°C) δ 143.0, 142.9, 141.3, 141.22, 141.2, 140.9, 140.7, 140.1, 139.9, 139.3, 138.3, 133.1, 129.1, 129.0, 128.6, 128.2, 128.1, 128.1, 128.0, 125.6, 125.5, 124.8, 124.1, 124.0, 123.9, 123.6, 118.0, 116.4, 114.4, 53.7, 53.6, 53.4, 53.2, 53.0, 33.9, 24.1, 24.0, 22.8, 22.7, 22.5, 22.1, 22.0, 21.1, 20.8, 20.7, 20.0, 0.2.

^{11}B-NMR (192 MHz, Methylene Chloride-d$_2$, Rif.BF$_3$OEt$_2$, +25°C) δ 54.64.

The product **11b** was obtained from general procedure with a yield of 54%.

Table 13. DFT calculations of GS and TSs state of compound **11b**.

State	2D structure	3D structure	Total Energy (a.u.)	Rel. E. Calculated (kcal/mol)
GS	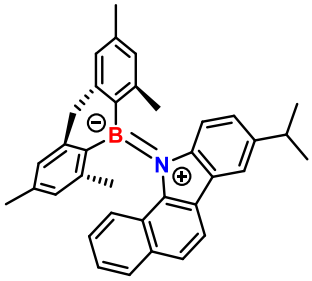	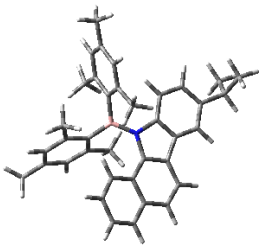	-1512.896562	0.0
2RF-TS (two-ring-flip) mes-mes	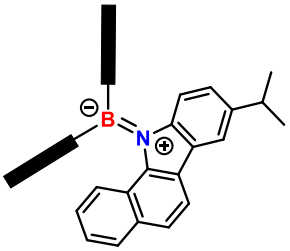	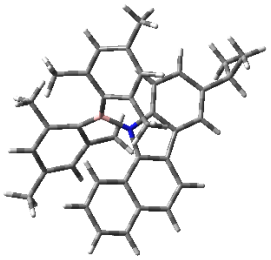	-1512.87041100	**16.4**
2RF-TS (two-ring-flip) mes-carb	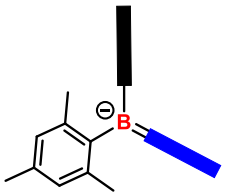	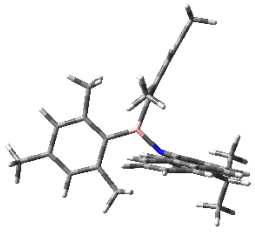	-1512.866307	**19.0**

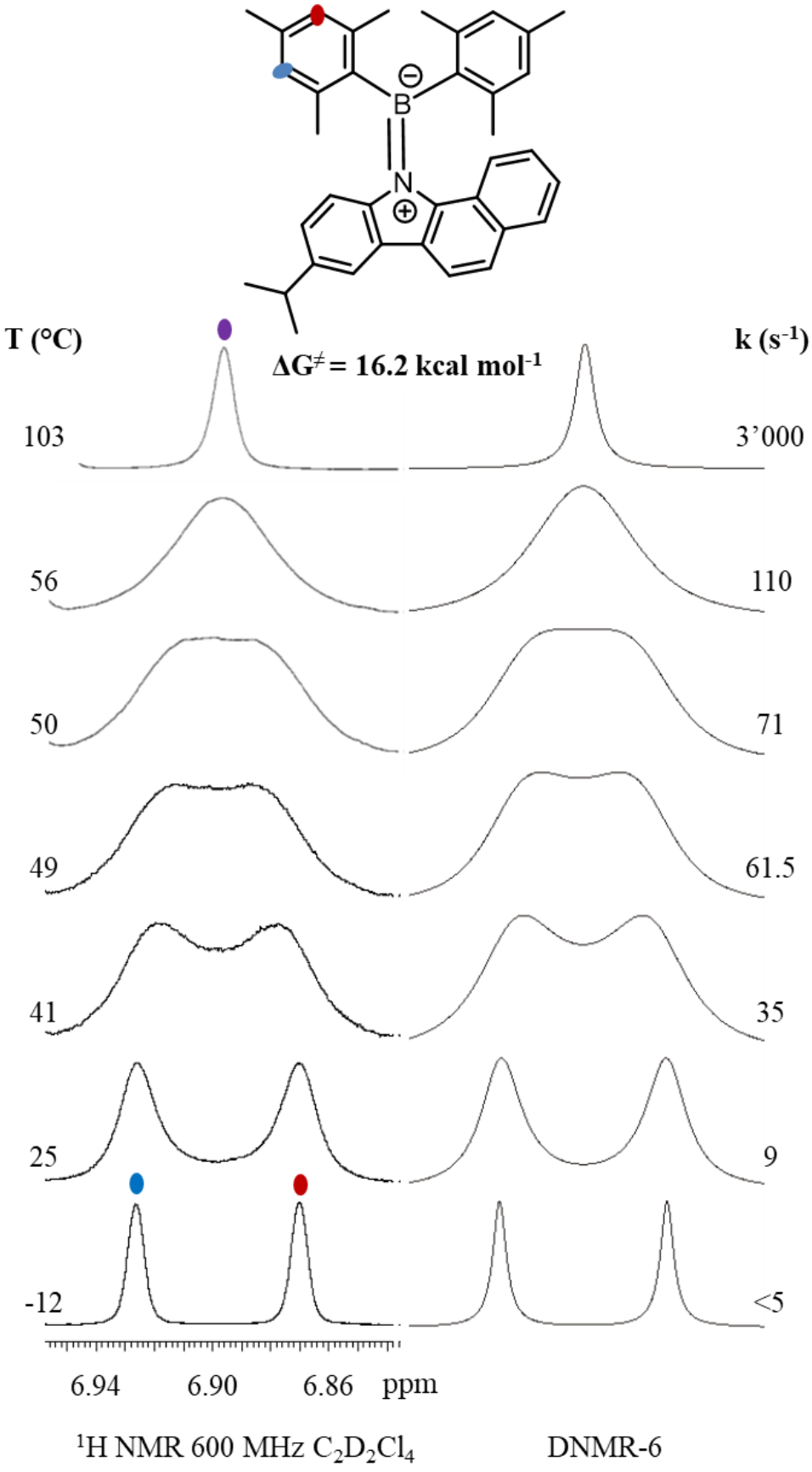

Fig.32 *DNMR of* ***11b****. left experimental spectra at different temperatures; right simulated spectra with different kinetic constants.*

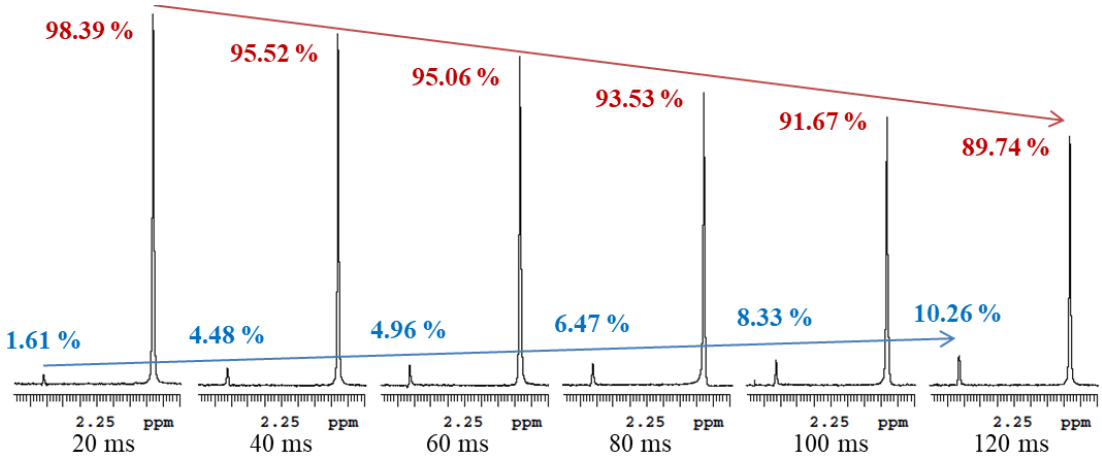

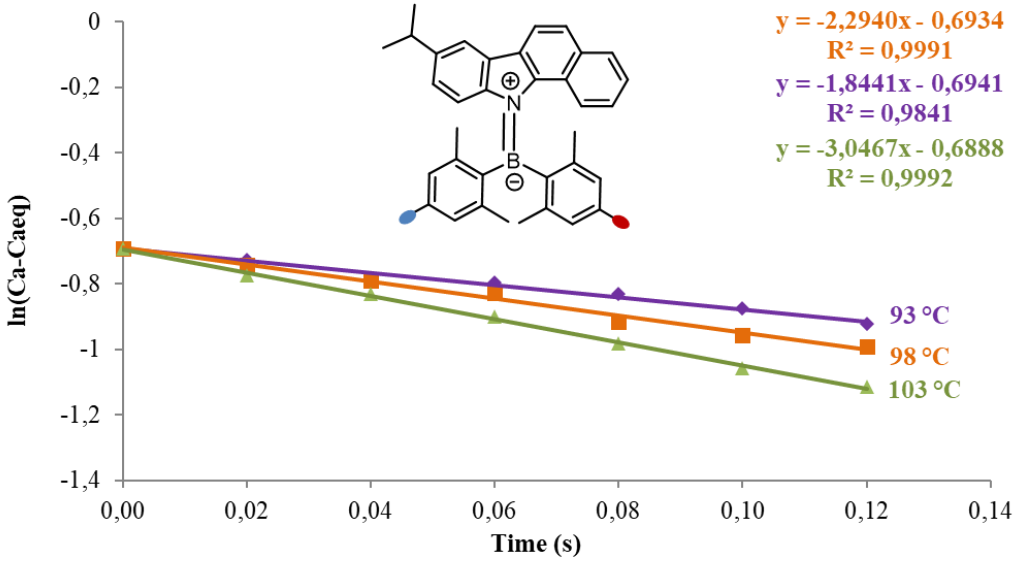

t (s)	T (°C)		
	93	98	103
	ln (Ca - Caeq)		
0	-0.693	-0.693	-0.693
0.02	-0.733	-0.743	-0.780
0.04	-0.779	-0.789	-0.844
0.06	-0.809	-0.828	-0.909
0.08	-0.839	-0.915	-1.002
0.1	-0.876	-0.957	-1.061
0.12	-0.924	-0.991	-1.141
$\Delta G^{\neq}$ (kcal/mol)	21.63	21.69	21.73
	21.7		

Fig.33 *EXSY of* ***11b****. Up experimental spectra at different mixing time; middle plotted mixing time and K values; down a tab. of k and relative* $\Delta G^{\neq}$ *at various T.*

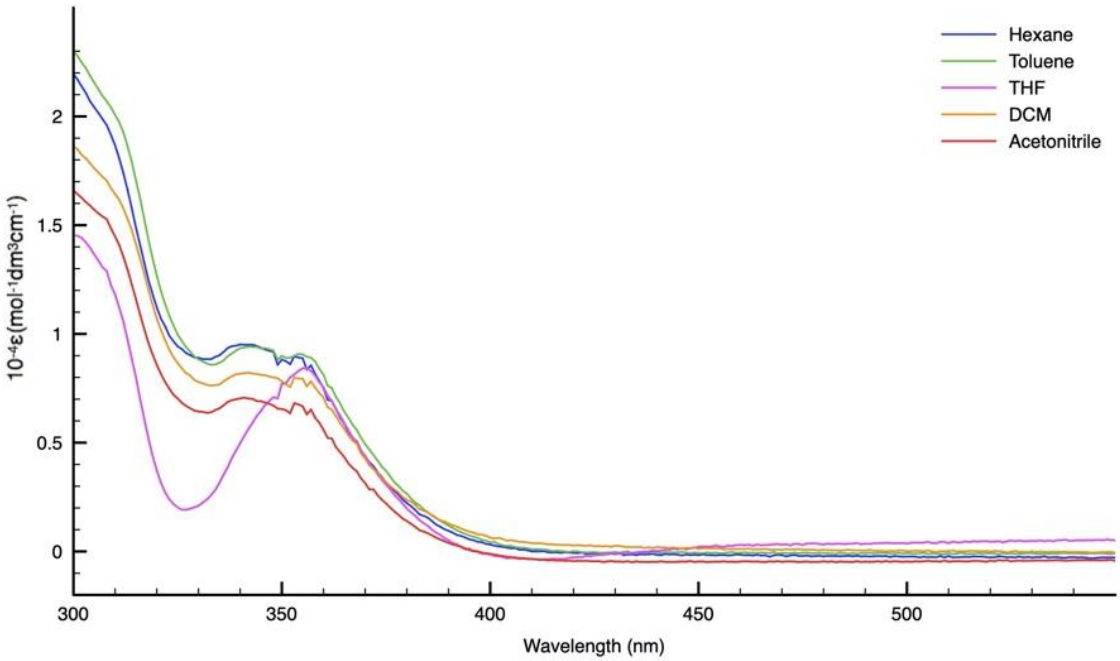

Fig.34 *Absorption Profiles of* ***11b*** *in different solvent at 298K.*

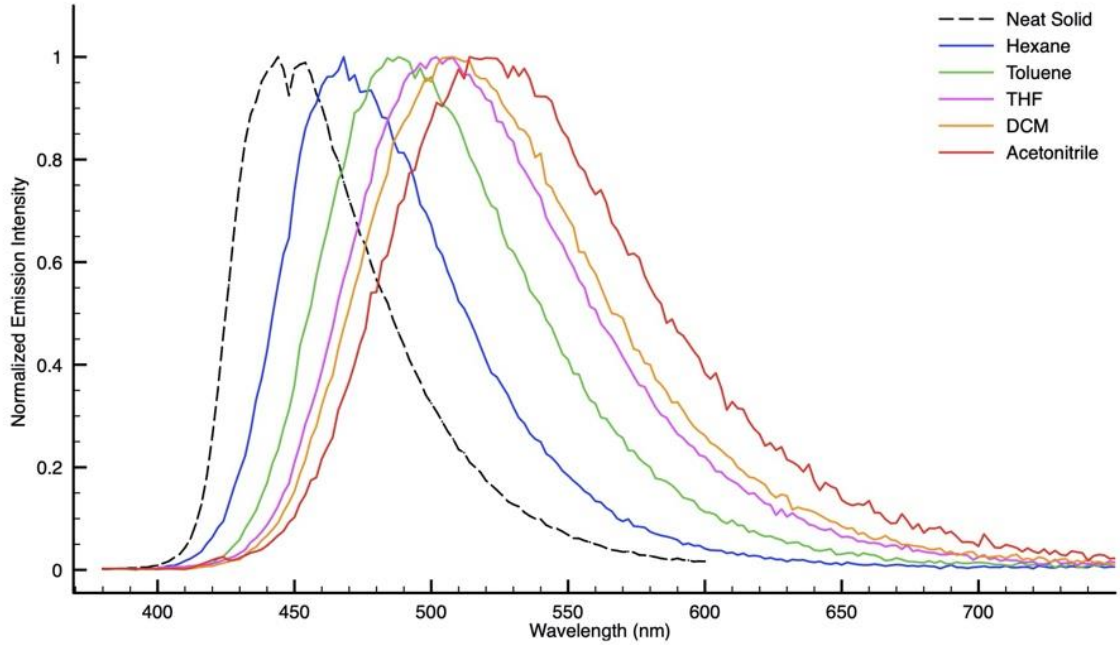

Fig.35 *Normalized Emission Profiles of* ***11b*** *in different solvent at 298K.*

Tab.14 *Fluorescence values for* ***11b*** *vs Quinine Sulphate/0.05 M H_2SO_4, Φ = 0.53 [v], λ_{exc} = 350 nm.*

Compound	Solvent	Absorption	Emission 298K			Emission Neat Solid Matrix 298K	
		λ(nm) $10^{-4}\varepsilon$ ($cm^{-1}M^{-1}$)	λ_{em} (nm)	τ_{ox} (ns)	ϕ_{ox}* (%)	λ_{em} (nm)	τ (ns)
11b	solid	/	/	/	/	450	5.6
	Hex	342 (0.95)	466	10	19.7	/	/
	Toluene	344 (0.94)	488	13.4	30.1	/	/
	THF	356 (0.84)	504	20	48.6	/	/
	DCM	343 (0.82)	510	19	25	/	/
	CH_3CN	343 (0.70)	520	14	21.4	/	/

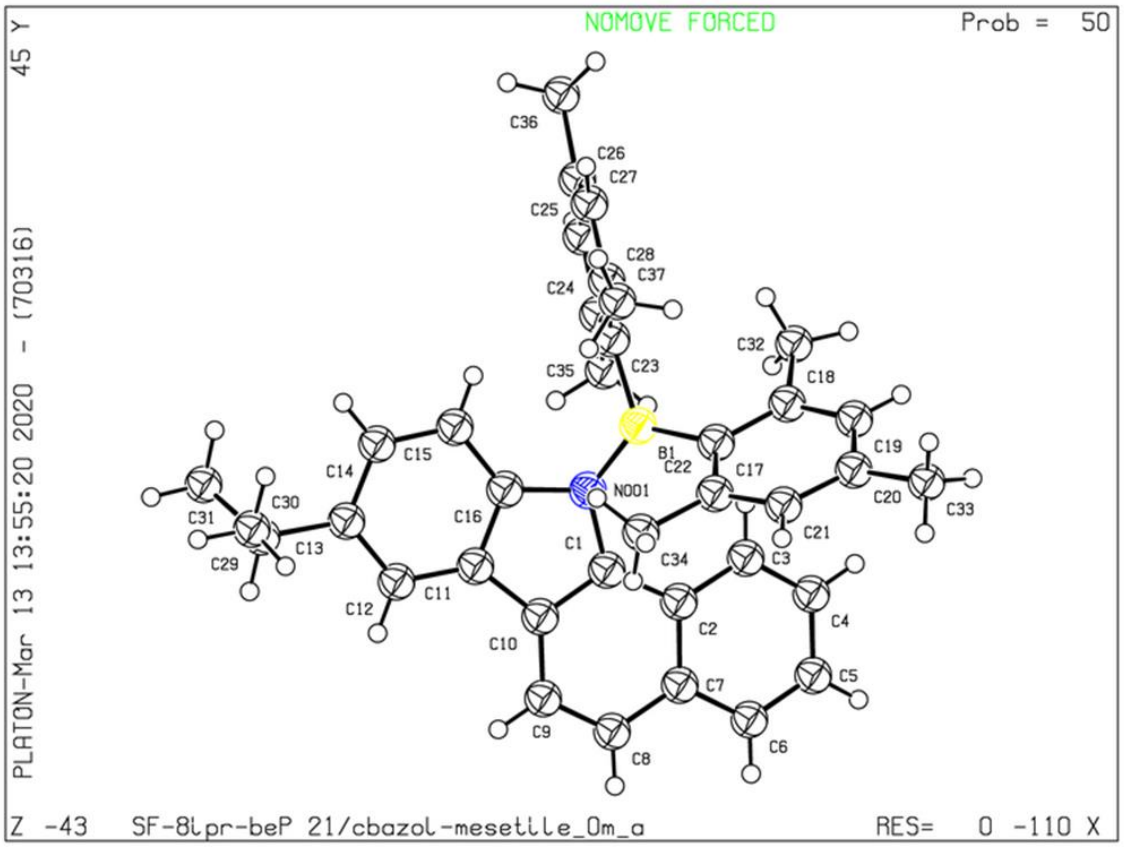

Cell: a=15.957(3) b=8.378(2) c=22.580(5)

alpha=90 beta=104.29(3) gamma=90

Fig.36 *Crystal structure and cell data of compound* ***11a****.*

6.5.9 Bis-mesityl-8-OMe-11-benzo[a]carbazole-borane 11c

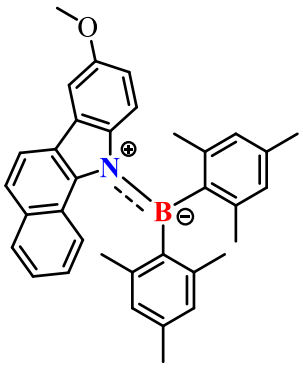

11c

^{1}H NMR (600 MHz, Tetrachloroethane-*d*$_2$, 6.0ppm, -10°C) δ 8.08 (d, *J* = 8.4 Hz, 1H), 7.98 (d, *J* = 8.5 Hz, 1H), 7.84 (dd, *J* = 8.3, 1.2 Hz, 1H), 7.76 (d, *J* = 8.5 Hz, 1H), 7.50 (d, *J* = 2.6 Hz, 1H), 7.27 (ddd, *J* = 8.0, 6.7, 1.1 Hz, 1H), 7.12 (ddd, *J* = 8.2, 6.8, 1.3 Hz, 1H), 6.94 (s, 1H), 6.88 (s, 1H), 6.78 (d, *J* = 9.2 Hz, 1H), 6.76 – 6.70 (m, 2H), 6.23 (s, 1H), 6.00 (s, 1H), 5.32 (s, 1H), 3.89 (s, 3H), 2.49 (s, 3H), 2.38 (s, 3H), 2.30 (s, 3H), 2.06 (s, 3H), 1.78 (s, 3H), 1.69 (s, 1H), 0.95 (s, 3H).

^{13}C NMR (151 MHz, Tetrachloroethane-*d*$_2$, 6.0ppm, -10°C) δ 155.2, 142.8, 141.4, 141.1, 140.9, 140.8, 139.9, 139.2, 137.3, 133.0, 129.3, 129.2, 128.8, 128.5, 128.3, 128.2, 125.6, 125.3, 124.6, 124.1, 124.0, 123.9, 118.4, 115.8, 114.0, 102.0, 74.2, 74.0, 73.8, 55.9, 54.1, 23.4, 23.3, 22.6, 21.8, 21.4, 20.5.

^{11}B-NMR (192 MHz, Methylene Chloride-d$_2$, Rif.BF$_3$OEt$_2$, +25°C) δ 54.57.

The product **11c** was obtained from general procedure with a yield of 66%.

Table 15. DFT calculations of GS and TSs state of compound **11c**.

State	2D structure	3D structure	Total Energy (a.u.)	Rel. E. Calculated (kcal/mol)
GS	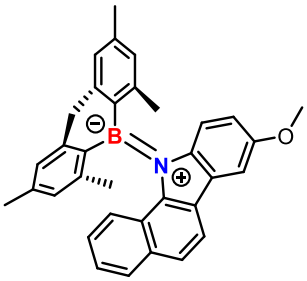	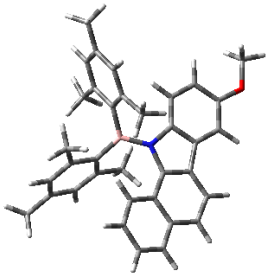	-1509.47332600	0.0
2RF-TS (two-ring-flip) mes-mes	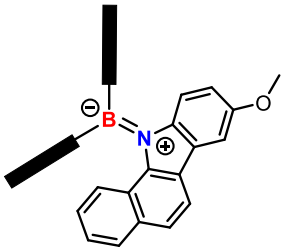	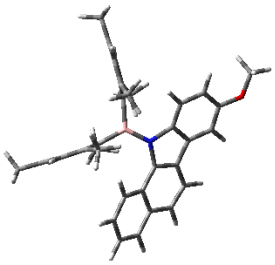	-1509.44770100	**16.1**
2RF-TS (two-ring-flip) mes-carb	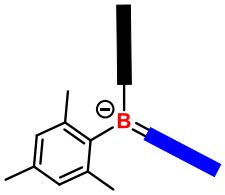	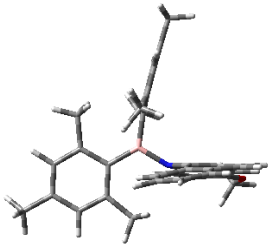	-1509.442472	**19.4**

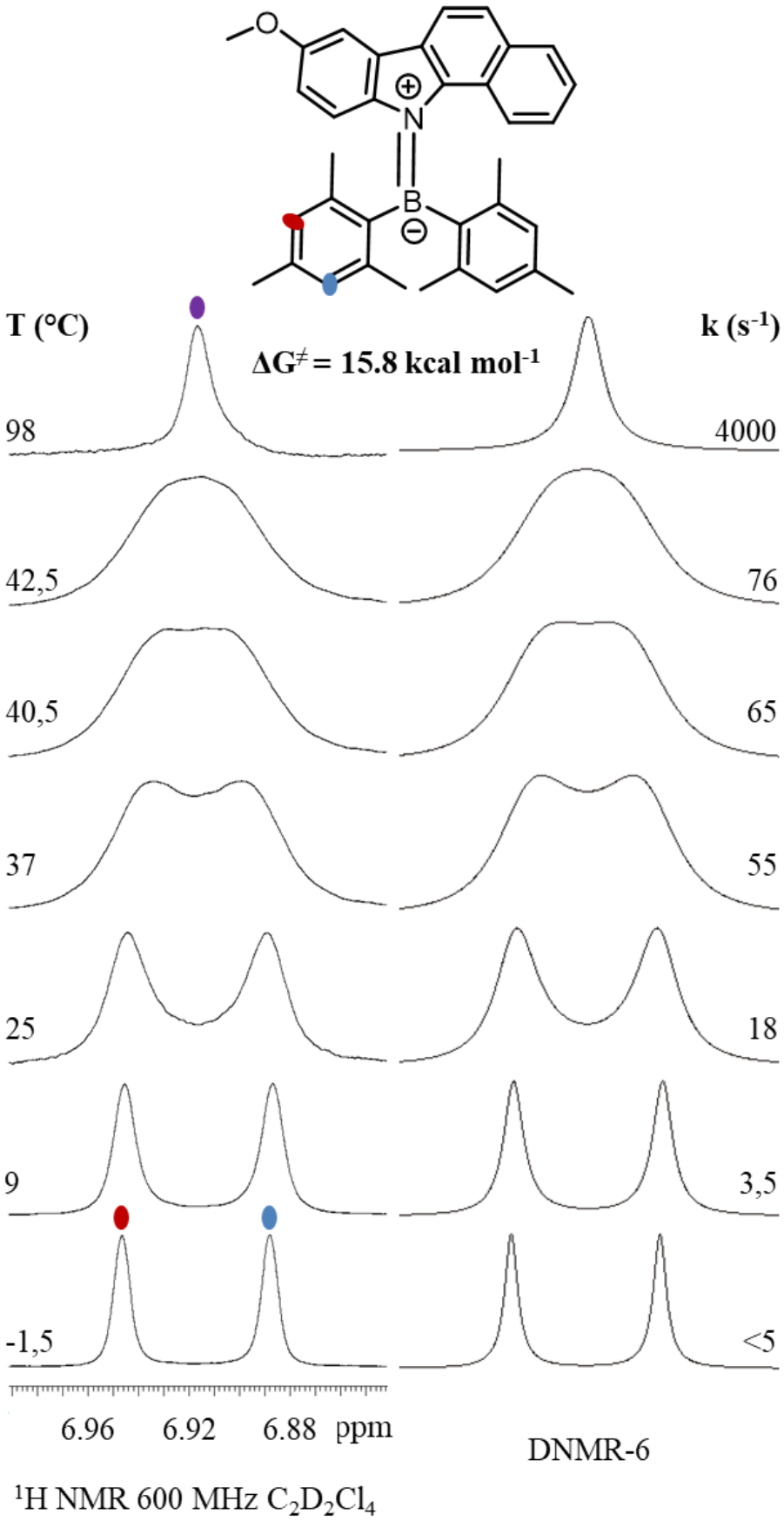

Fig.37 *DNMR of* ***11c****. left experimental spectra at different temperatures; right simulated spectra with different kinetic constants.*

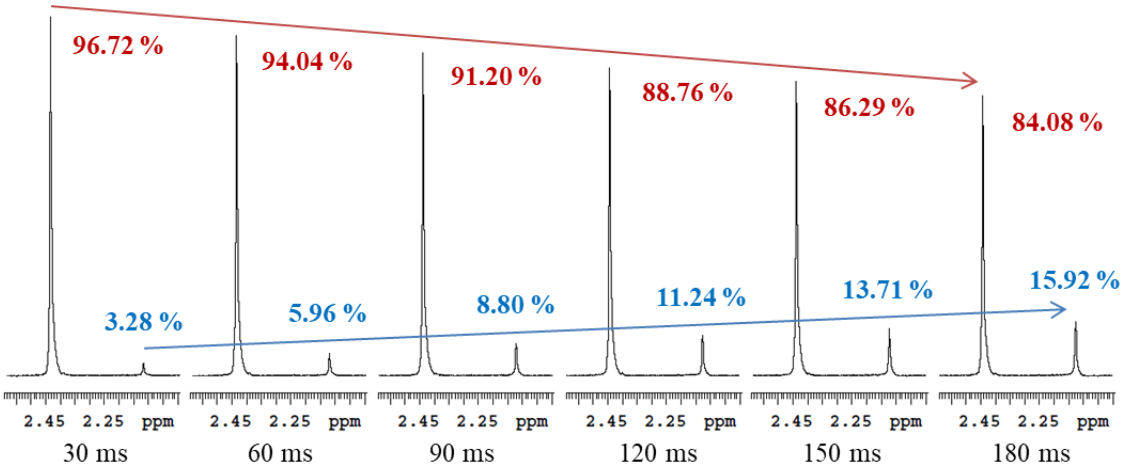

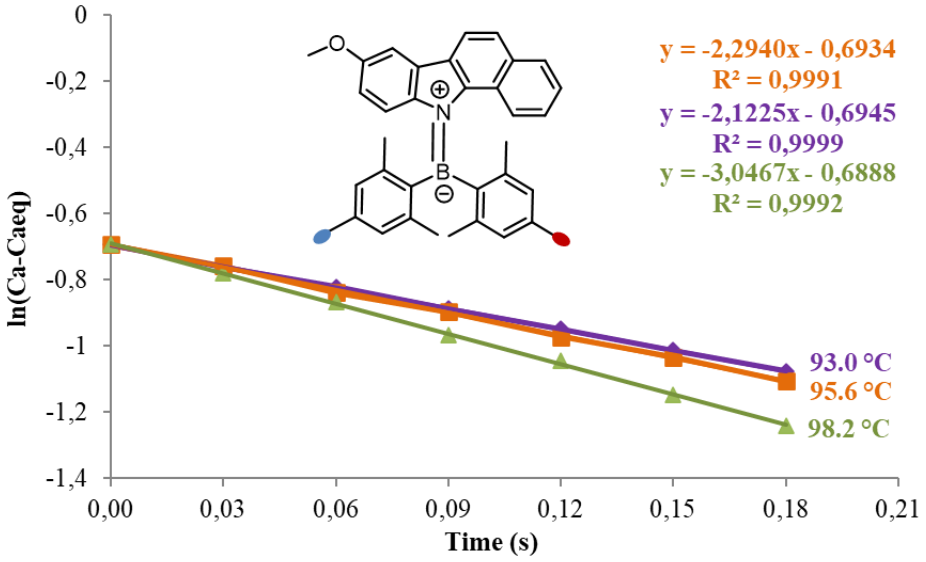

t (s)	T (°C)		
	93	95.6	98.2
	ln (Ca - Caeq)		
0	-0.693147181	-0.693147181	-0.693147181
0.03	-0.760997847	-0.757152511	-0.780013114
0.06	-0.820071874	-0.838635487	-0.867500568
0.09	-0.88673193	-0.897468978	-0.966531948
0.12	-0.947781399	-0.972067747	-1.044124103
0.15	-1.013627965	-1.033386504	-1.14696255
0.18	-1.076459484	-1.106846094	-1.242713633
$\Delta G^{\neq}$ (kcal/mol)	21.53	21.63	21.58
	21.6		

Fig.38 *EXSY of* ***11c****. Up experimental spectra at different mixing time; middle plotted mixing time and K values; down a tab. of k and relative* $\Delta G^{\neq}$ *at various T.*

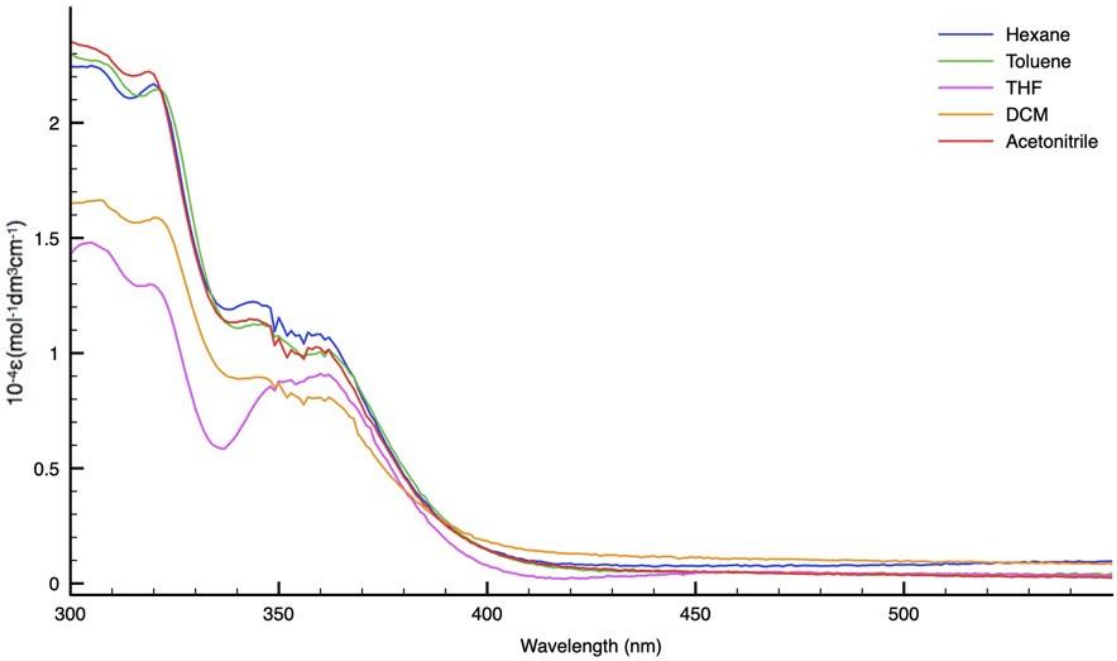

Fig.39 *Absorption Profiles of* ***11c*** *in different solvent at 298K.*

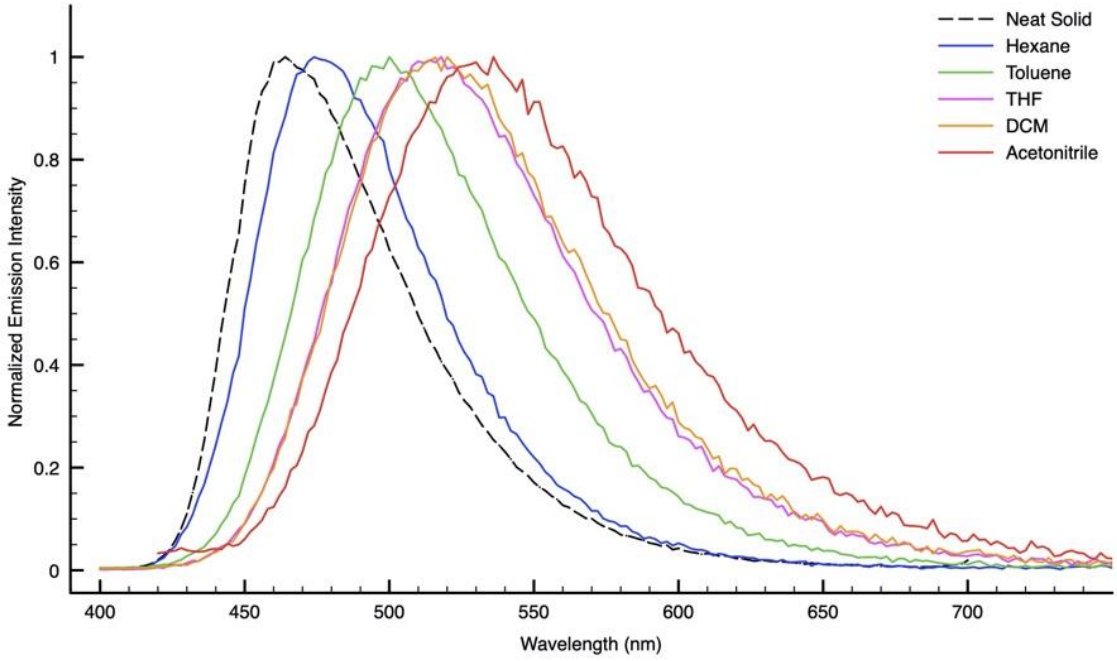

Fig.40 *Normalized Emission Profiles of* ***11c*** *in different solvent at 298K.*

Tab.16 *Fluorescence values for* ***11c*** *vs Quinine Sulphate/0.05 M H_2SO_4, Φ = 0.53 [vi], λ_{exc} = 350 nm.*

Compound	Solvent	Absorption	Emission 298K			Emission Neat Solid Matrix 298K	
		λ(nm) 10^{-4}ε ($cm^{-1}M^{-1}$)	λ_{em} (nm)	τ_{ox} (ns)	ϕ_{ox}* (%)	λ_{em} (nm)	τ (ns)
11c	solid	/	/	/	/	466	11
	Hex	307 (2.23), 320 (2.17), 344 (1.22), 361 (1.06)	478	9	15.4	/	/
	Toluene	309 (2.25), 320 (2.14), 345 (1.12), 360 (1.00)	498	12	23	/	/
	THF	305 (1.48), 320 (1.30), 360 (0.91)	516	18.6	33.9	/	/
	DCM	307 (1.66), 322 (1.58), 344 (0.89), 363 (0.80)	520	17	18.4	/	/
	CH_3CN	307 (2.31), 320 (2.21), 346 (1.13), 361 (1.00)	530	13	13	/	/

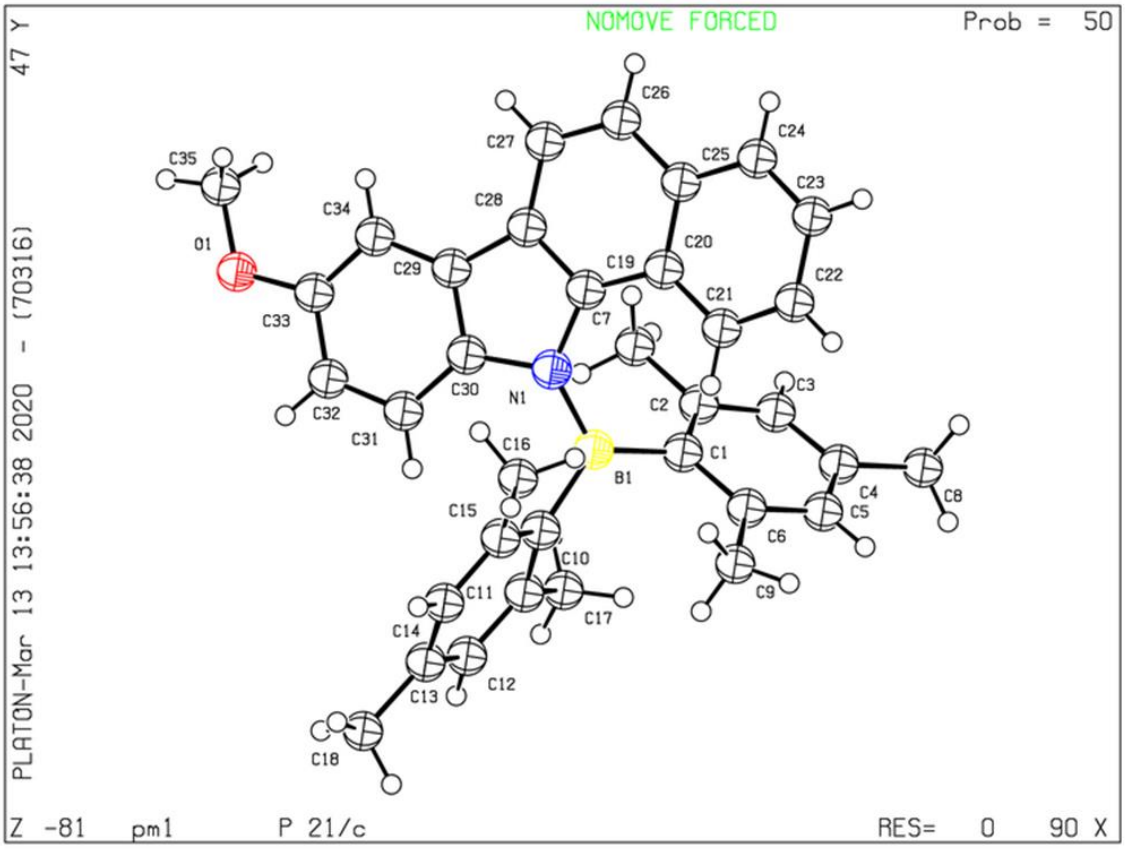

Cell: a=13.0769(10) b=8.4867(6) c=25.5513(19)

alpha=90 beta=93.326(2) gamma=90

Fig.41 *Crystal structure and cell data of compound* ***11c****.*

6.5.10 Bis-mesityl-8-CF_3-11-benzo[a]carbazole-borane 11d

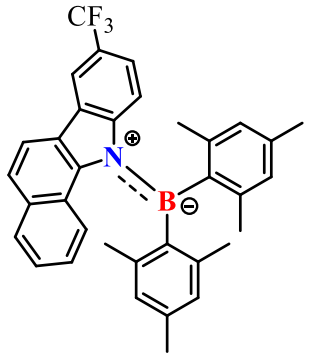

11d

^{1}H-NMR (600 MHz, Methylene Chloride-d_2, 5.36 ppm, -10°C)

δ 8.41 – 8.38 (m, 1H), 8.19 (d, *J* = 8.5 Hz, 1H), 8.09 – 8.04 (m, 1H), 7.92 (dd, *J* = 7.9, 1.2 Hz, 1H), 7.87 (d, *J* = 8.4 Hz, 1H), 7.41 – 7.33 (m, 2H), 7.22 (ddd, *J* = 8.2, 6.8, 1.3 Hz, 1H), 7.02 (d, *J* = 8.0 Hz, 2H), 6.97 (s, 1H), 6.83 (s, 1H), 6.32 (s, 1H), 2.50 (s, 3H), 2.39 (d, *J* = 29.4 Hz, 6H), 2.11 (s, 3H), 1.82 (s, 3H), 1.26 (s, 1H), 0.94 (s, 3H).

^{19}F NMR (376 MHz Methylene Chloride-d_2, Rif.BF_3OEt_2, +25°C) δ -61.27.

The product **11d** was obtained from general procedure with a yield of 31%.

Table 17. DFT calculations of GS and TSs state of compound **11d**.

State	2D structure	3D structure	Total Energy (a.u.)	Rel. E. Calculated (kcal/mol)
GS	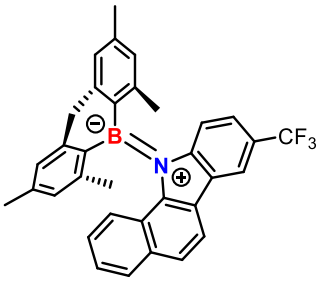	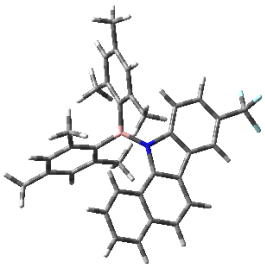	-1732.062604	0.0
2RF-TS (two-ring-flip) mes-mes	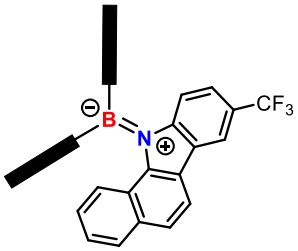	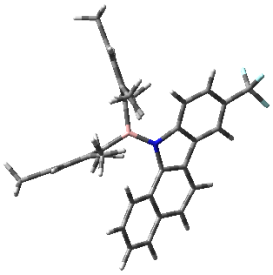	-1732.035733	**16.9**
2RF-TS (two-ring-flip) mes-carb	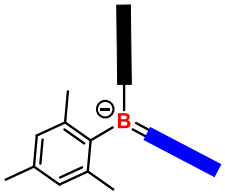	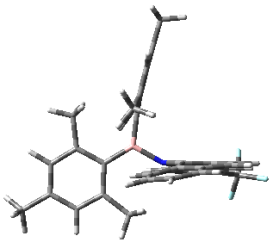	-1732.033272	**18.4**

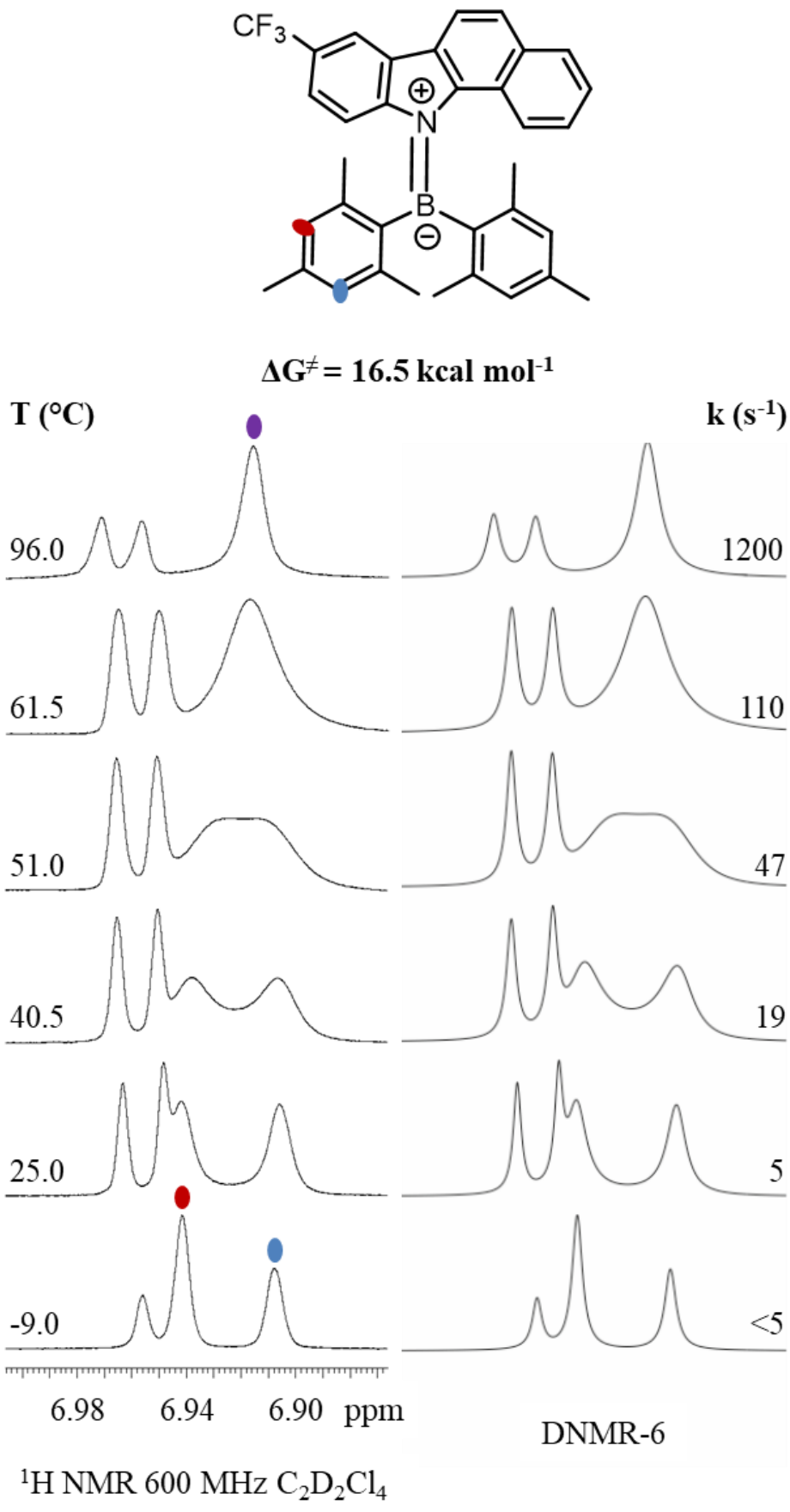

Fig.42 *DNMR of* ***11d****. left experimental spectra at different temperatures; right simulated spectra with different kinetic constants.*

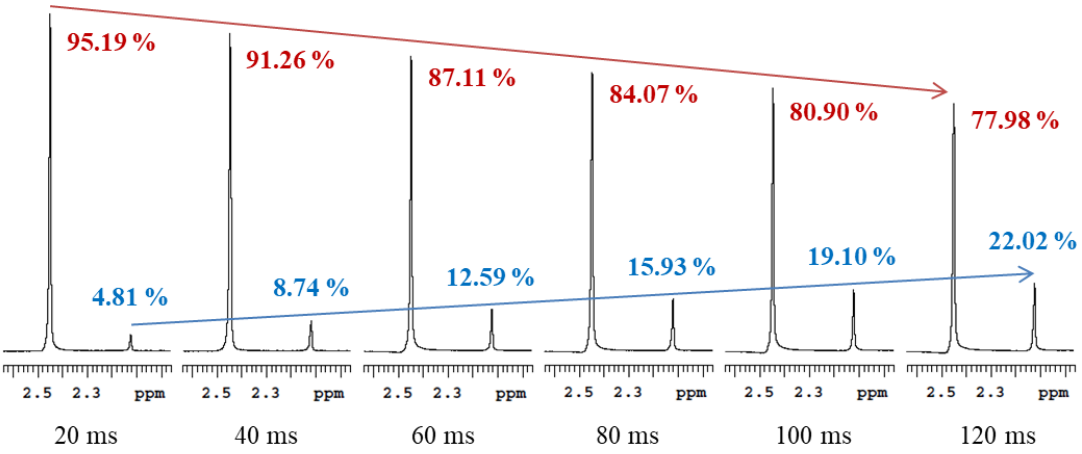

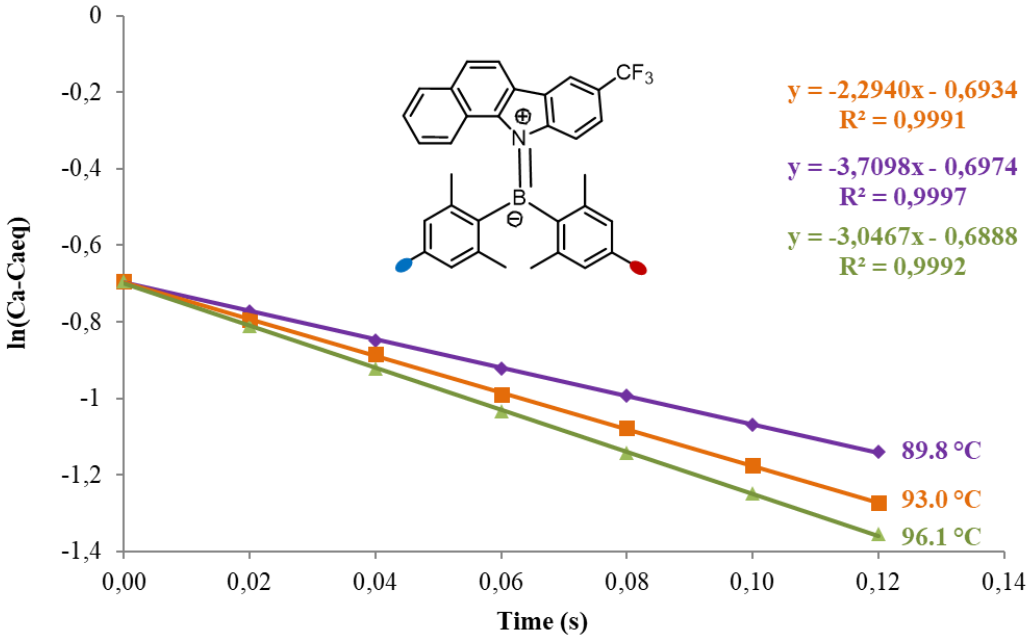

t (s)	T (°C)		
	89.8	93	96.1
	ln (Ca - Caeq)		
0	-0.693147181	-0.693147181	-0.693147181
0.02	-0.773489933	-0.794294363	-0.809680997
0.04	-0.849333264	-0.885276678	-0.923063616
0.06	-0.921303274	-0.991283711	-1.033105486
0.08	-0.993711879	-1.076752954	-1.141937413
0.1	-1.068277089	-1.174414002	-1.248621556
0.12	-1.140998005	-1.273680217	-1.355183366
$\Delta G^{\neq}$ (kcal/mol)	20.93	20.94	21.02
	21.0		

Fig.43 *EXSY of* ***11d.*** *Up experimental spectra at different mixing time; middle plotted mixing time and K values; down a tab. of k and relative $\Delta G^{\neq}$ at various T.*

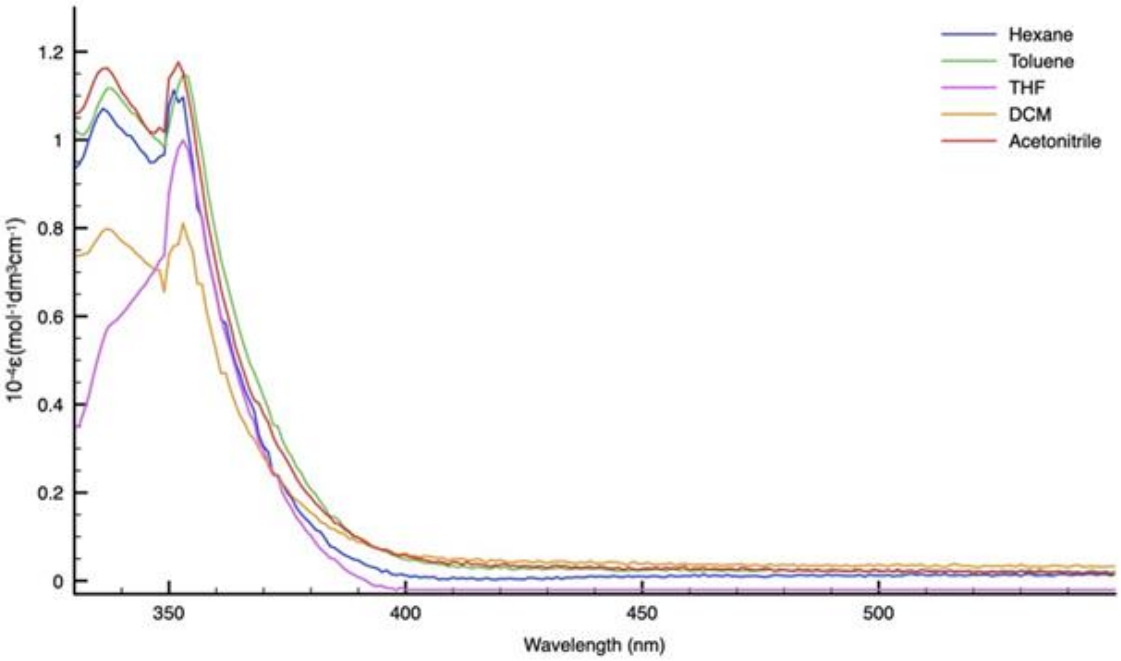

Fig.44 *Absorption Profiles of* ***11d*** *in different solvent at 298K.*

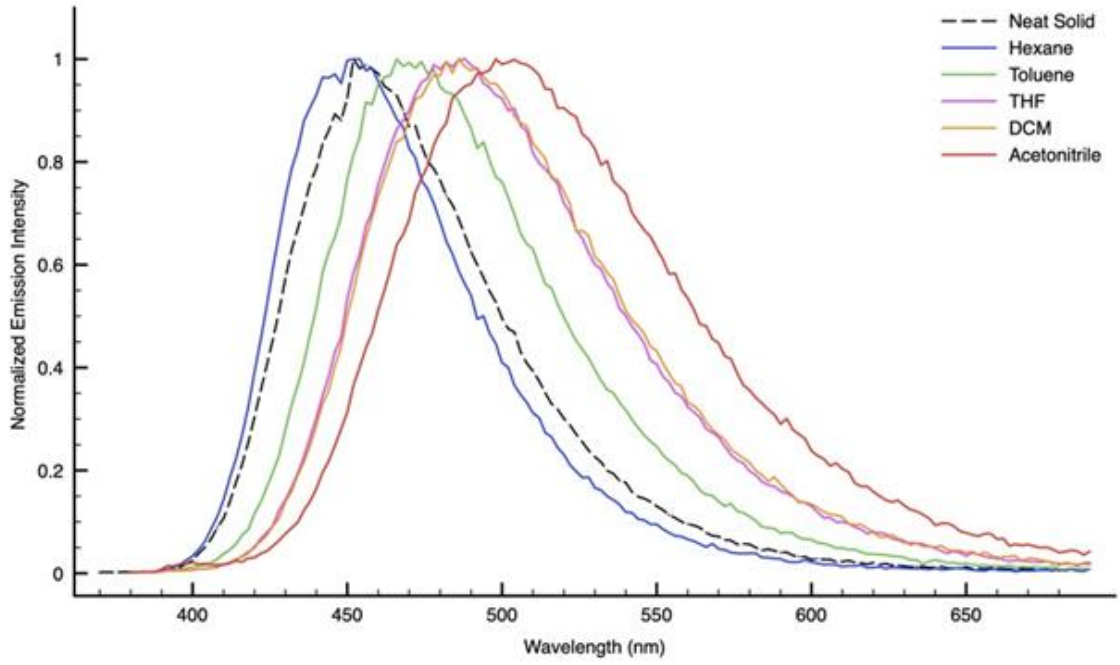

Fig.45 *Normalized Emission Profiles of* ***11d*** *in different solvent at 298K.*

Tab.18 *Fluorescence values for* ***11d*** *vs Quinine Sulphate/0.05 M H_2SO_4, $\Phi = 0.53$ [vii], $\lambda_{exc} = 350$ nm.*

Compound	Solvent	Absorption	Emission 298K			Emission Neat Solid Matrix 298K	
		λ(nm) $10^{-4}\varepsilon$ ($cm^{-1}M^{-1}$)	λ_{em} (nm)	τ_{ox} (ns)	ϕ_{ox}* (%)	λ_{em} (nm)	τ (ns)
11d	solid	/	/	/	/	456	10
	Hex	336 (1.07), 352 (1.09)	452	6	19.9	/	/
	Toluene	337 (1.12), 352 (1.12)	472	11.6	35.1	/	/
	THF	337 (0.57), 353 (0.99)	486	16.4	59.4	/	/
	DCM	337 (0.79), 353 (0.81)	486	16.9	36.5	/	/
	CH_3CN	336 (1.16), 352 (1.18)	502	15	25.4	/	/

6.5.113-isopropil-6-OMe-carbazole 6c

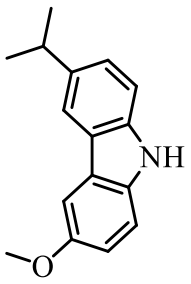

6c

^{1}H-NMR (600 MHz, Chloroform-d, TMS +25°C) δ 8.47 – 8.44 (m, 1H), 8.39 (s, 1H), 8.13 (d, J = 2.5 Hz, 1H), 7.91 (d, J = 8.3 Hz, 1H), 7.91 – 7.85 (m, 2H), 7.84 (s, 1H), 7.62 (dd, J = 8.7, 2.5 Hz, 1H), 4.52 (s, 3H), 3.67 (hept, J = 7.0 Hz, 1H), 2.13 (s, 3H), 1.95 (d, J = 6.9 Hz, 6H), 0.66 (s, 3H).

^{13}C-NMR (151 MHz, Chloroform-d, TMS, +25°C) δ 153.7, 139.8, 138.8, 134.7, 124.8, 123.8, 123.4, 117.3, 114.9, 111.3, 110.5, 103.0, 77.2, 77.0, 76.8, 56.0, 34.1, 24.7.

The product **6c** was obtained from general procedure with a yield of 30%.

6.5.123-isopropil-6-CF_3-carbazole 6d

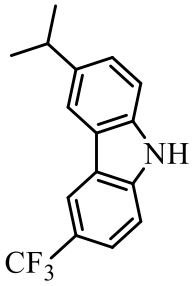

6d

^{1}H-NMR (400 MHz, Chloroform-d, TMS +25°C) δ 8.37 (dq, *J* = 1.7, 0.8 Hz, 1H), 8.19 (s, 1H), 7.98 (dq, *J* = 1.4, 0.7 Hz, 1H), 7.65 (ddd, *J* = 8.5, 1.8, 0.7 Hz, 1H), 7.49 (dt, *J* = 8.4, 0.7 Hz, 1H), 7.46 – 7.26 (m, 2H), 3.13 (hept, *J* = 6.9 Hz, 1H), 1.57 (s, 2H), 1.39 (d, *J* = 6.9 Hz, 6H), 0.09 (s, 3H).

^{19}F NMR (376 MHz Methylene Chloride-d_2, Rif.BF_3OEt_2, +25°C) δ -60.16.

The product **6d** was obtained from general procedure with a yield of 23%.

6.5.13 8-CF_3-11-benzo[a]carbazole 7d

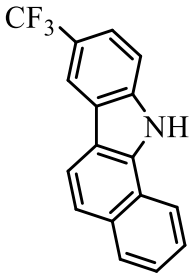

7d

^{1}H NMR (600 MHz, Chloroform-d, TMS +25°C) δ 8.96 (s, 1H), 8.39 (s, 1H), 8.13 (d, *J* = 8.4 Hz, 2H), 8.03 (d, *J* = 8.1 Hz, 1H), 7.71 (d, *J* = 8.6 Hz, 1H), 7.64 (p, *J* = 8.5 Hz, 3H), 7.60 – 7.54 (m, 1H), 1.24 (s, 1H), 0.06 (s, 4H).

^{13}C NMR (151 MHz, Chloroform-d, TMS, 76.9ppm, +25°C) δ 139.8, 135.7, 132.76, 129.2, 126.1, 125.9, 125.8, 124.3, 123.7, 122.7, 122.5, 122.3, 122.0, 121.6_2, 121.6, 121.5_7, 121.2, 121.0, 120.41, 119.0, 118.2, 117.6, 117.5_7, 117.5_5, 117.5_2, 111.1, 77.2, 77.0, 76.8, 1.0.

^{19}F NMR (376 MHz Methylene Chloride-d_2, Rif.BF_3OEt_2, +25°C) δ -61.27,

The product **7d** was obtained from general procedure with a yield of 17%.

6.5.14 Other synthesized carbazoles

- **3-isopropil-6-isopropil-carbazole 6b**

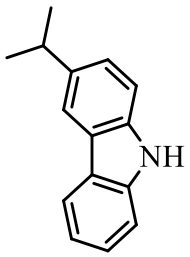

6b

^{1}H,^{13}C, ^{11}B-NMR spectra agree with that reported in letterature (Pub Chem CID 59346394).

The product **6b** was obtained from general procedure with a yield of 38%.

- ***8-isopropil-11-benzo[a]carbazole 7b***

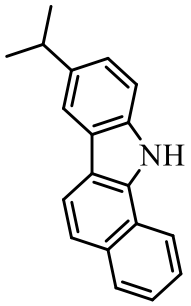

7b

^{1}H,^{13}C, ^{11}B-NMR spectra agree with that reported in letterature.[33]

The product **7b** was obtained from general procedure with a yield of 63%.

- ***8-OMe-11-benzo[a]carbazole 7c***

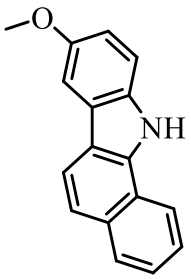

7c

^{1}H,^{13}C, ^{11}B-NMR spectra agree with that reported in letterature.[33]

The product **7c** was obtained from general procedure with a yield of 43%.

7 Bibliography

1. Mellerup, S. K. & Wang, S. Boron-based stimuli responsive materials. *Chem. Soc. Rev.* **48**, 3537–3549 (2019).
2. Cui, J., Kwon, J. E., Kim, H. J., Whang, D. R. & Park, S. Y. Smart fluorescent nanoparticles in water showing temperature-dependent ratiometric fluorescence color change. *ACS Appl. Mater. Interfaces* **9**, 2883–2890 (2017).
3. Liu, L., Wang, X., Wang, N., Peng, T. & Wang, S. Bright, Multi-responsive, Sky-Blue Platinum(II) Phosphors Based on a Tetradentate Chelating Framework. *Angew. Chemie - Int. Ed.* **56**, 9160–9164 (2017).
4. Beharry, A. A. & Woolley, G. A. Azobenzene photoswitches for biomolecules. *Chem. Soc. Rev.* **40**, 4422–4437 (2011).
5. Alemani, M. *et al.* Electric field-induced isomerization of azobenzene by STM. *J. Am. Chem. Soc.* **128**, 14446–14447 (2006).
6. Vyšniauskas, A. *et al.* Unravelling the effect of temperature on viscosity-sensitive fluorescent molecular rotors. *Chem. Sci.* **6**, 5773–5778 (2015).
7. Yu, X., Wang, Z., Jiang, Y., Shi, F. & Zhang, X. Reversible pH-responsive surface: From superhydrophobicity to superhydrophilicity. *Adv. Mater.* **17**, 1289–1293 (2005).
8. Kocak, G., Tuncer, C. & Bütün, V. PH-Responsive polymers. *Polym. Chem.* **8**, 144–176 (2017).
9. Martínez-Máñez, R. & Sancenón, F. *Fluorogenic and chromogenic chemosensors and reagents for anions*. *Chemical Reviews* vol. 103 (2003).
10. Bandara, H. M. D. & Burdette, S. C. Photoisomerization in different classes of azobenzene. *Chem. Soc. Rev.* **41**, 1809–1825 (2012).
11. Zhao, Q., Li, F. & Huang, C. Phosphorescent chemosensors based on heavy-metal complexes. *Chem. Soc. Rev.* **39**, 3007–3030 (2010).
12. Sagara, Y. & Kato, T. Mechanically induced luminescence changes in molecular assemblies. *Nat. Chem.* **1**, 605–610 (2009).
13. Arivazhagan, C. *et al.* Phenothiazinyl Boranes: A New Class of AIE Luminogens with Mega Stokes Shift, Mechanochromism, and Mechanoluminescence. *Chem. - A Eur. J.* **23**, 7046–7051 (2017).
14. Neena, K. K., Sudhakar, P., Dipak, K. & Thilagar, P. Diarylboryl-phenothiazine based multifunctional molecular siblings. *Chem. Commun.* **53**, 3641–3644 (2017).

15. Dong, H., Li, W., Sun, J., Li, S. & Klein, M. L. Understanding the Boron-Nitrogen Interaction and Its Possible Implications in Drug Design. *J. Phys. Chem. B* **119**, 14393–14401 (2015).
16. Burnham, B. Synthesis and Pharmacological Activities of Amine-Boranes. *Curr. Med. Chem.* **12**, 1995–2010 (2005).
17. Sudhakar, P., Mukherjee, S. & Thilagar, P. Revisiting borylanilines: Unique solid-state structures and insight into photophysical properties. *Organometallics* **32**, 3129–3133 (2013).
18. Fingerle, M., Maichle-Mössmer, C., Schundelmeier, S., Speiser, B. & Bettinger, H. F. Synthesis and Characterization of a Boron-Nitrogen-Boron Zigzag-Edged Benzo[fg]tetracene Motif. *Org. Lett.* **19**, 4428–4431 (2017).
19. Zhuang, F. D. *et al.* Efficient Modular Synthesis of Substituted Borazaronaphthalene. *Organometallics* **36**, 2479–2482 (2017).
20. Hegstrom_The_Handedness_of_the_universe.pdf.
21. Tokunaga, E., Yamamoto, T., Ito, E. & Shibata, N. Understanding the Thalidomide Chirality in Biological Processes by the Self-disproportionation of Enantiomers. *Sci. Rep.* **8**, 6–12 (2018).
22. Of, U. Basic terminology of stereochemistry (IUPAC Recommendations 1996). *Pure Appl. Chem.* **68**, 2193–2222 (1996).
23. Laplante, S. R., Edwards, P. J., Fader, L. D., Jakalian, A. & Hucke, O. Revealing Atropisomer Axial Chirality in Drug Discovery. *ChemMedChem* **6**, 505–513 (2011).
24. Benvenuto, D. *et al.* Accepted Article Accepted Article Accepted Article Accepted Article. *J. Med. Virol.* 0–3 (2020) doi:10.1002/jmv.25688.
25. Mislow, K. Stereochemical Consequences. **7019**, 26–33 (1975).
26. Driesschaert, B. *et al.* Configurationally stable tris(tetrathioaryl)methyl molecular propellers. *European J. Org. Chem.* 6517–6525 (2012) doi:10.1002/ejoc.201200801.
27. Grilli, S., Lunazzi, L., Mazzanti, A., Casarini, D. & Femoni, C. Conformational studies by dynamic NMR.78.1 Stereonmutation of the helical enantiomers of trigonal carbon diaryl-substituted compounds: Dimesitylketone, dimesitylthioketone, and dimesitylethylene. *J. Org. Chem.* **66**, 488–495 (2001).
28. Bretonnet, J. L. Basics of the density functional theory. *AIMS Mater. Sci.* **4**, 1372–1405 (2017).
29. Antony, J. & Grimme, S. Density functional theory including dispersion corrections for intermolecular interactions in a large benchmark set of biologically relevant molecules.

Phys. Chem. Chem. Phys. **8**, 5287–5293 (2006).

30. Demchenko, A. P. Introduction to fluorescence sensing. *Introd. to Fluoresc. Sens.* 1–586 (2009) doi:10.1007/978-1-4020-9003-5.
31. Ziessel, R., Ulrich, G. & Harriman, A. The chemistry of Bodipy: A new El Dorado for fluorescence tools. *New J. Chem.* **31**, 496–501 (2007).
32. Xiao, F., Liao, Y., Wu, M. & Deng, G. J. One-pot synthesis of carbazoles from cyclohexanones and arylhydrazine hydrochlorides under metal-free conditions. *Green Chem.* **14**, 3277–3280 (2012).
33. Shen, J., Li, N., Yu, Y. & Ma, C. Visible-light-induced oxidation/[3 + 2] cycloaddition/oxidative aromatization to construct benzo[a]carbazoles from 1,2,3,4-tetrahydronaphthalene and arylhydrazine hydrochlorides. *Org. Lett.* **21**, 7179–7183 (2019).

---

[i] A. M. Brouwer, *Pure Appl. Chem*., *83*, **2001**, 2213–2228.

[ii] A. M. Brouwer, *Pure Appl. Chem*., *83*, **2001**, 2213–2228.

[iii] A. M. Brouwer, *Pure Appl. Chem*., *83*, **2001**, 2213–2228.

[iv] A. M. Brouwer, *Pure Appl. Chem*., *83*, **2001**, 2213–2228.

[v] A. M. Brouwer, *Pure Appl. Chem*., *83*, **2001**, 2213–2228.

[vi] A. M. Brouwer, *Pure Appl. Chem*., *83*, **2001**, 2213–2228.

[vii] A. M. Brouwer, *Pure Appl. Chem*., *83*, **2001**, 2213–2228.